DOT/FAA/AR-07/7

Air Traffic Organization
Operations Planning
Office of Aviation Research
and Development
Washington, DC 20591

A Study of Normal Operational Landing Performance on Subsonic, Civil, Narrow-Body Jet Aircraft During Instrument Landing System Approaches

March 2007

Final Report

This document is available to the U.S. public through the National Technical Information Service (NTIS), Springfield, Virginia 22161.

U.S. Department of Transportation
Federal Aviation Administration

NOTICE

Technical Report Documentation Page

1. Report No.	2. Government Accession No.	3. Recipient's Catalog No.
DOT/FAA/AR-07/7		

4. Title and Subtitle	5. Report Date
A STUDY OF NORMAL OPERATIONAL LANDING PERFORMANCE ON SUBSONIC, CIVIL, NARROW-BODY JET AIRCRAFT DURING INSTRUMENT LANDING SYSTEM APPROACHES	March 2007
	6. Performing Organization Code

7. Author(s)	8. Performing Organization Report No.
Gerard W.H. van Es.[1], Peter J. van der Geest[1], Andrew Cheng, Ph.D.[2], Larry Hackler[3], and Archie E. Dillard, Ph.D.[4]	

9. Performing Organization Name and Address		10. Work Unit No. (TRAIS)
[1]National Aerospace Laboratory NLR Anthony Fokkerweg 2, 1059 CM Amsterdam P.O. Box 90502, 1006 BM Amsterdam, The Netherlands	[2]Hi-Tec Systems, Inc. 500 Scarborough, Suite 108 Egg Harbor Township, NJ 08234	
[3]Federal Aviation Administration William J. Hughes Technical Center Airport and Aircraft Safety R & D Division Flight Safety Branch Washington, DC 20591	[4]Federal Aviation Administration Mike Monroney Aeronautical Center Flight Simulation System, AFS-400 6500 South MacArthur Boulevard TSB Anex Oklahoma City, OK 73169	1. Contract or Grant No.

12. Sponsoring Agency Name and Address	13. Type of Report and Period Covered
U.S. Department of Transportation Federal Aviation Administration Air Traffic Organization Operations Planning Office of Aviation Research and Development Washington, DC 20591	Final Report
	14. Sponsoring Agency Code AFS-408

15. Supplementary Notes

16. Abstract

The need for improved capacity at airports to accommodate the rapid growth of domestic air traffic in the United States has led to the investigation of Land and Hold Short Operations (LAHSO) as a safe and feasible means to increase the traffic flow. While the capacity issue becomes important, it is imperative that the increase in capacity does not lead to a safety decline. A key task was to investigate the aircraft landing performance pertaining to operational safety guidelines for reducing the risks of incidents and accidents associated with LAHSO. For this, a clear knowledge of the day-to-day landing operations is required.

Data from quick-access recorders can be used to analyze aircraft performance. Aircraft landing field performance is influenced by many variables. Some variables were found to have a more dominating influence than others. Variables found to have a strong influence are height above the threshold, speed loss from flare initiation to touchdown, and the available runway length for landing. However, there is not one single factor that dominates the landing field performance.

This study used in-flight recorded data collected from day-to-day landing operations obtained from the quick-access recorders from two types of narrow-body jet aircraft.

17. Key Words	18. Distribution Statement
Operations safety, Threshold, Flare, Landing performance, Landing distance, Ground roll	This document is available to the U.S. public through the National Technical Information Service (NTIS), Springfield, Virginia 22161.

19. Security Classif. (of this report)	20. Security Classif. (of this page)	21. No. of Pages	22. Price
Unclassified	Unclassified	96	

TABLE OF CONTENTS

		Page
EXECUTIVE SUMMARY		ix
1.	INTRODUCTION	1
1.1	Background	1
1.2	Scope and Objective of the Study	1
1.3	Study Approach	1
1.4	Organization of the Report	2
2.	DATA COLLECTION	2
2.1	Aircraft Types	2
2.2	Data Sources	2
2.3	Flight Parameters Collected	3
2.4	Data Sample	4
2.5	Data Examples	5
3.	DATA PROCESSING	6
3.1	General	6
3.2	Derivation and Smoothing	7
3.3	The Airborne Distance	10
3.3.1	Threshold Crossing Height	11
3.3.2	Main Gear Touchdown	14
3.3.3	Airborne Distance Calculation	16
3.4	Nosewheel Touchdown	16
3.5	Flare Initiation	17
3.6	Other Parameters	19
3.7	Examples of Data Processing Performance	20
4.	RESULTS	25
4.1	Introduction	25
4.2	Characteristics of Miscellaneous Parameters	26
4.3	Airborne Part of the Landing	29
4.4	Ground Roll Part of the Landing	38
5.	BRIEF DISCUSSION OF THE RESULTS	46
5.1	Data Processing	46

5.2 Results 46

6. CONCLUSIONS 47

7. RECOMMENDATIONS 48

8. REFERENCES 48

APPENDICES

A—Example Time Histories
B—Demonstration of Data Processing Algorithms

LIST OF FIGURES

Figure		Page
1	Aircraft Types Considered in the Study	2
2	Sampling Process and Derivation of Pitch Rate From Sampled Pitch Angle	9
3	Gaussian Smoothing and Derivation of Pitch Rate From Sampled Pitch Angle Including Noise	10
4	Calculation of Height Above Threshold (H_{th}) From Glide Slope Deviation (Gs_{dev})	12
5	Difference Between RA and ILS Receiver Altitude	13
6	Time Histories of Normal Acceleration and Ground Spoiler Deflection During Landing (B-737)	15
7	Method of Estimating First Point of Main Gear Touchdown	16
8	Determination of Flare Initiation Point Based on Estimated Pitch Acceleration	18
9	A320 Landing Flare and Touchdown Recordings	21
10	B-737 Landing Flare and Touchdown Recordings	21
11	Runway Conditions Encountered	27
12	Prevailing Crosswind Conditions	27
13	Prevailing Head- and Tailwind Conditions	28
14	Prevailing Ceiling Conditions	28
15	Prevailing Visibility Conditions Below 10 km	29
16	Airborne Distance	30
17	Influence of Threshold Crossing Height on Airborne Distance for the B-737-400	31
18	Influence of Speed Loss on Airborne Distance	32
19	Time From Flare Initiation to Touchdown Versus Speed Loss	33
20	Difference in Actual Speed and Reference Speed at the Threshold	33
21	Influence of Speed Difference at Threshold On Airborne Distance for the B-737-400	34

22	Influence of Head- and Tailwind on Airborne Distance	35
23	Comparison of the Airborne Distance Autolands and Manual Landings (all Aircraft Types)	36
24	Flare Initiation Height	37
25	Influence Light Conditions on Airborne Distance	38
26	Frequency Distribution of Ground Roll Distance	39
27	Available Landing Distance Versus Ground Roll Distance	40
28	Time From Touchdown to Nose Down	41
29	Ground Distance During Nose-Down Rotation as Function of Time	41
30	Influence of Autobrake Use on Ground Roll Distance	42
31	Influence of Autobrake Setting on the Ground Roll Distance of the A320 and B-737-400	43
32	Influence of Runway Condition on Ground Roll Distance	43
33	Time From Touchdown to Thrust Reverser Engagement	44
34	Duration of Thrust Reverser Use	44
35	Airspeed at Idle Reverse Selection for the A319, A320, and A321 Aircraft	45
36	Influence of Thrust Reverser Use on Ground Roll Distance	46

LIST OF TABLES

Table		Page
1	List of Recorded Parameters	3
2	Landings in Data Sample	5
3	Parameter in the Landing Database	25
4	Visibility Conditions of 10 km or Better	29
5	Parameters That Influence the Airborne Distance	30

LIST OF ACRONYMS

A/THR	Autothrust
CAS	Calibrated airspeed
GMT	Greenwich Mean Time
GPS	Global positioning system
GS	Glide slope
ILS	Instrument landing system
kt	Knot
LAHSO	Land and Hold Short Operations
METAR	Aviation routine weather report
NLR	National Aerospace Laboratory
RA	Radio altitude (at main gear height)
rad/s	Radians per second
RDH	Reference datum height
TAS	True airspeed
THR	Thrust
Vref	Reference landing approach speed

EXECUTIVE SUMMARY

The need for improved capacity at airports to accommodate the rapid growth of domestic air traffic in the United States has led to the investigation of Land and Hold Short Operations (LAHSO) as a safe and feasible means to increase the traffic flow. While the capacity issue becomes important, it is imperative that the increase in capacity does not lead to a safety decline. The introduction of new technology and procedures for improving the airport capacity must be integrated into the existing infrastructure so that maximum benefits for safety and efficiency are realized. The key task was to investigate the aircraft landing performance pertaining to operational safety guidelines for reducing the risks of incidents and accidents associated with LAHSO. For this, a clear knowledge of the day-to-day landing operations in required. At the request of the Federal Aviation Administration, the National Aerospace Laboratory was commissioned by the Dutch Civil Aviation Authority to conduct an analysis of day-to-day landing operations using in-flight recorded data.

This present study is focused on analyzing the operational landing field performance of two different narrow-body, turbofan-engined aircraft under various weather conditions. Two aircraft types were selected for a statistical study of a number of performance and flight control parameters with respect to the landing phase of flight: the Boeing 737-400 and the Airbus A319, A320, and A321. The present study is conducted using in-flight recorded data collected from day-to-day landing operations. These data were obtained from the quick-access recorder, which stores a limited number of the important flight data parameters. The objective was not intended to be a complete and conclusive study regarding landing field performance in relation to LAHSO issues. However, the results and knowledge obtained from this study can be useful for further analysis of LAHSO flight performance-related issues.

The following objectives were made:

- Data from quick-access recorders can be used to analyze aircraft performance. During this study, valuable insight and knowledge were gained on using quick access recorded data for aircraft landing field performance analysis.

- Aircraft landing field performance is influenced by many variables. Some variables were found to have a more dominating influence than others. Variables found to have a strong influence are height above the threshold, speed loss from flare initiation to touchdown, and the available runway length for landing. However, there is not one single factor that dominates the landing field performance.

- Not all results presented in this study can be used for the analysis of LAHSO. The results show that the ground roll performance is strongly influenced by the available runway length for landing. Therefore, for this study, only landings on shorter runways should be considered.

1. INTRODUCTION.

1.1 BACKGROUND.

The need for improved capacity at airports to accommodate the rapid growth of domestic air traffic in the United States has led to the investigation of Land and Hold Short Operations (LAHSO) as a safe and feasible means to increase the traffic flow. While the capacity issue becomes important, it is imperative that the increase in capacity does not lead to a safety decline. The introduction of new technology and procedures for improving the airport capacity must be integrated into the existing infrastructure so that maximum benefits for safety and efficiency are realized.

A key task was to investigate the aircraft landing performance pertaining to operational safety guidelines for reducing the risks of incidents and accidents associated with LAHSO. For this, a clear knowledge of the day-to-day landing operations is required. At the request of the Federal Aviation Administration, the National Aerospace Laboratory (NLR) was commissioned by the Dutch Civil Aviation Authority to conduct an analysis of day-to-day landing operations using in-flight recorded data.

1.2 SCOPE AND OBJECTIVE OF THE STUDY.

This present study was focused on analyzing the operational landing field performance of two different narrow-body, turbofan-engined aircraft under various weather conditions. Two aircraft types were selected for a statistical study of a number of performance and flight control parameters with respect to the landing phase of flight: the Boeing 737-400 and the Airbus A319, A320, and A321.

The objective was to identify empirical distributions of the landing distance parameters such as the approach speed at threshold, the touchdown point, rollout distance, and total landing distance. Furthermore, the objective was to gain insight in those factors that affect the landing field performance. This study was explorative since it was the first attempt to analyze large quantities of flight data during landing.

The objective was not intended to be a complete and conclusive study regarding landing field performance in relation to LAHSO issues. However, the results and knowledge obtained from this study can be useful for further analysis of LAHSO flight performance-related issues.

1.3 STUDY APPROACH.

The present study was conducted using in-flight recorded data collected from day-to-day landing operations. These data were obtained from the quick-access recorder, which stores a limited number of the important flight data parameters.

1.4 ORGANIZATION OF THE REPORT.

This report is organized as follows: section 2 describes the data collection effort, section 3 describes the data processing applied to the collected data, and section 4 presents the results. In section 5, a brief discussion of the results is given, in section 6, the conclusions are summarized, and in section 7, recommendations are given.

2. DATA COLLECTION.

2.1 AIRCRAFT TYPES.

Two narrow-body jet aircraft were considered in this study: the Boeing 737-400 and the Airbus A319, A320, and A321 (see figure 1). Both aircraft are comparable in size and general performance (e.g., range and payload) and are used by many operators worldwide. One major distinctive feature of the two aircraft is the control system. One uses a conventional control system, and the other has a fly-by-wire control system. Although it was not the aim of this study to look at the advantages and disadvantages of these different control systems, it is likely that some differences in landing performance is attributable to the control system. This applies only to the airborne part of the landing and not to the ground roll part of the landing.

Figure 1. Aircraft Types Considered in the Study

2.2 DATA SOURCES.

All flight data analyzed in this study were obtained from a European airline. The flight data were obtained from the airline's flight data monitoring program. The recording effort lasted for more than 7 months and covered winter, spring, and summertime operations. In addition to flight data, aviation routine weather reports (METAR) were collected. METAR reports contain hourly observations of the weather conditions at an airport. For each landing, the METAR that was the closest to the landing time was linked with the recorded flight data of this landing.

2.3 FLIGHT PARAMETERS COLLECTED.

The list of collected comparable flight parameters for the A320 series and the B-737-400 is provided in table 1. It should be noted that some units and sample frequencies may differ between these aircraft types.

Table 1. List of Recorded Parameters

	Parameter List A320 Series	Unit	Sample Rate (Hz)		Parameter list B-737-400	Unit	Sample Rate (Hz)
1	Frame Counter	--	8	1	Frame Counter	--	8
2	RWY Heading	deg	8	2	Time	sec	8
3	GMT Hours	hr	1	3	Day of Month	--	1
4	GMT Minutes	min	1	4	Month	--	1
5	GMT Seconds	sec	1	5	Pressure Altitude	ft	1
6	Day of Month	--	1	6	Radio Altitude	ft	4
7	Month	--	1	7	Calibrated Airspeed	kt	1
8	Pressure Altitude	ft	1	8	True Airspeed	kt	1
9	True Airspeed	kt	1	9	Groundspeed	kt	1
10	Calibrated Airspeed	kt	1	10	N1 Engine 1	%	1
11	Groundspeed	kt	1	11	N1 Engine 2	%	1
12	N1 Engine 1	%	1	12	N2 Engine 1	%	1
13	N1 Engine 2	%	1	13	N2 Engine 2	%	1
14	N2 Engine 1	%	1	14	Normal Acceleration	g	8
15	N2 Engine 2	%	1	15	Longitudinal Acceleration	g	4
16	Normal Acceleration	g	8	16	Lateral Acceleration	g	4
17	Longitudinal Acceleration	g	4	17	Flap Position	deg	1
18	Lateral Acceleration	g	4	18	Training Edge Flap Position	deg	1
19	Flap	deg	1	19	Spoiler 2 Position	deg	1
20	Ground Spoiler Out	0/1	1	20	Spoiler 7 Position	deg	1
21	Thrust Reverser 1 Deployed	0/1	1	21	Thrust Reverser Deployed Left	0/1	1
22	Thrust Reverser 2 Deployed	0/1	1	22	Thrust Reverser Deployed Right	0/1	1
23	Air Ground	0/1	2	23	Air Ground	0/1	2
24	Glide slope Deviation	dot	1	24	Glide slope Deviation (Dots)	dot	1
25	Localiser Deviation	dot	1	25	Localiser Deviation (Dots)	dot	1
26	Autobrake High	0/1	1	26	Autobrake Level 1	--	1
27	Autobrake Medium	0/1	1	27	Autobrake Level 2	--	1
28	Autobrake Low	0/1	1	28	Autobrake Level 3	--	1
29	Gross Weight	kg	1	29	Auto Break Max	--	1
30	Magnetic Heading	deg	1	30	Gross Weight (lb)	lb	1
31	Pitch	deg	4	31	Gross Weight (kg)	kg	1
32	Angle of Attack	deg	1	32	Magnetic Heading	deg	1
33	Static Air Temperature	degC	1	33	Roll	deg	4
34	Radio altitude	ft	4	34	Pitch	deg	4
35	Roll	deg	4	35	Angle of attack	deg	2
36	Autopilot 1 cmd	0/1	1	36	Static air temperature	degC	1
37	Autopilot 1 cmd	0/1	1	37	Autopilot cmd A left	0/1	1

Table 1. List of Recorded Parameters (Continued)

	Parameter List A320 Series	Unit	Sample Rate (Hz)		Parameter List B-737-400	Unit	Sample Rate (Hz)
38	Autopilot engaged	0/1	1	38	Autopilot cmd A right	0/1	1
39	Brake 1 pressure	bar	1	39	Autopilot cmd B left	0/1	1
40	Brake 2 pressure	bar	1	40	Autopilot cmd B right	0/1	1
41	Brake 3 pressure	bar	1	41	Brake pressure alternate left	psi	1
42	Brake 4 pressure	bar	1	42	Brake pressure alternate right	psi	1
43	Brake 5 pressure	bar	1	43	Brake pressure main left	psi	1
44	Brake 6 pressure	bar	1	44	Brake pressure main right	psi	1
45	Brake 7 pressure	bar	1	45	Brake pedal left	deg	8
46	Brake 8 pressure	bar	1	46	Brake pedal right	deg	8
47	Target approach speed	kt	1	47	Target airspeed	kt	1
48	GPS longitude	deg	1	48	FMC longitude	deg	1
49	GPS latitude	deg	1	49	FMC latitude	deg	1
50	Drift angle	deg	1	50	Track angle magnetic	deg	1
51	Brake pedal left position	deg	1	51	Track angle true	deg	1
52	Brake pedal right position	deg	1	52	Inertial vertical speed	fpm	1
53	Inertial vertical speed	fpm	8	53	Elevator left	deg	1
54	Elevator left position	deg	4	54	Elevator right	deg	1
55	Elevator right position	deg	4				

Cmd = Command
FMC = Flight management computer
Fpm = Feet per minute
G = Gram
GMT = Greenwich Mean Time
psi = pounds per square inch
GPS = Global positioning system
kg = Kilogram
kt = Knot
RWY = Runway
ft = feet
min = minute
sec = second
hr = Hour
deg = Degree
lb = Pound

2.4 DATA SAMPLE.

The data collection effort was set to obtain landing data for 50,000 landings (all aircraft types combined). These data were checked for errors and inconsistencies. Landings were removed from the sample if significant errors and inconsistencies were identified. The landing data that was collected concerned both instrument and visual approaches. To calculate the airborne distance (i.e., distance covered when crossing the runway threshold to touchdown of the main landing gear), the position relative to the runway should be known. Although global positioning system (GPS) coordinates were recorded, these data were not accurate enough to determine the position of the aircraft relative to the runway threshold[1].

Therefore, a different approach was adopted to determine the position of the aircraft relative to the runway threshold. This approach is discussed in section 3 and is based on the use of glide slope deviation data. Such data is only available for those approaches flown using the instrument landing system (ILS) as guidance. Not every landing is conducted using the ILS as an approach aid. Therefore, a number of landings from the initial sample were not considered for further

[1] Although a GPS can accurately record the position of an aircraft, the flight data obtained from the quick-access recorder of an aircraft contains GPS coordinates that are stored with insufficient number of digits. Also, the sampling method of the GPS coordinates on the quick-access recorders influences the use in a negative matter.

analysis. In the end, data errors, inconsistencies, and the absence of ILS glide slope deviation data reduced the initial data sample of 50,000 landings to 40,764. The number of landings in the final data sample is listed in table 2.

Table 2. Landings in Data Sample

Aircraft Type	Number of Landings
A319	7,474
A320	13,245
A321	5,952
B-737-400	14,093

2.5 DATA EXAMPLES.

Example time histories for the four aircraft models in the data sample are provided in appendix A. Figures A-1 to A-8 show recorded data for the B-737-400, A320, A319, and A321, respectively. These data have not been processed in any way and are depicted as recorded by the aircrafts' onboard quick-access recorders.

The time histories are given in two series of 12 graphs each. The first series relates mainly to flight technical parameters, such as velocity, pitch, altitude, heading, and accelerations. The second series shows mainly aircraft controls, such as engine parameters, flaps, spoiler, thrust reversers, and brake pedal.

It should be noted that the data sets for the Boeing and Airbus types are not exactly identical, as addressed in section 2.3. Also, the units in which data are recorded differ between these aircraft types. For instance, the B-737 data set contains spoiler deflection in degrees, whereas in the Airbus types, spoiler deflection is recorded as a discrete (in/out).

In general, it was concluded—as also illustrated by these example time histories—that the data quality is fairly good, and there is good consistency among the data. However, a few remarks have to be made in this respect.

First, the recording of the GPS position (latitude and longitude) as recorded by the Airbus types appears to be anomalous. These anomalies were observed in the large majority of cases, but not in all cases. The reason for this behavior was not clear. The data processing, discussed in section 5.1, was not relevant because the actual position coordinates were not used to determine the landing performance indicators.

Another observation that was made from the example time histories concerned the characteristics of the various recorded velocities. The calibrated airspeed (CAS) was limited to a lower value of 45 kt for the B-737 and to 30 kt for the Airbus models. Similarly, the true airspeed (TAS) was limited to minimum values of 100 kt for the B-737 and 60 kt for the Airbus models.

3. DATA PROCESSING.

3.1 GENERAL.

This section treats the processing of the recorded data before they can be used for further statistical analysis. This processing consists of two steps:

- Data error check and removal
- Determination of derived parameters

The first step is performed to check whether the recorded data are consistent and do not contain obvious errors. If errors are found it is determined whether the data can be repaired or if the recording has to be rejected as a valid recording.

The second step concerns the processing of the data to establish a number of parameters that are not part of the original data set, such as instantaneous pitch rate and pitch acceleration. Subsequently, the data is further processed to determine a number of event parameters, such as threshold crossing height and the touchdown point.

This second step data processing is explained further in sections 3.2 through 3.7. Here, only the first step processing will be described.

This processing contains a number of subsequent elements:

- Altitude check—It is checked whether the initial altitude is sufficiently high. It appeared that a substantial number of recordings started at rather low altitude (<60 ft). Since this altitude is within the range of the expected threshold crossing height, all recordings with an initial altitude of less than 60 ft are rejected. If these recordings would be included, this could lead to a statistical bias in the threshold crossing height.

- Spikes—A number of relevant time histories (i.e., velocities, radio altitude (RA), vertical speed, and glide slope deviations) are checked for the presence of spikes. Spikes are effectively detected by a spike detection algorithm. This algorithm triggers on steep flanks in the data and can detect whether the spike occurs over single or multiple subsequent data samples. If the algorithm detects a single point spike, it will repair the data by replacing the spike by interpolation between the data samples before and after the anomaly. If the spike comprises multiple samples, the data from this landing will be rejected.

- Frozen data—A number of parameters appear to sometimes exhibit a frozen behavior. That means that a constant value is recorded. The glide slope deviation and vertical speed are parameters that appear to be especially susceptible to this phenomenon. For the glide slope deviation, this can occur when a nonprecision approach is carried out, and no ILS is used as a landing aid. For the vertical speed, it is not clear what the background of this behavior is. A special algorithm was developed to detect when data was frozen. If frozen data is detected, the data from that landing is rejected.

- Reasonableness—Parameters are checked to determine whether the recorded data are within reasonable limits. It appears that, in particular, recordings of vertical speed and ground speed are susceptible to being outside reasonable limits (e.g., ground speed < -50 kt). If data is found outside reasonable limits, the data from that landing is rejected.

Due to the initial data processing described above, approximately 10% of the available recordings were rejected for further processing.

3.2 DERIVATION AND SMOOTHING.

A number of the selected landing performance indicators, such as the flare initiation and the main gear and nose wheel touchdown points, require the determination of certain parameters that are not part of the recorded data list as presented in section 2.3. These parameters pertain mainly to derived signals, such as pitch rate, pitch acceleration, and change of normal acceleration. Determination of these parameters requires the calculation of the time derivatives of the recorded pitch attitude and normal acceleration.

It is well known that exact differentiation of continuous, real-time signals is theoretically impossible. For this reason, it is necessary to devise processing algorithms to estimate the actual time derivative signals as accurately as possible. For real-time data processing, various methods have been developed that can estimate time derivative signals, such as simple rate taking filters, complementary filters, and Kalman filters. It is beyond the scope of the present report to discuss these methods in more detail. However, the general drawback of these real-time processing methods is that they inherently introduce some time delay in the resulting time derivative signals, and, in addition, they may amplify the noise level of the original signal.

Consequently, in-flight data analysis, it is common practice to use postprocessing methods. The advantage of such methods is that they can use, in the point estimate process, the information of both past and future neighboring samples. By doing so, it is possible to minimize the effects of time delay and effectively reduce the noise level of the resulting signal.

A simple and effective method to estimate the time derivative of a signal in postprocessing is to determine the slope of the signal during the time interval before and after the actual data point and to average them, thus minimizing time delay. More advanced methods may make use of more data samples before and after the actual data point using, for instance, spline methods or moving averaging. However, it should be noted that the noise level can be reduced by using more data samples in the estimating process, but in general, at the expense of the frequency content (bandwidth) of the resulting signal. Therefore, the best method to use depends on the application at hand, which is based on required bandwidth, the basic sampling frequency, and the data quality.

In this respect, it should be noted that the sampling rate of the recorded parameters in the present study is relatively low, especially in comparison with dedicated flight test programs. For instance, in flight test programs, it is general practice to record the pitch angle at 16 or 32 Hz and accelerations at 64 or 128 Hz. In the present data set, the pitch angle is recorded at 4 Hz and

accelerations at 8 Hz. Clearly, this presents some conflict between retaining sufficient bandwidth and required noise reduction.

As a rule of thumb, the bandwidth of pitch dynamics of a commercial transport aircraft (size of a B-737 or A320) is typically on the order 1.5 to 2.5 radians per second (rad/s), in the approach and landing phase. To record the aircraft motion of such frequency content with sufficient accuracy, it is necessary to sample the pitch angle with a sampling frequency that is at least 10 times the bandwidth. In this particular case, that is 10 x 2.5= 25 rad/s ~ 4 Hz.

From this simple analysis, it is clear that the sampling rate of the pitch angle in the present data set is the bare minimum to describe the pitch dynamics. For this reason, one should be careful in the determination of the pitch rate (the time derivative of the pitch angle) not to introduce noise-reducing filtering that would decrease the bandwidth of the resulting signal.

However, smoothing algorithms do exist, which can effectively reduce noise while minimizing the effects on bandwidth. Forward/backward moving averaging is such a method that can be applied in postprocessing to provide this smoothing. Forward/backward moving averaging is a method that takes the average value of a number of samples before and after the data point and averages over these samples to provide noise reduction without introducing time delay. Noise reduction is obtained because random noise, when averaged over a number of samples, will largely cancel out the noise. At the same time, however, the actual frequency content of the signal is averaged over a number samples and, therefore, somewhat reduced.

This particular problem arose about 20 years ago, during the flight test program of the Fokker 100, when it was required to accurately determine the vertical speed of the aircraft during the landing and touchdown as part of the autoland performance analysis. Vertical speed is a signal that cannot be measured directly, but has to be derived from either differentiating the RA or integrating the vertical acceleration. Both methods had their drawbacks, the first leads to amplifying noise, and the second may lead to large bias errors. Various filtering schemes were devised to solve those problems without affecting the dynamics of the vertical speed and without introducing time delays. It was shown that most real-time processing methods were not able to meet the requirements, but that postprocessing methods were most effective. Finally, it appeared that Gaussian forward/backward moving averaging of the RA provided the best results. This method is a variant of uniform forward/backward moving averaging by weighing the involved data samples according to a Gaussian function. The exact mathematical details of this method are still considered proprietary and, therefore, are not presented here.

An illustrative example is presented here to demonstrate how the procedure works on a data set, with similar properties as the recorded data used in this study. First, true data are generated by using a nonlinear, 6 degrees-of-freedom, aircraft simulation program of the Fokker 100 that is available at the NLR. In this particular example, the true data consist of the time histories of the pitch angle and pitch rate of a Fokker 100 during approach, in response to an elevator step-type of input. These time histories are calculated at small time intervals (1/64 sec). Subsequently, the pitch angle is sampled at 4 Hz, corresponding to the sample rate in the present recorded data set. Next, the pitch rate is determined by numerical forward/backward differentiation of the (4 Hz)

sampled pitch angle. The result is the estimated pitch rate, which is also provided at 4 Hz. The results are depicted in figure 2.

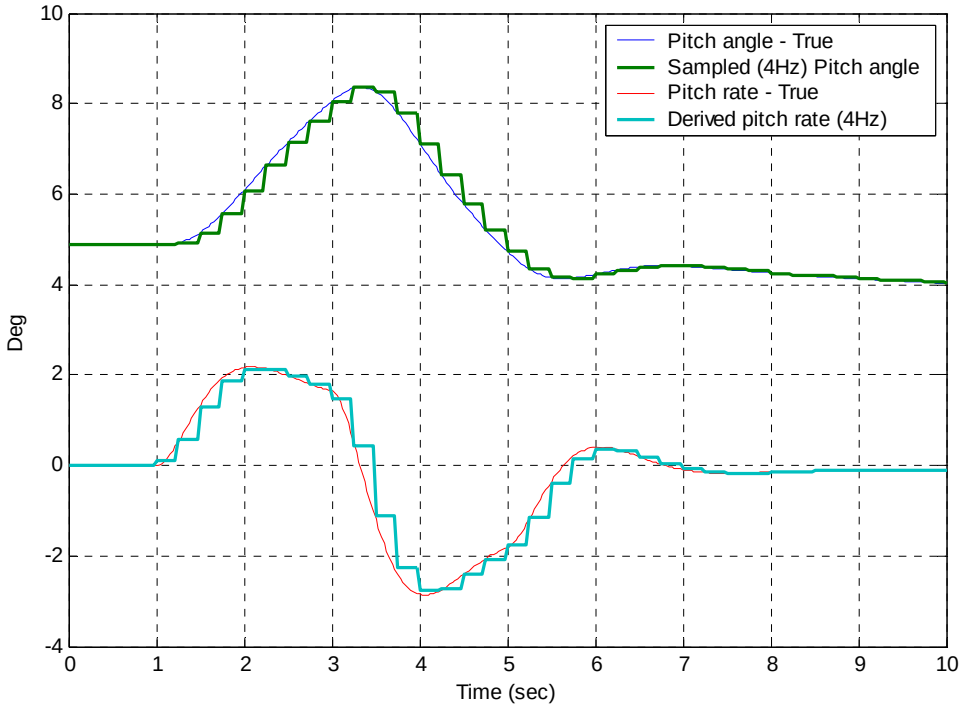

Figure 2. Sampling Process and Derivation of Pitch Rate From Sampled Pitch Angle

It is clearly shown that the forward/backward differentiation process provides an accurate estimate of the true pitch rate, and no time delay is introduced. Evidently, this performance can only be achieved when the original signal is fully noise free, as is the case here. In a second example, the effects of noise and the effectiveness of the Gaussian moving average method is demonstrated. In this example shown in figure 3, the true pitch angle signal is corrupted with random noise of a magnitude corresponding to a (low performance) Attitude and Heading Reference System. Now, the 4-Hz sampled pitch angle signal also includes the random noise values, as shown in figure 3. The noise-corrupted sampled pitch angle is now again numerically differentiated to obtain the estimate of the pitch rate signal.

As shown in figure 3, this leads to strong amplification of the noise in the derived rate signal and results in significant distortion. To reduce the effect of noise, the Gaussian moving average method is now applied to the derived pitch rate signal. Figure 3 clearly illustrates the effectiveness of this method. The resulting estimate of the pitch rate signal closely resembles the true pitch rate signal. Noise is significantly reduced, and no time delay is introduced. Figure 3 also shows that the derived rate signal is distorted at the start and end of the time series. This is a consequence of the forward/backward averaging process. At the start of the recording, data was missing from samples before the recording was started. Likewise, data was missing at the end of the recording, after the recording was ended.

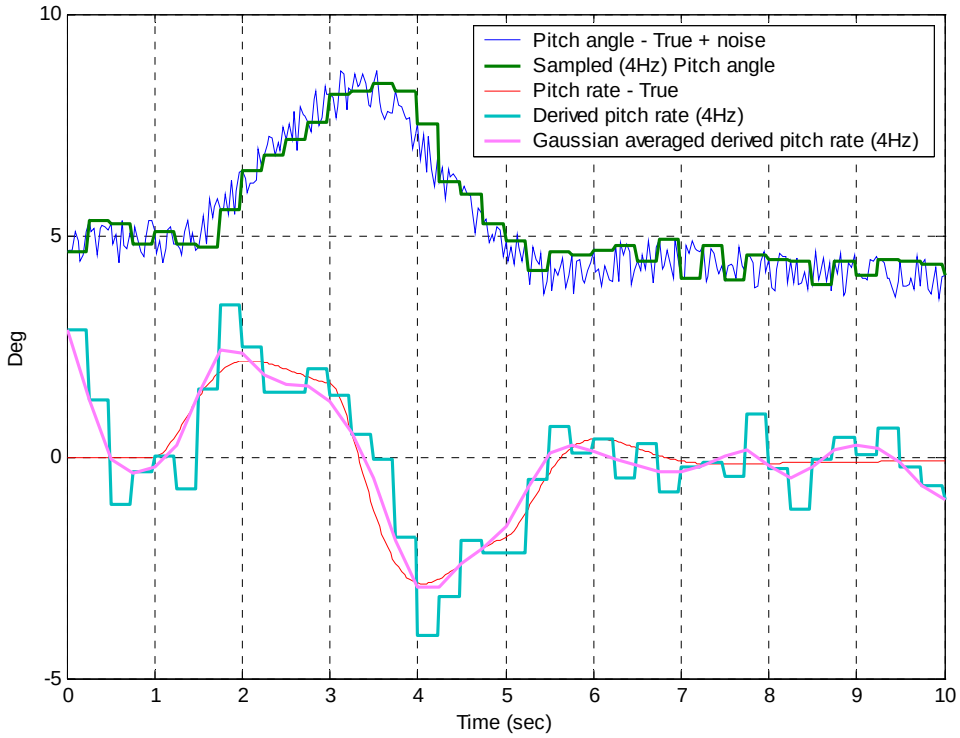

Figure 3. Gaussian Smoothing and Derivation of Pitch Rate From Sampled Pitch Angle Including Noise

To summarize, a short empirical analysis was performed to illustrate the problems that can arise from deriving rate signals from low rate sampled data. Moreover, the effectiveness of a smoothing algorithm that is used to remove noise from the resulting signals without significantly affecting the bandwidth of the signal or introducing time delay was demonstrated. The following sections show how these algorithms are applied to determine a number of landing performance related parameters.

3.3 THE AIRBORNE DISTANCE.

According to Title 14 Code of Federal Regulations Part 25.125 [1], the landing distance of an aircraft is defined as the horizontal distance from the point at which the main gear of the airplane is 50 ft above the landing surface to the point at which the aircraft is brought to a stop. To determine the landing distance, two parts are to be considered: the airborne distance (from 50 ft to touchdown) and the ground distance from touchdown to stop.

In this study, the focus is on the determination of the airborne distance from the recorded operational data. For this, it is essential to determine the point where the targeted 50-ft height above the runway is crossed and the actual point of touchdown. The determination of both parameters from operational data is discussed in section 3.3.1.

3.3.1 Threshold Crossing Height.

As indicated in Advisory Circular 25-7A, "Flight Test Guide for Certification of Transport Category Airplanes" [2], the airborne distance should be measured from a targeted -3 degrees glide slope that should be maintained prior to reaching a height of 50 ft above the landing surface. The reason for this requirement is that the usual glide slope of the ILS is -3 degrees, and 50 ft coincides with the usual ILS Reference Datum Height (RDH) that marks the height of the intersection of the glide slope beam with the runway threshold. The airborne distance, calculated in this way, will, therefore, be representative of common operational practice. However, in particular cases, the ILS glide slope or the ILS RDH may deviate from the standard -3 degrees and 50 ft, respectively. This might influence the actual airborne distance in practice.

For the present investigation, the interest is not in the airborne distance that is applicable to a particular airport, but in the actual air distance in operational practice when the -3 degrees glide slope and 50-ft height above landing surface would be targeted. For this reason, it is assumed that, for all airports in the data sample, a -3 degrees glide slope and 50-ft RDH is applicable[2].

Based on this assumption, the geometric point where the 50-ft RDH is passed is located 50/tan(3°) = 954 ft (~290 meters) in front of the ILS glide slope transmitter. For the determination of the airborne distance, it is, therefore, essential to determine when the airplane passes this geometric location.

Of course, in practice, the aircraft will not follow the glide slope exactly and, therefore, will not pass precisely at 50 ft over the threshold. These deviations are, however, measured as glide slope deviations by the ILS receiver onboard the aircraft. The glide slope deviation is an angular signal that provides the angular deviation from the reference glide slope. The actual deviation is measured according to the following relationship:

$$i_{gs} = \frac{625}{|\gamma_{gs}|} \cdot \varepsilon_{gs} \tag{1}$$

where:

i_{gs} is the current in μA, measured by the ILS glide slope receiver
γ_{gs} is the reference glide slope angle in degrees
ε_{gs} is the angular deviation in degrees

So, for a reference glide slope of 3 degrees, the angular glide slope deviation would be 0.0048° per μA of deviation measured by the ILS glide slope receiver. Since the full-scale deflection of the glide slope deviation pointer in the cockpit (i.e., two dots) is equivalent to 150 μA, the angular glide slope deviation would be equal to 0.36° per dot of deviation shown on the glide slope deviation pointer.

[2] The published glide slope threshold crossing height does not represent the height of the actual glide path on-course indication above the runway threshold. It is used as a reference for planning purposes and represents the height above the runway threshold that an aircraft's glide slope antenna should be, if that aircraft remains on a trajectory formed by the 4-mile-to-middle marker glide path segment.

By measuring the glide slope deviation, the absolute line of sight angle to the glide slope transmitter is also established, i.e.,: $\gamma_{total} = \gamma_{gs} + \varepsilon_{gs}$.

Because the actual height (H) relative to the runway surface is known from the radio altimeter, the distance (R) to the glide slope transmitter can be computed, according to the following equation, see figure 4:

$$R = \frac{H}{\tan(\gamma_{gs} + \varepsilon_{gs})} \tag{2}$$

The actual threshold crossing point is found when R equals 50/tan(3°)≈954 ft.

When the threshold crossing point is established, the corresponding threshold crossing time (t_{TH}) and the actual threshold height (H_{TH}) also are determined.

$$\tan\,(GS + GSDev) = \frac{H}{R}$$

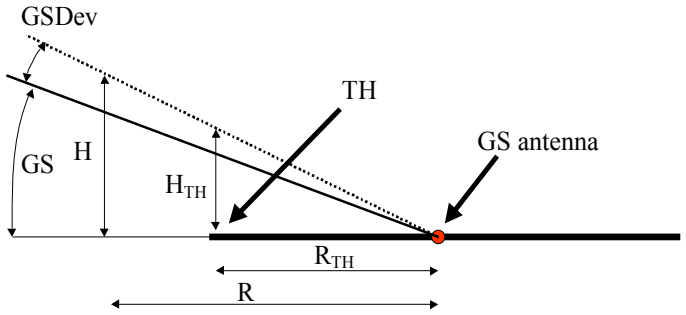

Figure 4. Calculation of Height Above Threshold (H_{th}) From Glide Slope Deviation (GS_{dev})

Clearly, the above described procedure is only accurate if the reference glide slope angle is 3 degrees. To get an indication of how the actual glide slope angle affects the calculated threshold height, the following analysis is presented.

Based on equations 1 and 2, the threshold crossing height is given by:

$$H_{TH} = \frac{50 \cdot \tan(\gamma_{gs} + \varepsilon_{gs})}{\tan(\gamma_{gs})} = \frac{50 \cdot \tan(\gamma_{gs}(1 + \frac{i_{gs}}{625}))}{\tan(\gamma_{gs})} \tag{3}$$

For small angles, it is known that, by good approximation, $\tan(\gamma) \approx \gamma$. Herewith, equation 3 can be written as:

$$H_{TH} \approx 50 \cdot (1 + \frac{i_{gs}}{625}) \tag{4}$$

Since the sensitivity of the glide slope receiver depends on the actual glide slope angle, the determination of the threshold crossing height is, by good approximation, independent of the glide slope angle.

Another aspect that has to be addressed is the fact that the actual glide slope deviation in the aircraft is measured at the location of the glide slope antenna in the nose of the airplane. The radio altimeter provides the height of the main gear above the earth's surface. The height of the ILS antenna above the surface needs to be compensated for this difference in location and the pitch attitude of the aircraft, as illustrated in figure 5. The height of the ILS antenna can be calculated as follows:

$$H_{ILS} = H_{RA} + x_{ILS} \cdot \sin\theta + y_{ILS} \cdot \cos\theta \tag{5}$$

where:

H_{RA} = Height to main gear as given by radio altimeter
x_{ILS} = Longitudinal distance from ILS antenna to main gear (+ fwd)
y_{ILS} = Vertical distance from ILS antenna to main gear (+ up)
θ = Pitch attitude

So, the threshold crossing height is computed based on the crossing height of the ILS antenna and then, subsequently, the corresponding height of the main gear at that point in time is determined.

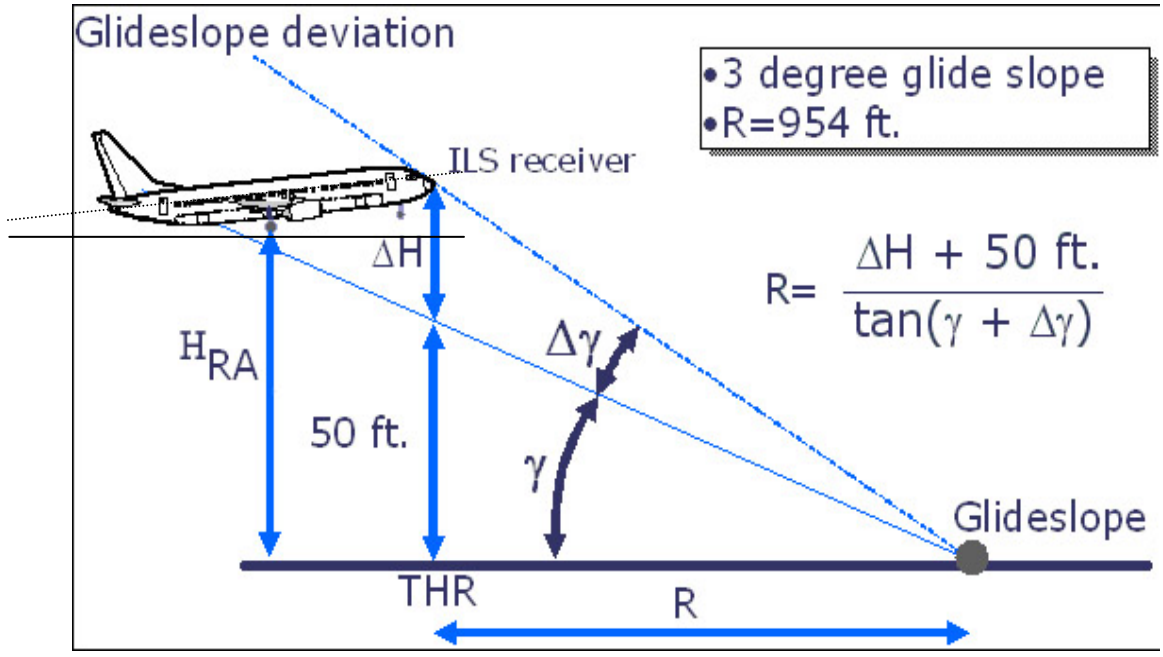

Figure 5. Difference Between RA and ILS Receiver Altitude

3.3.2 Main Gear Touchdown.

The second parameter that has to be determined to establish the airborne distance is the main gear touchdown point. In particular, it is important to determine the point in time of touchdown as accurately as possible. It should be noted that the airspeed of the aircraft types at hand during the landing phase is approximately 140 kt. This means that each second, a distance of approximately 200 ft is covered, which is about 15% of the average airborne distance. For this reason, it is necessary to determine the actual touchdown time with an accuracy of 0.1 to 0.2 second. Since the smallest sampling time interval in the data sample (pertaining to normal acceleration) is 0.125 second, it is important that the correct touchdown sample is found, and that the processing method should not introduce any additional time delay. The objective of this section is to briefly describe the method used to determine the touchdown point during the aircraft landing maneuver.

The available flight data comprises a number of indicators that could be used for the estimation of first ground contact. These are:

- Air-ground switch
- Ground spoiler deployment
- Normal acceleration

At first sight, the most logical choice is to use the air-ground switch. In practice, this switch is triggered by wheel spin-up and/or main gear strut deflection. However, for the aircraft types under consideration (B-737 and A320), this parameter appeared to be less suited for the intended purpose for several reasons. Inspection of the available test data showed that there were substantial differences in the method with which the air-ground switch was sampled for both aircraft types. (For the B-737, it was an alpha-numerical value, and for the A320, it was a digital value). This hampers the automatic processing of these data. Moreover, the sample rate of the air-ground switch is relatively low (2 Hz), which would preclude achieving the required timing accuracy. Finally, some inconsistencies were noted in the available data, showing that the air-ground switch was sometimes triggered after the ground spoiler deflection due to sampling delay.

For this reason, it has been decided to discard the use of the air-ground switch as an indicator and to use instead the point of first ground spoiler deflection. This parameter shows consistent behavior. Obviously, the ground spoiler deflection does not represent the actual point of first ground contact, because there will be some delay between first ground contact and ground spoiler deflection. For this purpose, the normal acceleration signal is used in combination with the ground spoiler deflection signal.

Figure 6 shows an example of the normal acceleration and the ground spoiler deflection for one case out of the test data set. Again, it may seem logical to use the first peak of the normal acceleration signal just before the ground spoiler activation as the trigger for the first ground contact. However, in practice, this procedure cannot be used for two reasons. First, in many cases, there can be a relatively soft touchdown such that a real peak can not be discriminated. Figure 6 presents a relatively firm touchdown. Second, the peak in the normal acceleration

represents the point of maximum ground reaction forces, and that point will be somewhat later than the point of first ground contact. As shown in figure 6, the anticipated point of first ground contact is approximately 0.2 to 0.3 second before the point of maximum normal acceleration.

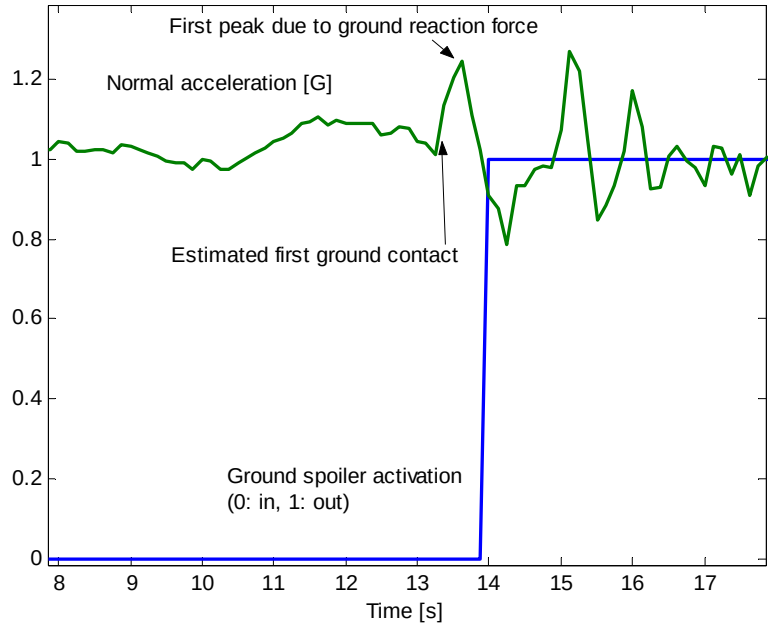

Figure 6. Time Histories of Normal Acceleration and Ground Spoiler Deflection During Landing (B-737)

Based on these observations, it was concluded that it is necessary to take into account the change of the normal acceleration to more accurately estimate the actual point of first ground contact. The procedure followed is to differentiate the normal acceleration signal (by means of forward/backward numerical differentiation, discussed in section 3.2). This derived signal is called the jerk.

It appears that the characteristics of the jerk are clearly correlated with the airborne and ground phase of the landing. Consequently, this signal is well suited to identify the transition from airborne to ground. Figure 7 provides an illustration how the jerk can be used to accurately identify the point of first ground contact. This method is also suited to be used, in an automated way, to process large quantities of flight data. A problem with this method is that after main gear touchdown, the jerk signal becomes rather noisy due to the ground surface reaction forces, leading to peaks that can be higher than the original first touchdown peak. To avoid false identification of the touchdown point, a procedure is used to first identify the time of ground spoiler activation and then search for the peak in the jerk signal in the time period of 2.5 seconds before this point. For the available test data, this appeared to provide consistent results, yielding an accuracy of one sample period (0.125 sec).

It is concluded here that the described methodology provides sufficiently accurate results and is usable in an automated data processing scheme.

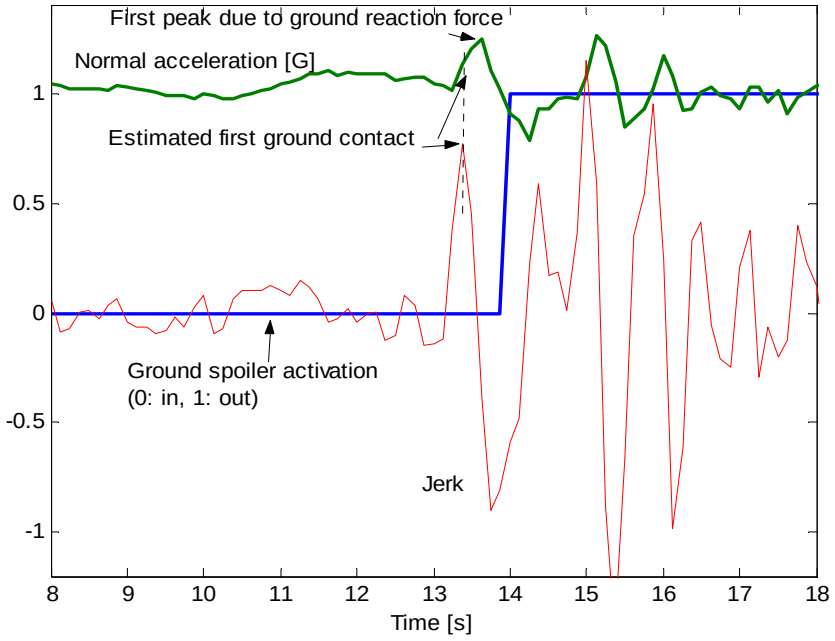

Figure 7. Method of Estimating First Point of Main Gear Touchdown

Examples of the performance of the described algorithm are presented in section 3.7.

3.3.3 Airborne Distance Calculation.

Once the point in time of crossing the threshold and the first main gear ground contact is established, the air distance can be computed by integrating the recorded ground speed of the aircraft over this time period, according to the next equation:

$$D_{airborne} = \int_{T_{THR}}^{T_{TD}} V_{ground} \cdot dt \tag{6}$$

For this integrating process, the ground speed has been used directly as recorded, i.e., it has not been smoothed or filtered. It is assumed that random noise on the ground speed will not affect the calculated airborne distance because the integration process will cancel out random noise. Bias errors on the ground speed could affect the calculated airborne distance. However, bias errors on the ground speed are usually small due to the way the ground speed has been calculated by the airborne Inertial Reference Systems/GPS systems. For this reason, it is expected that direct integration of the measured ground speed over the given time interval from threshold crossing to main gear touchdown provides a good approximation of the airborne distance.

3.4 NOSEWHEEL TOUCHDOWN.

An important parameter in the assessment of the aircraft touchdown dynamics is the time required to lower the nosewheel to the runway surface after main gear touchdown. To identify

the instantaneous moment where the nosewheel hits the ground, it may appear that normal acceleration (or its time derivative) are suited signals. However, in general, the normal acceleration signal is, after main gear touchdown, significantly corrupted by high-frequency noise due to the main gear reaction forces on the runway. Moreover, the reaction force resulting from nosewheel touchdown will be, in general, much lower than that of the main gear. For that reason, it is difficult to identify nosewheel touchdown accurately based on the normal acceleration signal.

An alternative method is to use pitch rate or pitch acceleration. In general, the aircraft's nose will be lowered slowly until the nosewheel hits the pavement. At that point in time, the aircraft's pitch rate will reduce quickly to zero, which is associated with a short positive peak in the pitch acceleration. This peak can easily be identified by an automated process that detects the maximum positive (nose up) pitch acceleration after main gear touchdown. Obviously, this process requires the derivation of pitch rate and pitch acceleration from the available pitch attitude signal. This process was described in section 3.2. In section 3.5, the application of pitch rate and pitch acceleration is further elaborated to demonstrate its application for the identification of the flare initiation point. This is a more challenging application than the identification of the nosewheel touchdown point. Therefore, it suffices here to conclude that nosewheel touchdown can be accurately determined by this method. Examples demonstrating the performance of the identification process will be provided in section 3.7.

3.5 FLARE INITIATION.

To assess the aircraft dynamics during the airborne part of the landing maneuver, it is necessary to identify the point in time when the pilot is initiating the flare maneuver. In general, the flare maneuver is initiated by a discrete elevator pilot command input to raise the nose of the aircraft such that the vertical speed is reduced to an acceptable level at touchdown. In practice, however, the discrete command input is, in many cases, masked by the control activities of the pilot to correct flight path deviations and stabilize the aircraft in response to external disturbances. For this reason, the actual initiation of the flare maneuver is not clearly defined and cannot be directly derived from the pilot's control inputs.

An important characteristic of the flare maneuver is the noticeable increase in pitch attitude and the subsequent reduction of the vertical speed. Based on this characteristic, it is possible to make an estimate of the flare initiation point by identifying the initiation of the pitch increase close the ground and before the actual reduction in vertical speed takes place. The initiation of the pitch increase can be identified by finding the maximum pitch rate within a specific search window. However, the maximum pitch rate will be reached after the flare is initiated, and therefore inherently, this method would lead to some time delay in the identified flare initiation point. A better solution is to use the maximum pitch acceleration. From a flight physics point of view, the pitch acceleration is directly related to the pitch control input and, therefore, appears to be a logical choice for identifying the flare initiation point. The problem is whether the pitch acceleration can be derived with sufficient accuracy from the recorded pitch attitude signal to serve as a proper indicator for the flare initiation. It requires double differentiation of the pitch attitude signal, and therefore, it can be expected that the resulting signal will be severely corrupted by noise. To demonstrate that the derivation and smoothing process, as described in

section 3.2, can be successfully tuned and applied to estimate the double derivative of the pitch angle, the following test case is presented here.

With the nonlinear Fokker 100 simulation program, available at NLR, a schematized flare maneuver has been simulated. In this particular simulation, the aircraft was subject to moderate to severe turbulence, such that the aircraft was continuously disturbed. Furthermore, the simulated pitch attitude signal (the truth signal) was contaminated with measurement noise and subsequently sampled at 4 Hz. This sampled signal is processed by the derivation and smoothing algorithms to estimate the pitch rate and pitch acceleration signals. These signals are subsequently compared with the true pitch rate and pitch acceleration computed by the simulation program. Results are presented in figure 8.

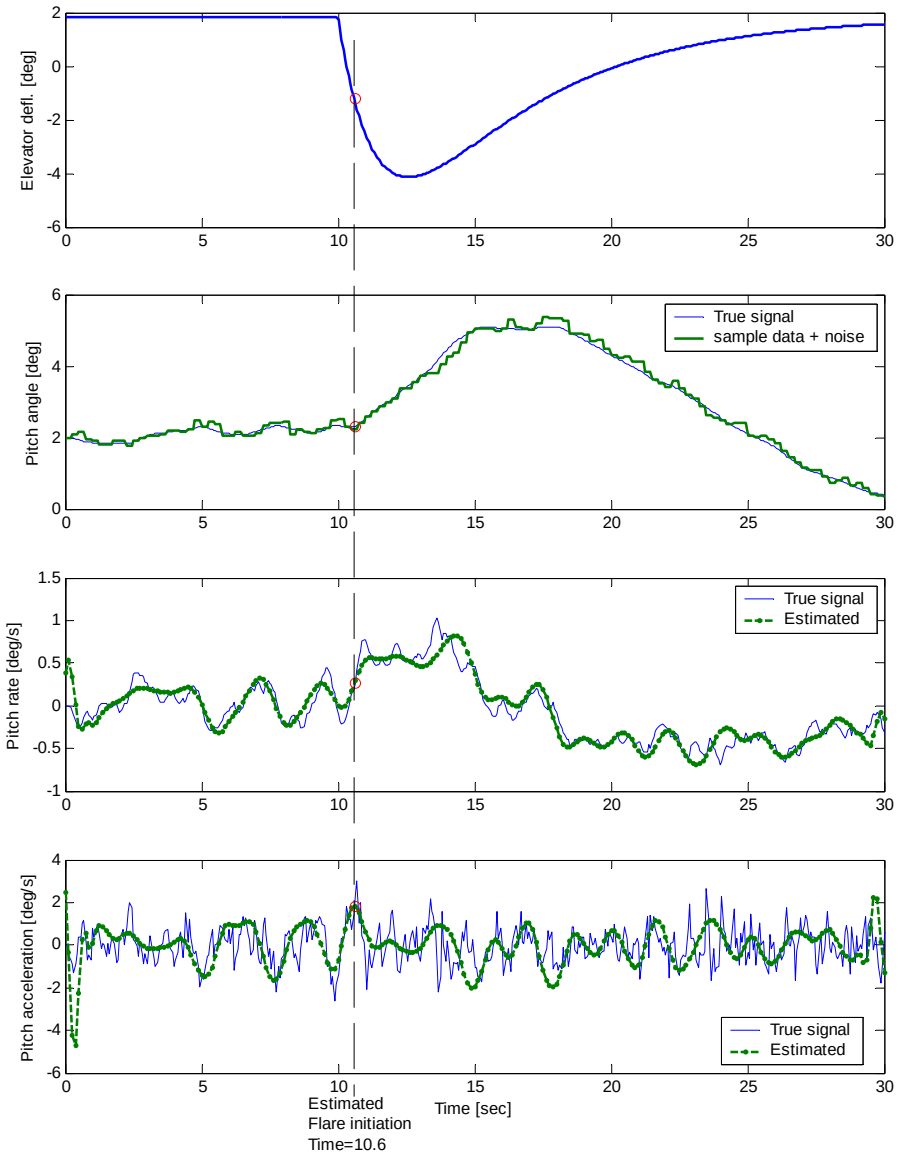

Figure 8. Determination of Flare Initiation Point Based on Estimated Pitch Acceleration

Figure 8 shows that the derived pitch rate signal compares well with the true pitch rate signal. The general dynamics of the aircraft are well matched, despite the fact that some high-frequency disturbances, resulting from the encountered turbulence, are somewhat filtered out. It is also clear that pitch rate could not be used as an indicator to identify the flare initiation point because the maximum pitch rate occurs approximately 5 seconds after the flare initiation.

In the lower graph of figure 8, the derived pitch acceleration is compared with the true pitch acceleration signal. It is clear that the true pitch acceleration is significantly affected by the turbulence. Due to the applied smoothing in the calculation of the derived pitch acceleration signal, much of these disturbances are filtered out. Nevertheless, the basic dynamics of the pitch acceleration is well matched by the derived signal. Apparently, the peak pitch acceleration, associated with the flare initiation, is correctly identified. Based on finding the maximum pitch acceleration in the full-time history, the flare initiation point is found at 0.6 second after the actual flare maneuver was first initiated. Given the fact that the aircraft requires some time to respond to pilot input, this is considered an excellent result. Based on visual inspection of the results, the identified flare initiation point exactly corresponds to the initiation of the pitch increase. Therefore, it is concluded that the method to identify the flare initiation point, as presented here, is in principle feasible for application to the available data set.

To minimize potential false identifications in the actual processing, a search window has been applied. This search window covers the time period from descending through 60-ft radio altitude to the moment that the vertical speed has reduced to 350 ft/min. This has been based on the concept that, in general, the flare will not be initiated above 60-ft altitude (which is above screen height). Also, once the vertical speed was reduced to 350 ft/min, this must have been caused by a deliberate action of the pilot to initiate the flare.

In appendix B, some results are presented to demonstrate the accuracy of the flare initiation determination process in practice. These will be further discussed in section 3.7.

3.6 OTHER PARAMETERS.

The complete list of parameters that are established for each of the recorded flights is presented in section 4. The determination of most of these parameters is straight forward and needs no further explanation. Nevertheless, a few important remarks have to be made here.

A number of the parameters are composed of combined signals. For instance, N1 at flare initiation provides an indication of the engine thrust at that particular point. However, the aircraft types in the data sample all have two engines, and therefore, the N1 is recorded for both the right and left engine. The actual presented parameter is the mean of the left and right engine N1 at that particular point. The same is true for thrust reverser deflection.

One of the established parameters concerns the maximum negative elevator deflection during the flare. This parameter provides an indication of the amount of elevator command that is used during the flare. It should be noted, however, that the sign conventions of the elevator deflection differs between the Boeing and Airbus types. For Boeing, elevator trailing edge up is considered

a positive deflection, whereas for Airbus the reverse definition is used (trailing edge down is positive). The latter is the standard European convention. For this reason, in the determination of this parameter, the sign of the elevator deflection has been reversed as if it were for a Boeing aircraft. In this way, the maximum negative elevator deflection always corresponds to the maximum pitch up command during the flare.

A number of parameters require the determination of when full reverse thrust is applied. In practice, various levels of reverse thrust can occur and it is not clearly defined when full reverse thrust is actually selected. In the present analysis, it has been assumed, based on operational practice, that full reverse thrust has been applied if N1 exceeds 55%.

Furthermore, it should be noted that a number of parameters are related to either CAS or TAS at specific points. As mentioned already in section 2.5, those recorded speeds can have relatively high lower limits (e.g., for the B-737 the lower limit of TAS is 100 kt). For this reason, some of the mentioned parameters have lost their significance, such as the TAS at runway exit.

Finally, it is important to note that the glide slope deviation signal can also be subject to limiting values. For the B-737, the glide slope deviation signal has been limited to ±2.7 dots as long as the aircraft is airborne. In some cases, this affects the determination of the threshold crossing height. Based on a standard sensitivity of 0.36°/dot, the highest threshold crossing height to be calculated is limited at 66.2 ft. For the Airbus-type aircraft such a limitation does not exist.

3.7 EXAMPLES OF DATA PROCESSING PERFORMANCE.

In the previous sections, the processing algorithms that determine the key aircraft landing performance indicators were described. In this section, the effectiveness and validity of these algorithms are demonstrated using a number of illustrative example recordings. These examples concern cases with

- small and large glide slope tracking errors,
- calm wind, high wind, and severe turbulence,
- short and long air distances,
- hard and soft landings,
- high and low descent rates, and
- gradual and aggressive flaring.

Time histories of these 30 examples are presented in appendix B (figures B-1 to B-30). The results of these cases are addressed shortly hereafter.

However, before examining the examples mentioned above, figures 9 and 10 show a random sample of approximately 150 recordings from the entire data set that concerns the landing flare and touchdown of the A320 and B-737, respectively.

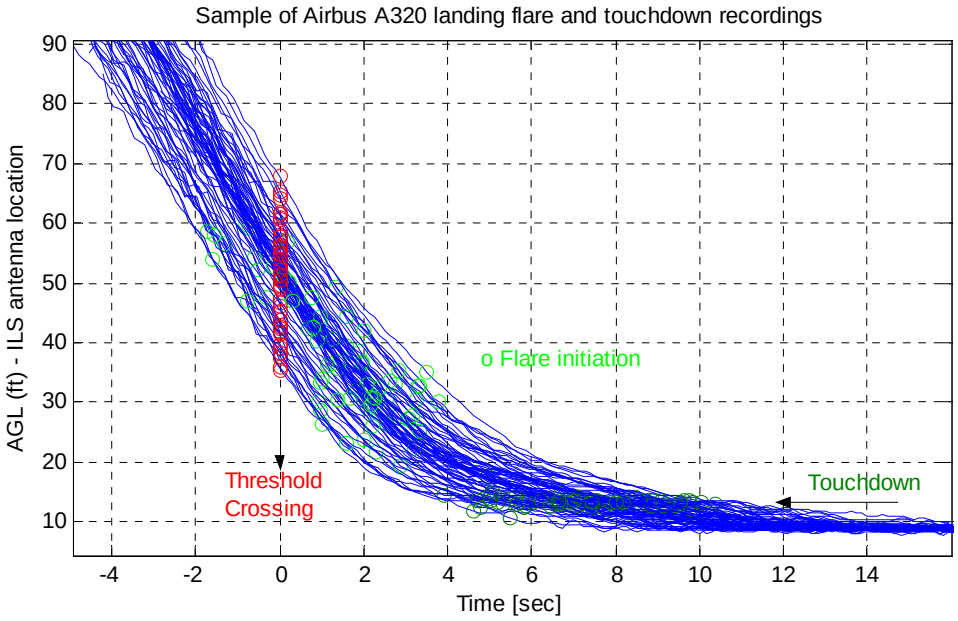

Figure 9. A320 Landing Flare and Touchdown Recordings

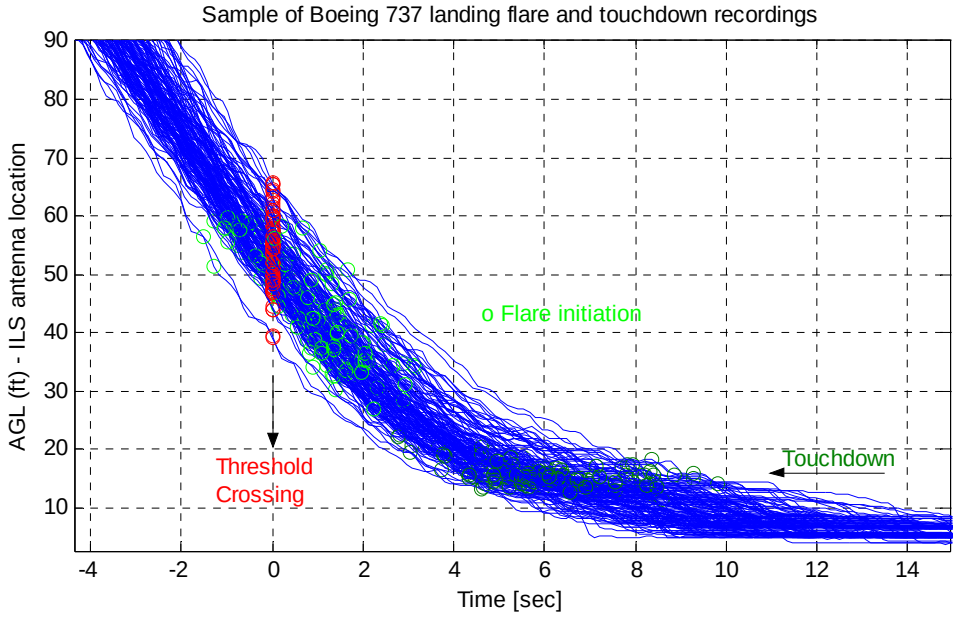

Figure 10. B-737 Landing Flare and Touchdown Recordings

For both aircraft types, these recordings cover approximately 1% of the available data set for each type. The graphs also show the estimated threshold crossing height, flare initiation, and the touchdown point for each of the time histories. The recordings have been synchronized in time such that crossing of the threshold coincides with T = 0 sec.

Figures 9 and 10 show that both aircraft types exhibit similar flare and touchdown behavior. However, some slight differences can be noted. It appears that flare initiation with the A320 occurs, on average, at approximately 30 ft, whereas the B-737 is slightly higher at approximately 40 ft. It is also noticeable that the recorded altitude signal for the B-737 appears to be slightly more affected by noise than that of the A320.

In the following paragraphs, the example cases presented in appendix B will be further discussed. For each example case, a series of selected parameters are presented. Because the examples are intended to demonstrate the validity of the determination of the threshold crossing height, flare initiation and touchdown relevant parameters are selected to be displayed. These are the radio altitude, pitch attitude, CAS, glide slope deviation and normal acceleration, and its time derivative (jerk) and spoiler deflection. Particular cases that were aimed to further demonstrate the identification of the flare initiation point (appendix B), the elevator deflections, derived pitch rate, and pitch acceleration are presented instead of glide slope deviation, normal acceleration, and jerk.

Example cases with small and large glide slope tracking errors are presented in figures B-1 through B-8. Figures B-1 and B-2 show landings of an A320 and B-737, respectively, while they were precisely positioned at the glide slope, and thus passed the threshold at 50 ft. In the case of the A320, a very soft touchdown was made that was, nevertheless, accurately identified. Also, the flare initiation point appears to be correctly identified. In both cases, the time from threshold to touchdown was approximately 6 seconds, resulting in an airborne distance of between 1200 and 1300 ft.

Figures B-6 through B-8 are cases where the aircraft passed high over the threshold (>2 dots deviation high). Figure B-3 shows a particular case with a clear floating tendency during the flare. In this case, the time from threshold to touchdown took approximately 12 seconds, which lead to an airborne distance of slightly over 3000 ft. Figures B-4 and B-5 show rather regular, but quite gradual, flare behavior despite the high threshold crossing.

Figures B-6 through B-8 show cases where the aircraft passed low over the threshold (>2 dots deviation low). In two cases, this leads to flare initiation before the threshold is crossed. The figures also show that the low threshold crossing leads to fairly aggressive and discrete flare maneuvers and that the time from threshold to touchdown is reduced. In the case shown in figure B-8, the time between crossing the threshold and touchdown was 2.5 seconds, resulting in a very short airborne distance and a very firm touchdown (>1.4 g).

Example cases with calm wind, high wind, and severe turbulence are presented in figures B-9 through B-12. The first two cases were selected based on wind reports indicating calm wind (<3 kt) and no turbulence. These two cases represent nominal landing cases undisturbed by external turbulence or wind. Both cases show (A320 and B-737, respectively) a smooth flare maneuver resulting in and a fairly normal touchdown (~1.15 g).

The two subsequent cases were selected based on weather reports indicating high wind (30 kt or more) and severe turbulence (gust values of 45 kt or more). Both cases show that the wind and turbulence significantly affect the aircraft response. During the airborne part, pitch excursions of

±1 degree are shown and normal acceleration varies between 0.8 and 1.2 g. Nevertheless, in both cases, a fairly normal touchdown is being made. In figure B-11, even a very smooth touchdown is realized, such that the acceleration due to the ground reaction can not be discriminated from the normal acceleration variations. Clearly, this is a challenging case for the touchdown determination algorithm. Nevertheless, the algorithm provides a reasonable estimate of the touchdown point, although one could argue that, in this particular case, it is perhaps slightly early.

Example cases with short and long air distances are presented in figures B-13 through B-16. The first two cases were selected based on an extremely short air distance (≈500 ft). Both cases are characterized by a low threshold crossing height, flare initiation before the threshold was crossed, and a hard landing (>1.4 g). These cases are fairly easy cases for the processing algorithms. The subsequent cases have been selected based on an extremely long air distance (>2600 ft).

In both cases, a fairly gradual flare maneuver is shown with a noticeable change in pitch, and a floating tendency can be observed. Nevertheless, a fairly normal touchdown was made (~1.12 g). It is clear that, due to the gradual flare maneuver, no distinct flare initiation point can be distinguished. However, the flare initiation point found by the algorithm appears to be reasonable.

Example cases with hard and soft landings are presented in figures B-17 through B-20. The first two cases have been selected based on high touchdown acceleration (>1.5 g). These cases are characterized by a relatively aggressive flare initiation at rather low altitude. The second case, figure B-18, is particularly interesting. It appears that the aircraft bounces back after a very hard touchdown to become almost airborne again. Apparently, the air-ground switch is deactivated after first touchdown, such that the spoilers are retracted again. Spoilers are deployed again approximately 8 seconds after initial touchdown. In this time frame, the aircraft is clearly unable to decelerate. As shown, the algorithm is able to identify the first touchdown point, despite the bouncing effect, and the subsequent activation and deactivation of the spoilers.

The next two cases have been selected on the basis of very low touchdown acceleration (~1.02 g). These can be expected to be challenging cases for the touchdown determination algorithm. As shown in figures B-19 and B-20, the variation in the acceleration level in the airborne phase is on the same order as the touchdown acceleration itself. Nevertheless, a credible estimate of the touchdown point is made. A particularly interesting case is shown in figure B-20 where a noticeable peak in normal acceleration can be seen after touchdown. This is caused by lowering the nosewheel aggressively towards the ground after very smooth main gear touchdown, which leads to a normal acceleration of approximately 1.15 g due to the nosewheel response. It is considered a favorable feature of the touchdown determination algorithm that the soft main gear touchdown was correctly identified and not confused with the marked peak due to the nosewheel touchdown.

Example cases with high and low descent rates are presented in figures B-21 through B-24.

The first two cases have been selected based on high descent rate at the threshold (>850 ft/min). It is shown that, in both cases, a rather aggressive flare maneuver is initiated (approximately 1.2 g during the flare). This maneuver is apparently sufficient to arrest the sink rate. In both cases, a relatively soft touchdown was made and was correctly identified.

The next two cases were selected based on low descent rate at the threshold (< 350 ft/min). In both cases, a very gradual flare was executed, which led to a very soft touchdown. Despite the gradual flare maneuver and soft touchdown, the flare initiation points and the touchdown points were estimated credibly.

Example cases with gradual and aggressive flaring are presented in figures B-25 through B-30. The first two cases have been selected based on being representative for a normal, average flare. From analyzing the complete data set, it appears that the maximum normal acceleration during the flare is, on average, 1.12 g. Evidently, many cases in the data set are present that satisfy this criterion. Two cases have been selected to represent normal flare behavior. These cases are given in figures B-25 and B-26. In both cases, a marked pitch increase of approximately 3 degrees was observed during the flare, and the flare initiation points were identified correctly.

The next two examples concern cases with aggressive flare behavior. From analysis of the data set, it was found that the highest values of normal acceleration during the flare amount to approximately 1.4 g. Two cases with such high acceleration levels during the flare are presented in figures B-27 and B-28. In both cases, a low threshold crossing occurred and required a fast pitch up, and the flare initiation point was identified accurately.

The final two examples concern cases with very gradual flare behavior. From analysis of the data set, it was found that a gradual flare is characterized by a normal acceleration level of approximately 1.05 g. Two of such cases are presented in figures B-29 and B-30. Evidently, these are challenging cases for the determination of the flare initiation point. Both cases show an almost continuous and gradual increase of pitch attitude during the landing flare maneuver. The derived pitch acceleration signal shows oscillatory behavior, from which it is difficult to identify which peak would coincide with flare initiation. However, due to the fact that a specific search window is being used, several peaks were discarded. The actual peaks identified by the algorithm to coincide with flare initiation can easily be disputed because, in these particular examples, the flare initiation is not sharply defined. However, if the elevator commands given by the pilot are taken into account, it appears that the identified flare initiation points correspond well with the initial flare command of the pilot. Therefore, it is concluded that, even in the case of a smooth and gradual flare, the algorithm was able to provide a credible estimate of the flare initiation point.

To conclude, based on the above examples, the processing algorithms (as discussed in sections 3.2 through 3.5) provide a valid method to determine threshold crossing height, touchdown point, and flare initiation with sufficient accuracy. It can also be concluded that these algorithms are suited for automatic data processing. Results obtained with these methods are further analyzed in the section 4.

4. RESULTS.

4.1 INTRODUCTION.

In this section, the results from the data analysis are presented and discussed. The airborne and ground roll parts of the landing are presented separately. Also, the results for the different aircraft types are discussed individually in most cases. The parameters derived from the data are listed in table 3. The metrological data were either obtained from, or were calculated from, METAR reports. The available runway landing distances were obtained from an airport database, which was matched with each individual landing. The sunset and sunrise times[3] were calculated using the date of the landing and the location of the airport.

Table 3. Parameter in the Landing Database

Airborne Part		Ground Roll Part	
Parameter	Unit	Parameter	Unit
Distance from THR to touchdown	m	Time from touchdown to thrust reverser engagement	s
Height of ILS receiver over THR	m	Distance from touchdown to thrust reverser engagement	m
Height of wheels over THR	m	TAS at T/R deselection	m/s
Height of wheels at touchdown	m	Ground speed at T/R deselection	m/s
Height of flare initiation	m	Time from touchdown to T/R deselection	s
Time from touchdown to nose wheel touchdown	s	Distance from touchdown to T/R deselection	m/s
Bug speed	m/s	Time period of full reverse	s
Autopilot setting	----	TAS at full reverse selection	m/s
Flight path angle over the THR	deg	TAS at idle reverse selection, after full reverse	m/s
CAS over the THR	m/s	Time from touchdown to nose wheel touchdown	m/s
TAS over the THR	m/s	Distance from touchdown to nose wheel touchdown	m
Ground speed over the THR	m/s	TAS at initial manual braking	m/s
Vertical speed over the THR	m/s	Groundspeed at initial manual braking	m/s
Pitch angle over the THR	deg	Distance from touchdown to manual braking	m
N1 over the THR	%	Time from touchdown to spoiler deflection	s
CAS at flare initiation	m/s	Distance from touchdown to spoiler deflection	m
TAS at flare initiation	m/s	TAS at runway exit	m/s
Ground speed at flare initiation	m/s	Groundspeed at runway exit	m/s
Pitch angle at flare initiation	deg	Localizer deviation at THR	m
N1 at flare initiation	%	Autobrake setting	----
Max Nz during flare	g	Distance from touchdown to runway exit	m
Max negative elevator deflection during flare	deg	Miscellaneous Parameters	

[3] Sunrise and sunset refer to the times when the upper edge of the disk of the sun is on the horizon. The times of sunrise and sunset cannot be precisely calculated, because the actual times depend on unpredictable atmospheric conditions that affect the amount of refraction at the horizon. Thus, even under ideal conditions, the times computed for rise or set may be in error by a minute or more. However, for the present project, such small errors are not of great concern.

Table 3. Parameter in the Landing Database (Continued)

Airborne Part		Ground Roll Part	
Parameter	Unit	Parameter	Unit
CAS at touchdown	m/s	Airport code	----
TAS at touchdown	m/s	Date/time	----
Ground Speed at touchdown	m/s	Temperature	C
Pitch angle at touchdown	deg	Mean wind	m/s
N1 at touchdown	%	Gusts	m/s
Nz at touchdown	g	Wind direction	deg
Vertical speed at touchdown	m/s	Visibility	m
Heading at touchdown	deg	Ceiling	m
Bank angle at touchdown	deg	Runway condition	----
Time from flare to touchdown	s	General weather	----
Distance from flare to touchdown	m	Sunrise time	----
Speed loss from flare initiation to touchdown	m/s	Sunset time	----
		Landing distance available	m
		Runway heading	deg
		Flaps	deg
		Weight	kg

THR = Thrust
T/R = Thrust reverser

4.2 CHARACTERISTICS OF MISCELLANEOUS PARAMETERS.

The frequency distribution of the runway conditions prevailing at the time of each landing by the different aircraft types are shown in figure 11. These frequencies are estimations based on the precipitation conditions approximately the time the aircraft landed and are not based on the actual assessment of the runway. The results should, therefore, be treated with some caution. Figures 12 and 13 present the crosswind and head- and tailwind conditions that prevailed at the time of each landing for each aircraft type. The crosswind distributions were more or less symmetrical approximately the zero crosswind condition, suggesting that there was an equal probability of having wind coming from the left- or right-hand side of the aircraft. The distributions of the crosswind conditions are comparable for each aircraft type. However, the A319 data showed a slightly higher probability of wind coming from the right. When the direction of the crosswind was disregarded, the distribution became more similar. The head- and tailwind conditions were practically the same for the aircraft types considered. Figures 12 and 13 clearly show the preference for making headwind landings.

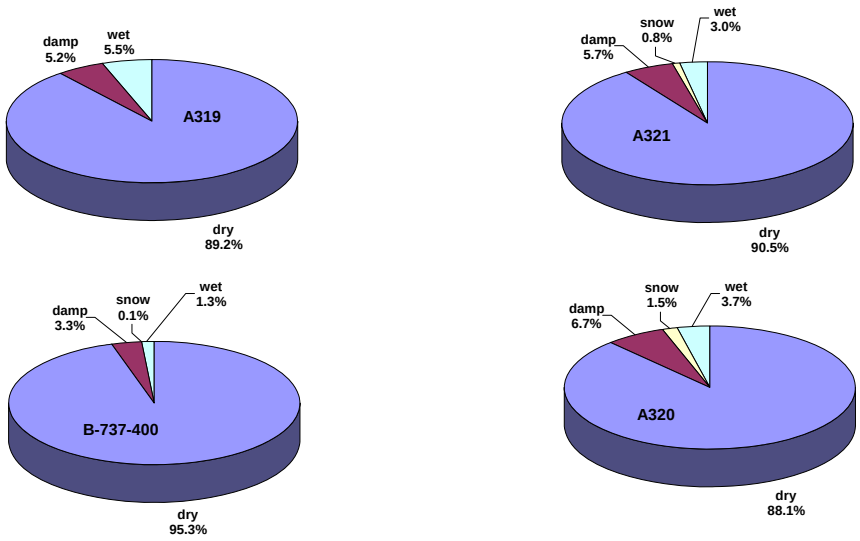

Figure 11. Runway Conditions Encountered

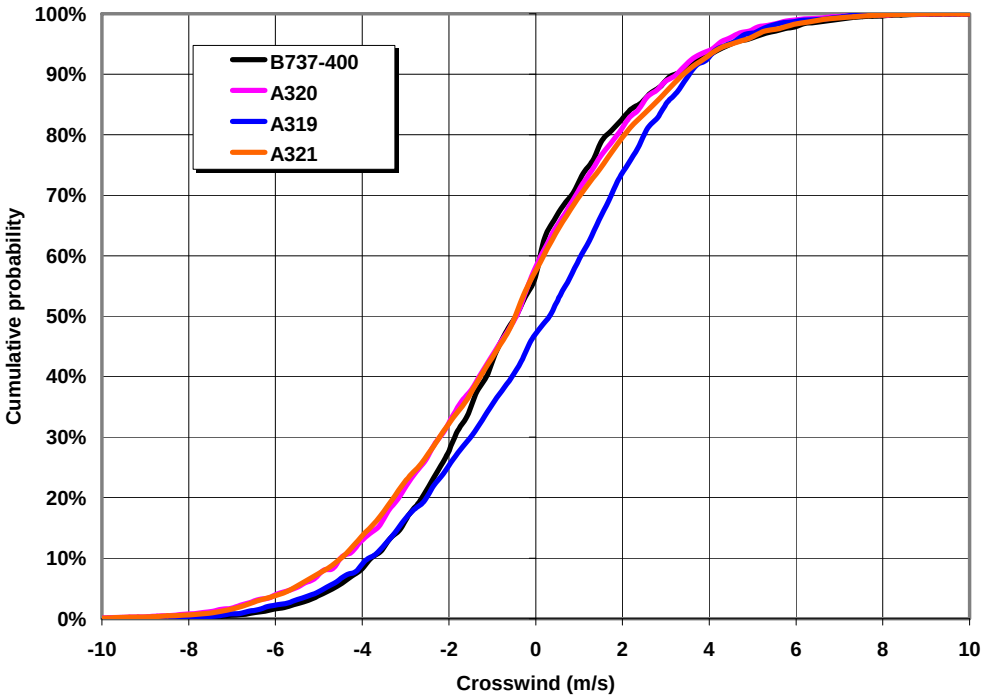

Figure 12. Prevailing Crosswind Conditions

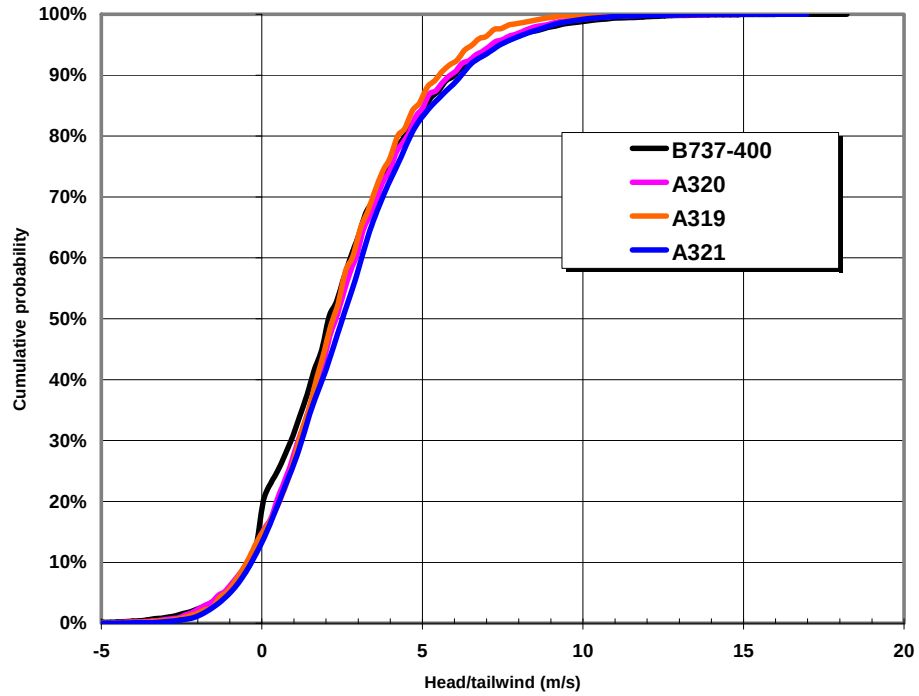

Figure 13. Prevailing Head- and Tailwind Conditions

The ceiling was only recorded for cases where the sky condition was broken or overcast (14% of all landings in the database). The ceiling conditions prevailing at the time of each landing for each aircraft type are shown in figure 14.

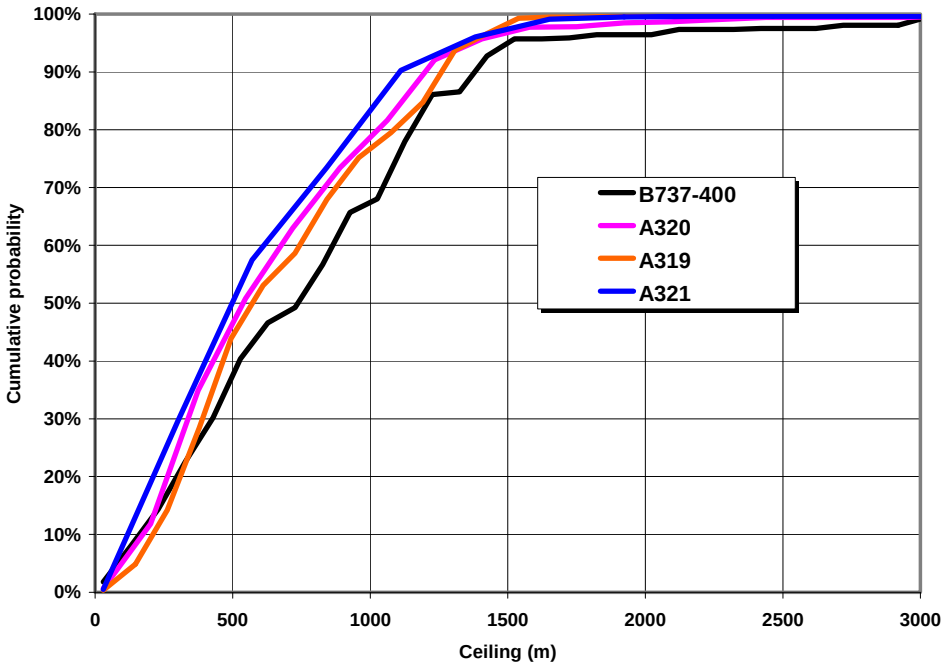

Figure 14. Prevailing Ceiling Conditions

A large number of landings in the database were in visibility conditions of 10 km or more. The visibility values were recorded as >10000 m whenever the visibility exceeded 10 km. In the database, these were changed into a visibility of 10 km. Table 4 shows the percentage of landings in which such visibilities existed. Figure 15 shows the visibility distribution for conditions below 10 km.

Table 4. Visibility Conditions of 10 km or Better

Aircraft Model	Landings with visibility condition 10 km or more
A319	92%
A320	81%
A321	80%
B-737-400	74%

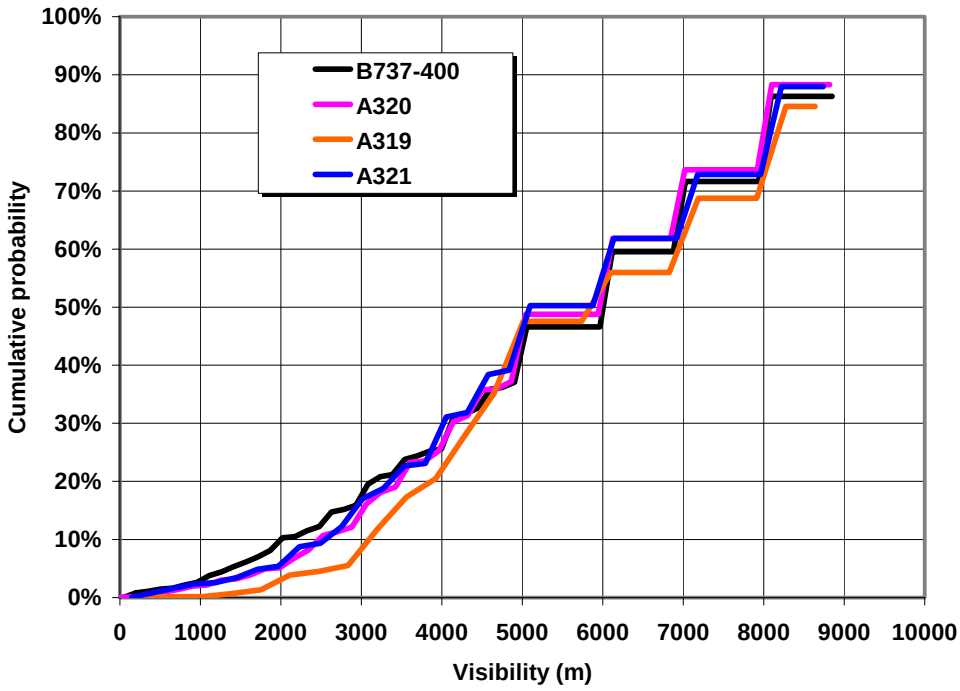

Figure 15. Prevailing Visibility Conditions Below 10 km

4.3 AIRBORNE PART OF THE LANDING.

Table 3 lists the parameters that were recorded in the database, which relate to the airborne part of the landing. Many of these parameters are related to the airborne distance (i.e., the ground distance covered from threshold to touchdown). The distribution of the airborne distance for the different aircraft types is shown in figure 16.

There are a number of parameters recorded in the database that can influence the airborne distance. To find the subsets of independent parameters that best contribute to the airborne distance, a linear best subsets regression analysis is conducted. Best subsets regression is a technique for selecting variables in a multiple linear regression by systematically searching through the different combinations of the independent variables and then selecting the subsets of variables that best contribute to predicting the dependent variable. The regression technique also looks at redundant information in the other independent parameters. This analysis was applied to the data and resulted in a list of parameters that influenced the airborne distance the most (table 5).

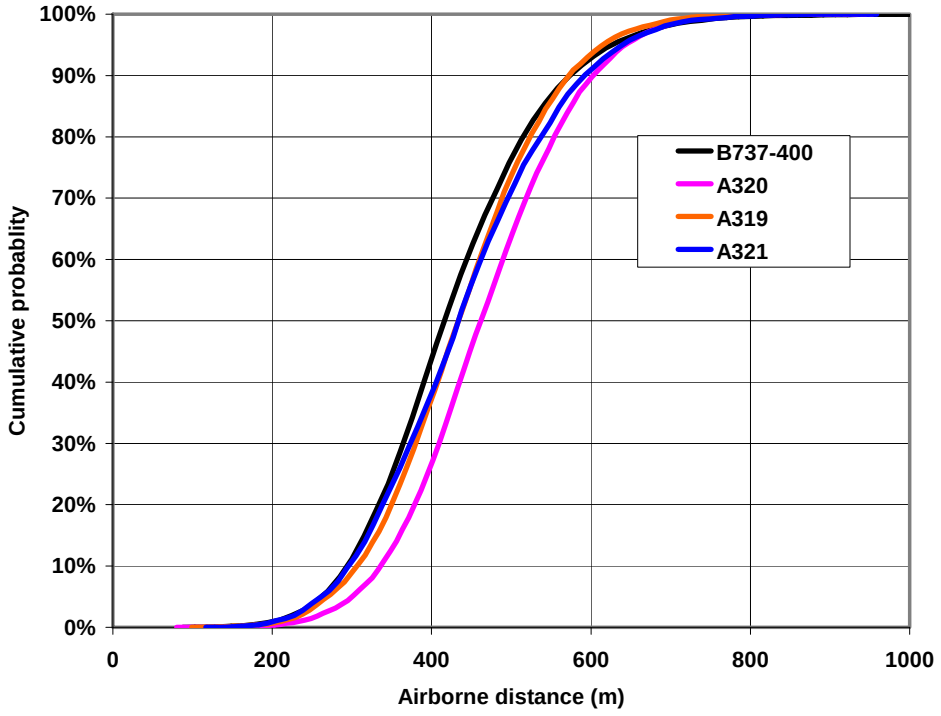

Figure 16. Airborne Distance

Table 5. Parameters That Influence the Airborne Distance

Parameter	Influence*	Correlation**
Height of ILS receiver over threshold	+++	+
Height of flare initiation	+	+
Flight path angle over the threshold	++	+
Ground speed over the threshold	++	+
Max Nz during flare	-	
Max negative elevator deflection during flare	++	-
N1 over the threshold	-	
Ground speed at flare initiation	-	

Table 5. Parameters That Influence the Airborne Distance (Continued)

Parameter	Influence*	Correlation**
CAS at flare initiation	+	+
N1 at flare initiation	-	
Head- and tailwind mean (m/s)	±	-
Difference between actual and reference speed over threshold	++	+
Speed loss from flare initiation to touchdown	+++	+
Difference in rate of descent at threshold and touchdown	+	-

* +++: very strong influence, ++: strong influence, +: minor influence, -: no influence.
** +: positive correlation, -: negative correlation.

The influence of the threshold crossing height appears to have the strongest influence on the airborne distance. The higher the aircraft crosses the threshold, the longer the airborne distance gets. Figure 17 clearly illustrates this relation for each of the four aircraft types. The glide slope deviations for the B-737-400 are limited to 2.7 dots, which explains the cutoff in data shown in the top left chart of figure 17.

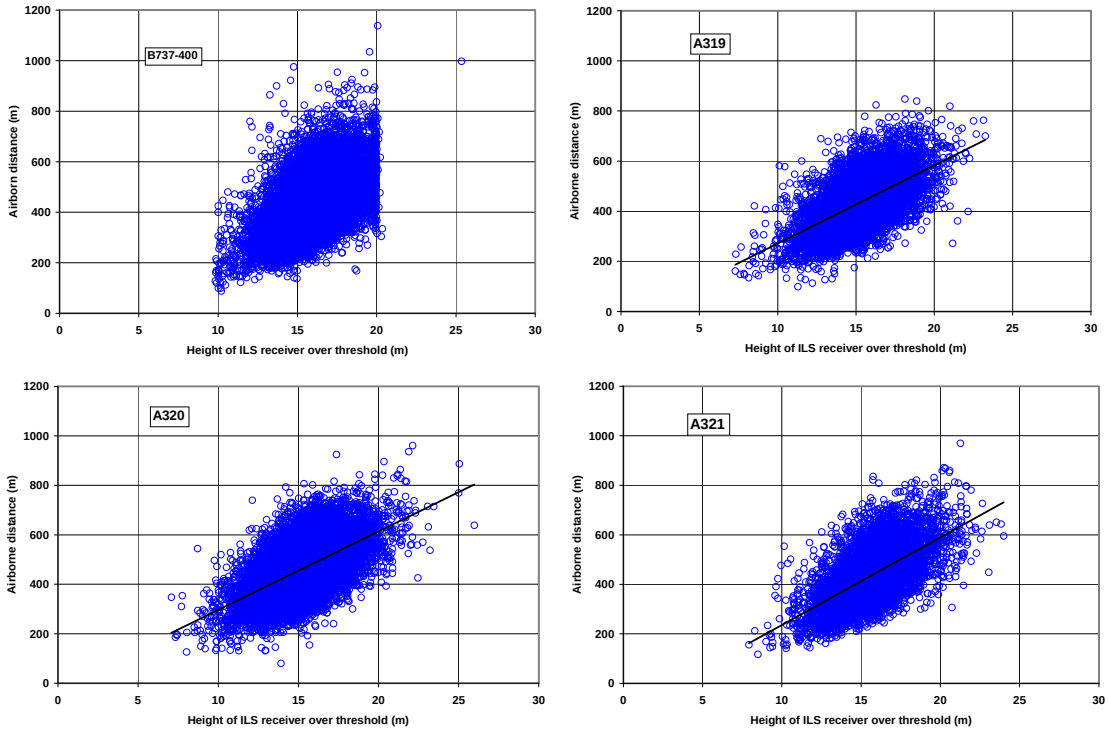

Figure 17. Influence of Threshold Crossing Height on Airborne Distance for the B-737-400

The speed loss from flare initiation to touchdown has a very significant influence on the airborne distance, as illustrated in figure 18. In this figure, the loss in speed is positive, and the airborne distance increases with a higher speed loss. As shown in figure 19, the time from flare initiation

and touchdown increases with a higher speed loss. It takes time, and therefore ground distance, to reduce the speed. Note that it is normal to reduce some speed during the flare. Boeing, for instance, recommends touching down with a speed that is equal to the reference landing approach speed (Vref) plus the gust correction.[4]

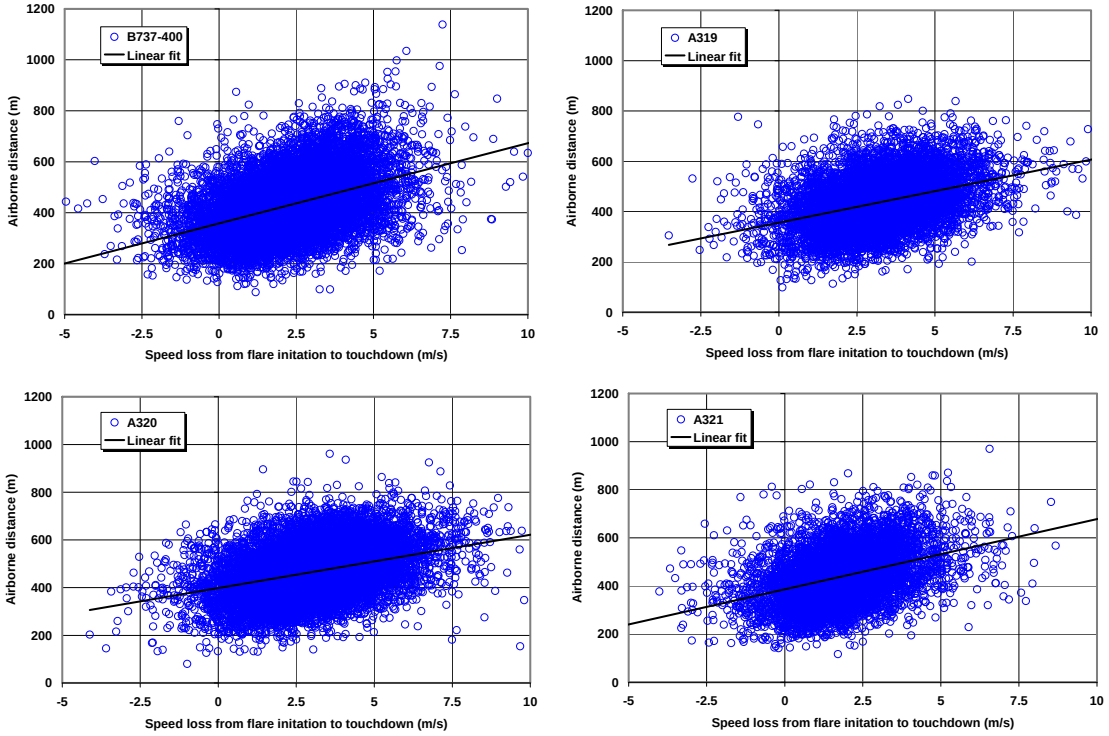

Figure 18. Influence of Speed Loss on Airborne Distance

The difference in the actual speed and the reference speed over the threshold has a strong influence on the airborne distance. This speed difference for the different aircraft types is shown in figure 20. The B-737-400 data shows a higher tendency to be faster than the reference speed at the threshold compared to the Airbus models. The reason for this is unknown. It may be because the standard practice for fly-by-wire aircraft is to fly with the autothrust (A/THR) engaged during a landing, whereas standard practice for a conventionally controlled aircraft with wing-mounted engines is to disengage the A/THR as soon as the autopilot is disengaged. With A/THR engaged, the speed control is more accurate, possibly explaining the results shown in figure 20. In figure 21, the influence of the speed difference at the threshold on the airborne distance is shown for the B-737-400. The linear fit is only shown to illustrate the general correlation between airborne distance and the speed difference at the threshold.

[4] The wind corrections made on Vref are not the same for the Boeing and the Airbus aircraft. Boeing recommends to use an approach speed wind correction of half the steady headwind component plus all the gust increment above the steady wind, whereas Airbus recommends to use one third the total headwind component.

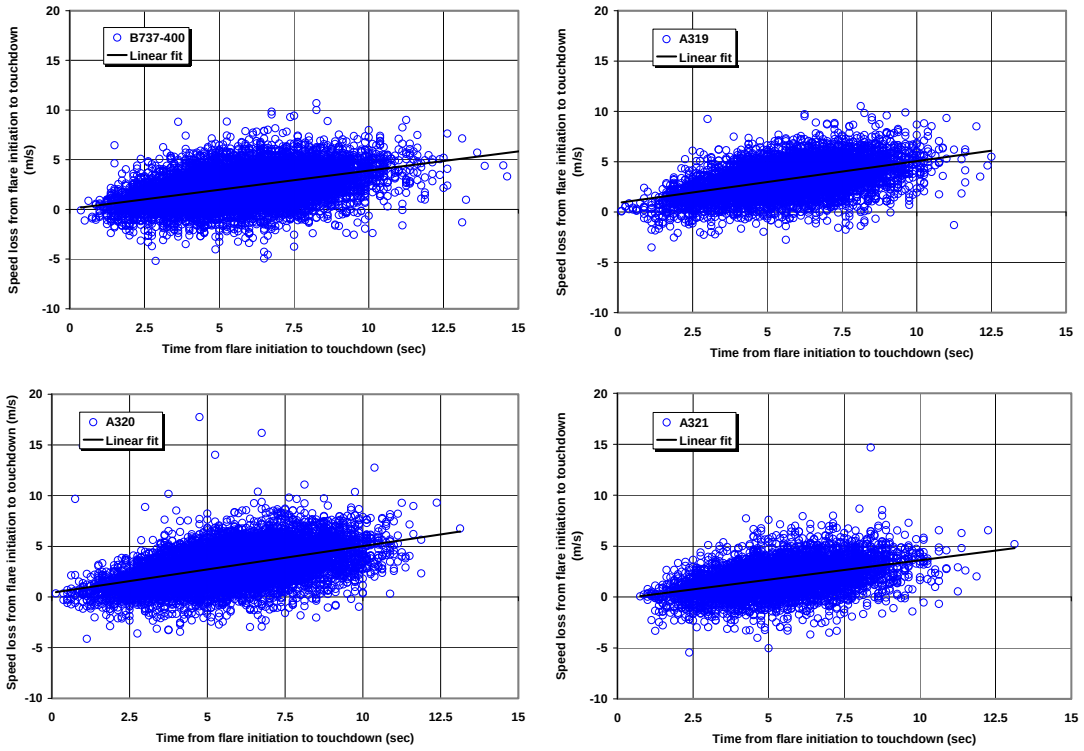

Figure 19. Time From Flare Initiation to Touchdown Versus Speed Loss

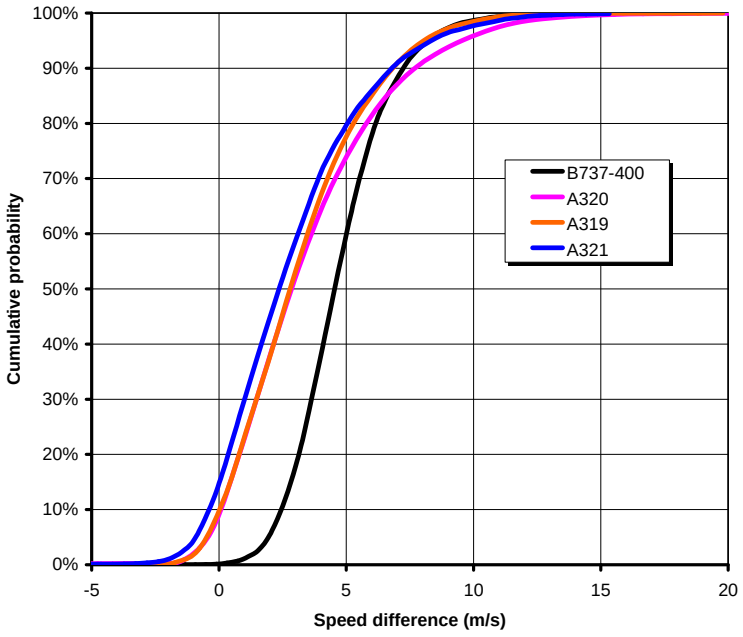

Figure 20. Difference in Actual Speed and Reference Speed at the Threshold

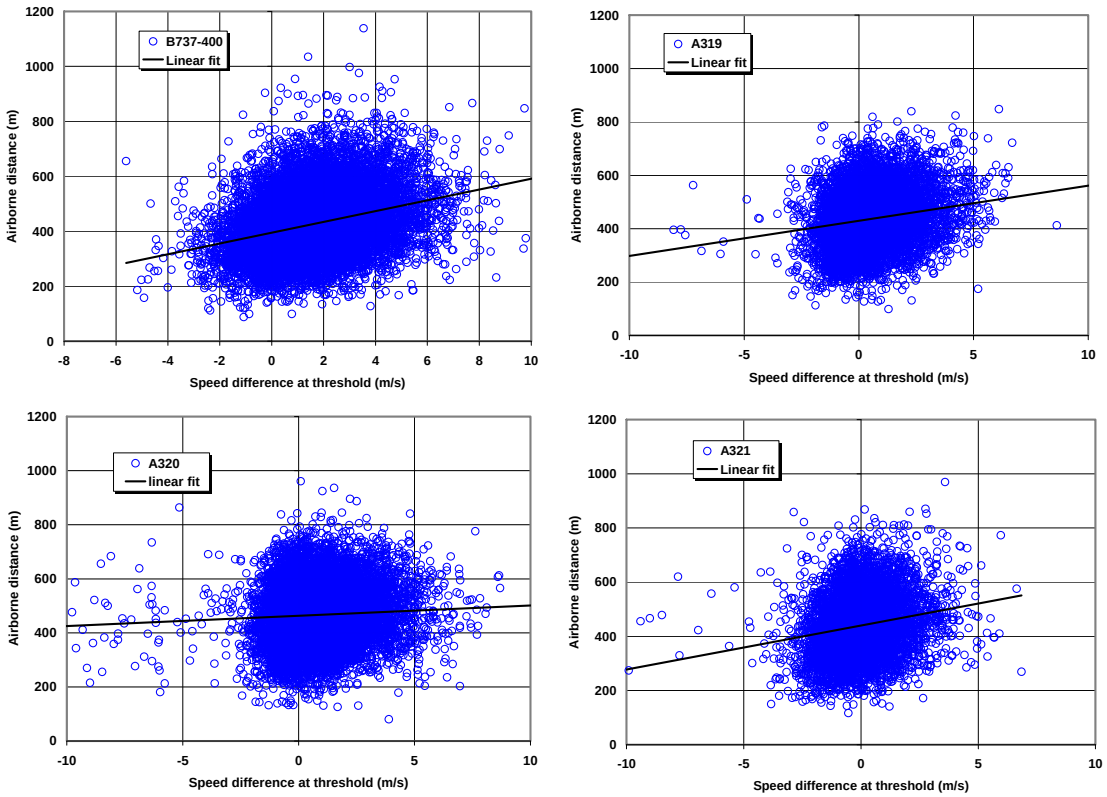

Figure 21. Influence of Speed Difference at Threshold on Airborne Distance for the B-737-400

The best subsets regression analysis showed that head- or tailwind does not have a large influence on the airborne distance. The final approach speeds of the aircraft considered in this study are corrected for wind conditions as part of the standard operating procedures of those aircraft. In case of headwind conditions, the final approach speed is increased and for tailwind conditions no corrections are made. However, when reaching the threshold, these wind corrections may be bled off according to recommended practices given by Boeing and Airbus. The results from figure 20 suggest that most landings are conducted with some additional speed above the reference speed. It seems that not all the speed additives are bled off. The data showed that this is particularly true during headwind landings. This could mean that the reduction in ground speed due to headwind is counteracted by the tendency to overspeed. As a result, there is not a large effect on airborne distance. Tailwind could increase the airborne distance; however, tailwind conditions only existed in 15% of all landings (see figure 13). The runways used for landing are normally selected with a preference for headwind conditions (see figure 13). Furthermore, for these cases, the tailwind itself was small in magnitude and, as a result, its effect on the airborne distance was also small. This explains the fact that head- or tailwind conditions have a small influence on the airborne distance. Figure 22 gives an example of the influence of head- and tailwind on the airborne distance of an A320.

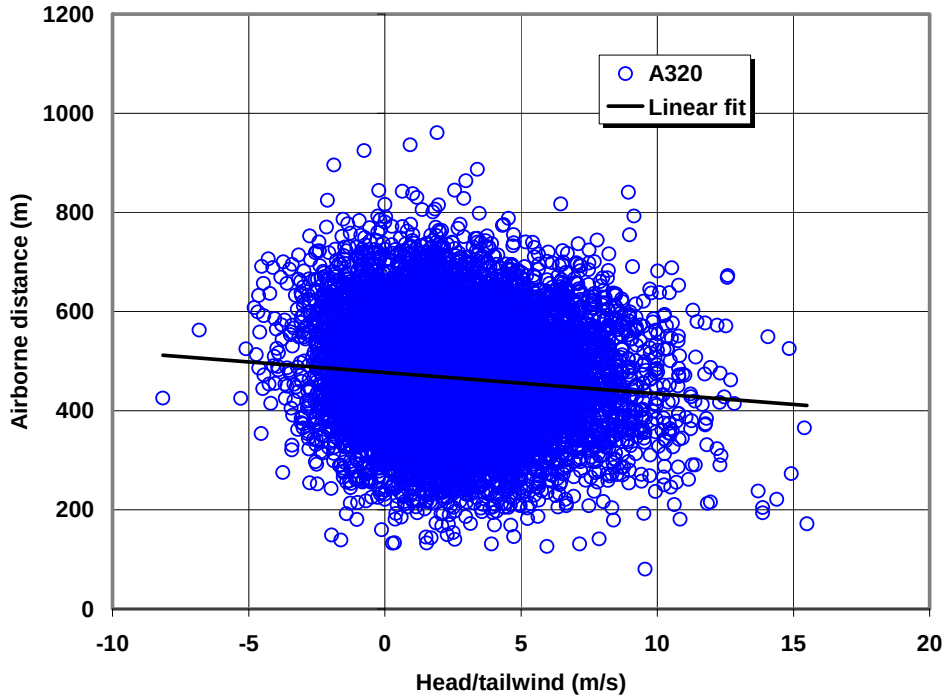

Figure 22. Influence of Head- and Tailwind on Airborne Distance

A limited number of landings were conducted with the autopilot and A/THR engaged until touchdown (511 in total). This number of autolands conducted by each of the four aircraft types is too small for meaningful statistical analysis. Therefore, only the results of all aircraft types together are considered. Figure 23 shows the comparison of airborne distance of autolands and manual landings for all aircraft types. As can be expected, the autolands have a lower average airborne distance than manual landings and also show less deviation from the average airborne performance. These findings are logical because autolands are not influenced by any human performance during the airborne maneuver. As a result, a more consistent and shorter airborne distance is realized during an autoland.

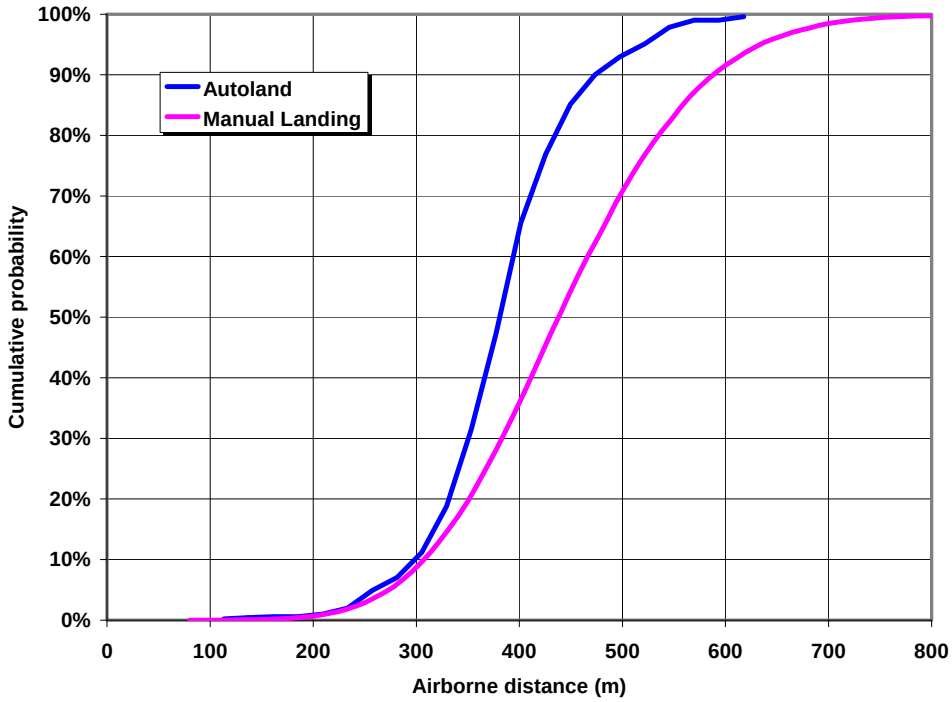

Figure 23. Comparison of the Airborne Distance Autolands and Manual Landings (All Aircraft Types)

The fly-by-wire aircraft in this study use a special flare law. When reaching 50-ft RA, the autotrim ceases and the pitch law is modified to a flare law. Through 30-ft RA, the system begins to reduce the pitch attitude at a predetermined rate. Consequently, as the speed reduces, the pilot will have to move the stick rearwards to maintain a constant path. The flare technique is, thus, very conventional to the pilot flying. The aircraft with the conventional flight control system in this present study does not have a flare law like the fly-by-wire aircraft. The flight crew training guide for the B-737-400 advises pilots to initiate the flare when the main gear is approximately 15 feet above the runway by increasing pitch attitude approximately 2° to 3°. Figure 24 shows the flare initiation heights as derived from the flight data for the four different aircraft models. These heights are relative to the ILS receiver position. Since the pitch angle is small at flare initiation, the height relative from the main gear wheels (RA) is approximately 2.5 and 3 meters lower than these heights for the B-737 and the A319, A320, and A321 aircraft. The data show that the A319, A320, and A321 aircraft have a lower flare initiation height than the B-737-400. Some care must be taken when analyzing the results shown in figure 24 because it is not always easy to derive the flare initiation height from the data. Sometimes there is no clear flare initiation due to the way the pilot handles the aircraft.

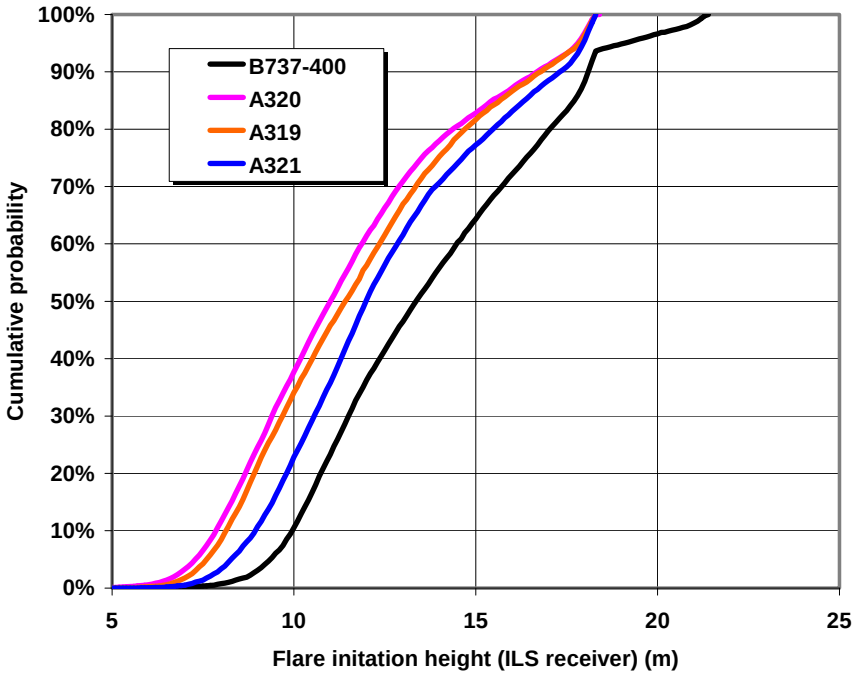

Figure 24. Flare Initiation Height

Approximately 25% of all landings in the data sample were conducted between sunset and sunrise (nighttime conditions). The influence of such conditions could not be addressed by the linear best subsets regression analysis. The airborne distance data for landings conducted between sunrise and sunset (daytime conditions) were compared to landings conducted between sunset and sunrise (nighttime conditions). The results are shown in figure 25 for all aircraft models considered in this study. From this figure, it appears that lighting conditions do not have an affect on airborne distance.

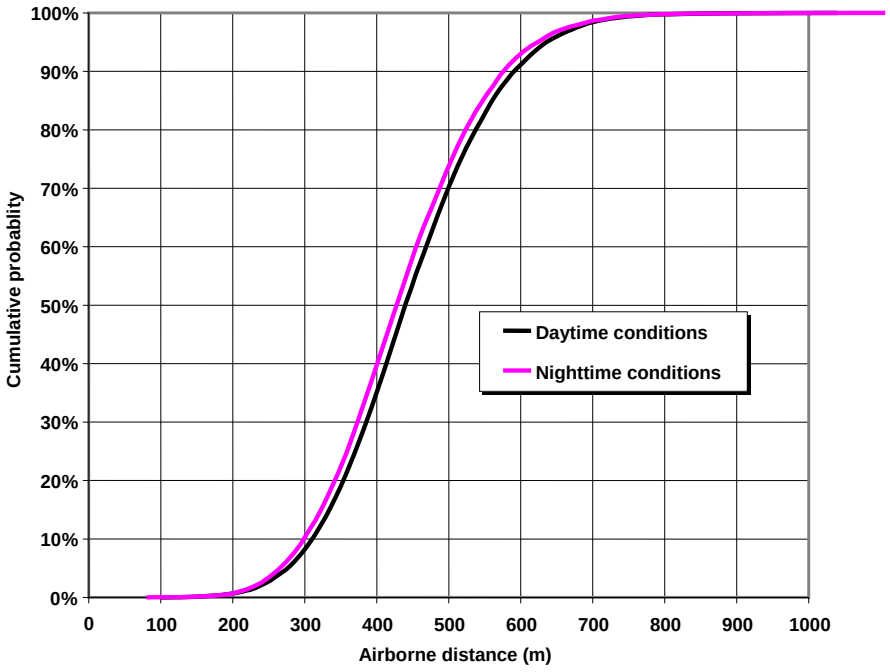

Figure 25. Influence Light Conditions on Airborne Distance

4.4 GROUND ROLL PART OF THE LANDING.

There are a number of parameters recorded in the database that can influence the ground roll distance. Unlike for the airborne distance, it was not possible to conduct a linear best subsets regression analysis to find the subsets of independent parameters that best contribute to the ground roll distance[5]. However, based on the theoretical background on aircraft landing performance and expert judgment, it was possible to identify those parameters that influence the ground roll distance. The following factors are important: thrust reverser use, runway conditions, autobrake use, time to lower the nose after touchdown, available runway length, speed at touchdown, and use of high-speed exits. Some factors are related to each other. For instance, the autobrake setting can be influenced by runway condition, available runway length, and the exit the pilot wants to take. If the runway is long and the pilots want to take the last available exit, the autobrake setting is normally set to a low value. Further, in this same example, the pilot might elect to overrule the autobrake system and continue using manual braking. If the runway is short or the pilot wants to take a high-speed exit, the autobrake setting is most likely high regardless of the runway condition. There are many more combinations of these and other factors possible. This makes the analysis of the ground roll somewhat difficult. Nevertheless, a number of results are discussed next.

The frequency distributions of the overall ground roll distance from touchdown to leaving the runway at the exit for the four aircraft are shown in figure 26. The ground roll distance for Airbus aircraft change, as can be expected, according to their increasing average landing mass

[5] The autobrake setting has a significant impact on the ground roll distance. However, this parameter cannot be taken into the linear best subset regression analysis.

(54, 58, and 66 metric tons for the A319, A320, and A321 respectively). The B-737-400 shows a higher ground roll distance than the Airbus aircraft, which cannot be explained from the average landing mass (48 metric tons). The difference is most likely because the B-737-400 in the data sample frequently operated at an airport that had a high-speed exit at approximately 1350 m from the threshold. Analysis of the landing data for the B-737-400 at this airport showed that it often used this high-speed exit.

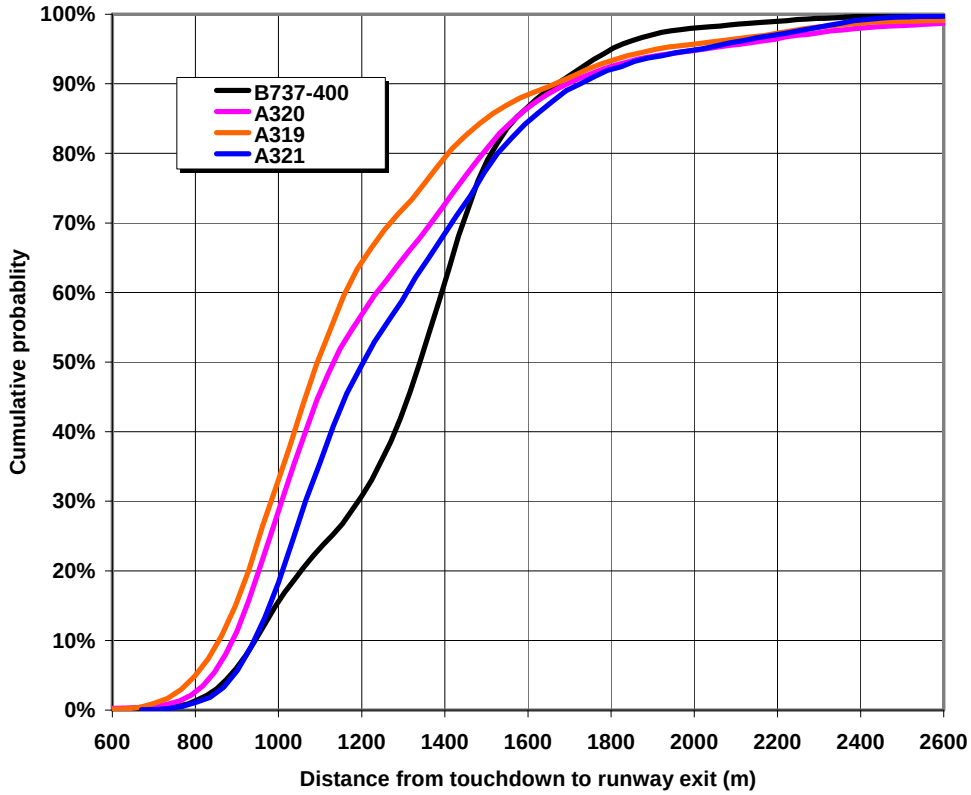

Figure 26. Frequency Distribution of Ground Roll Distance

The available landing distance of the runway that the aircraft lands on can also influence the ground roll distance. In figure 27, the available landing distance is shown as a function of the actual ground roll distance. This figure clearly shows that as the available distance to land, the aircraft increases the scatter in actual ground roll distance increases too. Long runways often have more (high speed) exits available than short runways. The aircraft considered in the present study can use most of these exists. Typically, depending on air traffic control instructions or the location of the gate, the pilots decide to take a particular exit. This is one reason why the scatter in ground roll distance increases as the available landing distance increases.

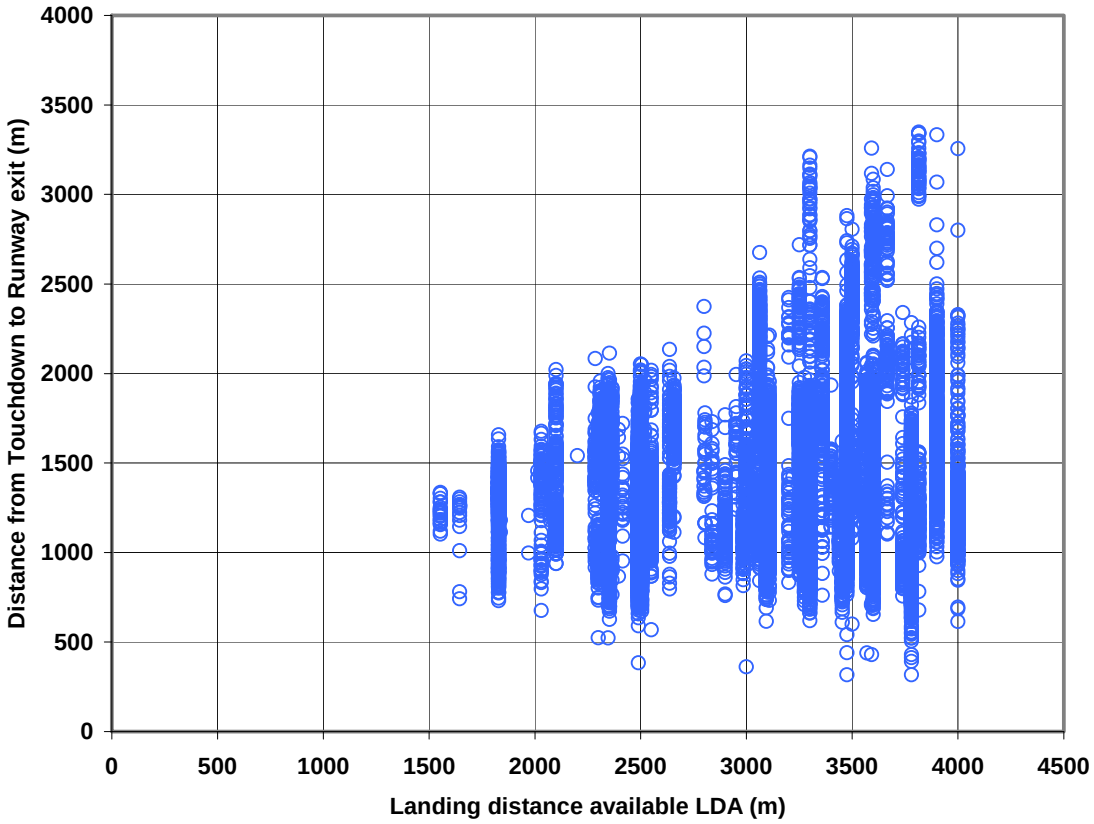

Figure 27. Available Landing Distance Versus Ground Roll Distance

After touchdown of the main wheels, the nose should be lowered without delay to maximize the load on the tires. Some fighter jet pilots tend to keep the nose up as long as possible to increase aerodynamic drag and shorten the required runway length. This technique is called aerodynamic braking and is an acceptable technique on some fighter jets. However, it is not a recommended technique for commercial transport aircraft. The stopping forces associated with this technique are only a fraction of those forces achieved when the aircraft is braked with the nose down. The time from touchdown to nose down for the four aircraft is shown in figure 28. The data show a strong variation in rotation duration. The ground distance covered in the time from touchdown to nose down increases proportionally to the rotation time, as illustrated in figure 29.

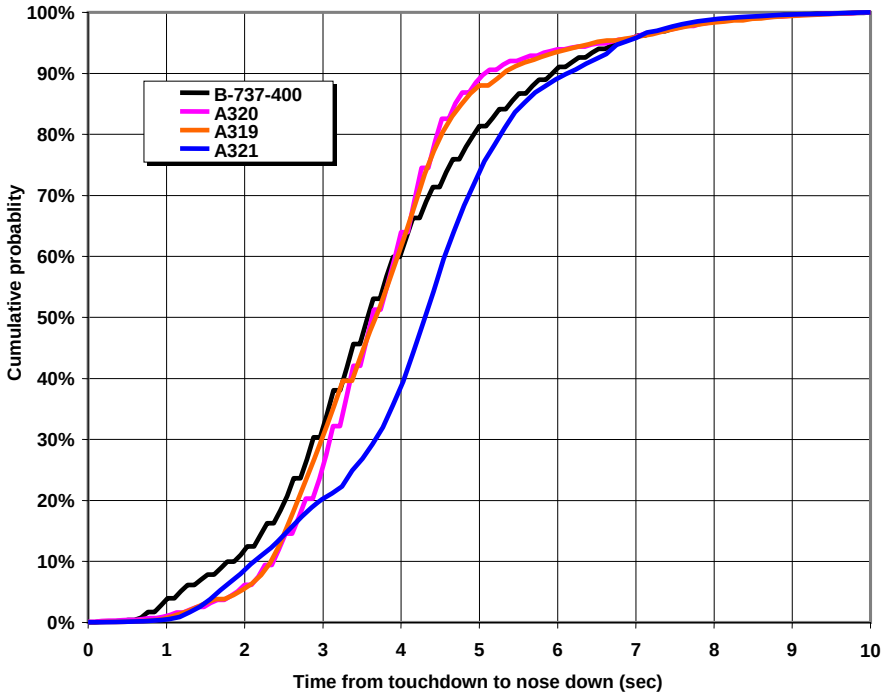

Figure 28. Time From Touchdown to Nose Down

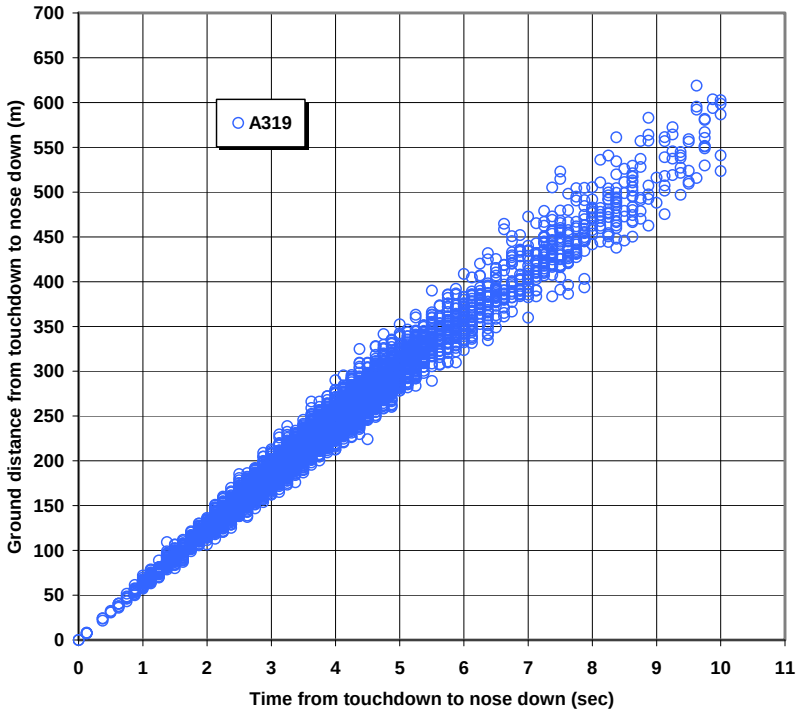

Figure 29. Ground Distance During Nose-Down Rotation as Function of Time

The use of autobrakes can have a significant impact on ground roll distance. Autobrakes decelerate the aircraft with a fixed predefined deceleration. In general, they produce a more consistent deceleration than manual braking by the pilot. Figure 30 shows the effect of autobrake selection on the ground roll distance of the four aircraft analyzed. Clearly, those landings in which no autobrakes were selected show a significantly longer ground distance than when the autobrake was selected. These results do not consider the actual autobrake setting used nor do they reflect situations where maximum manual braking effort is needed. Figure 31 gives an example of the influence of the actual autobrake setting on the ground roll distance for the A320 and the B-737-400. It is clearly shown that the average ground roll distance reduces rapidly from the no autobrake setting to the medium level[6] for the A320 and from no autobrakes setting to setting 3 for the B-737-400[7].

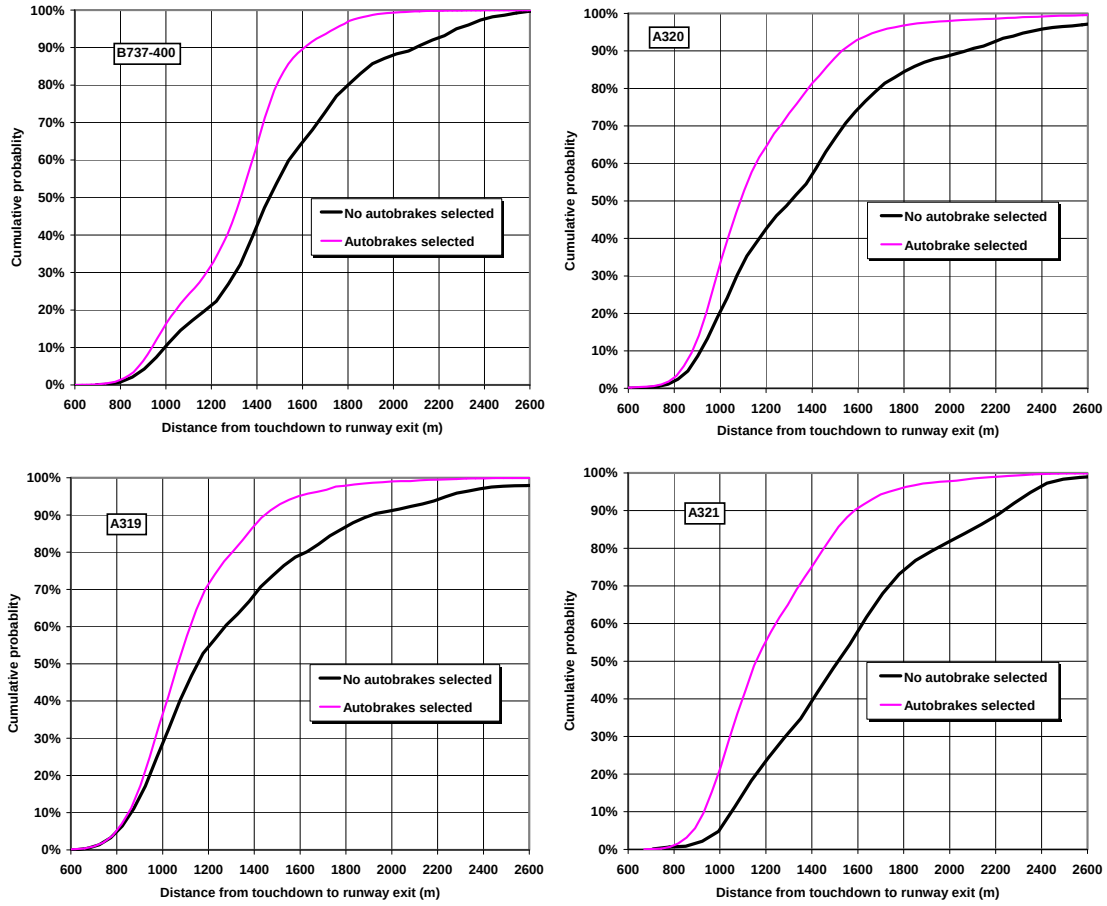

Figure 30. Influence of Autobrake Use on Ground Roll Distance

6 The Airbus aircraft have four autobrake settings: no autobrakes, low, medium, and high. Normally, medium is the highest autobrake setting used. The data sample contains only 148 landings with autobrake setting high.

7 The B-737-400 has five settings for the autobrake available for landing: no autobrakes, 1, 2, 3, and max. The maximum setting is not normally used. The data sample contains only three landings with autobrake setting max.

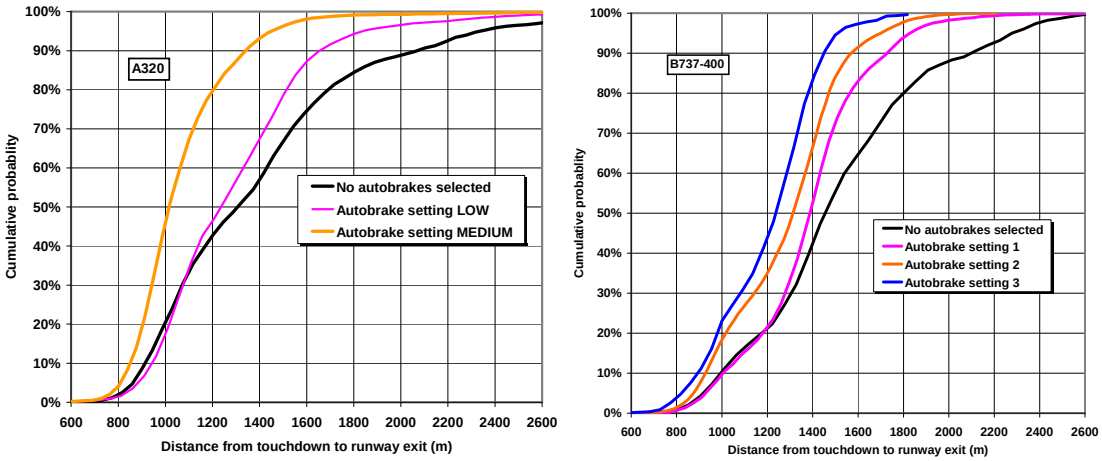

Figure 31. Influence of Autobrake Setting on the Ground Roll Distance of the A320 and B-737-400

Runway condition affects the braking friction between the tires and the runway. Runways covered with water or snow generate lower frictional forces than dry runways. This could result in longer ground distances to stop the aircraft. However, figure 32 shows that, for the data collected for this study, the runway condition had no influence on the ground roll distance. This is partly the result of higher autobrake settings being selected by the pilots that landed on damp, wet, and snow-covered runways. High autobrake settings were used in 35% of the landings on damp, wet, and snow-covered runways compared to the 21% on dry runways.

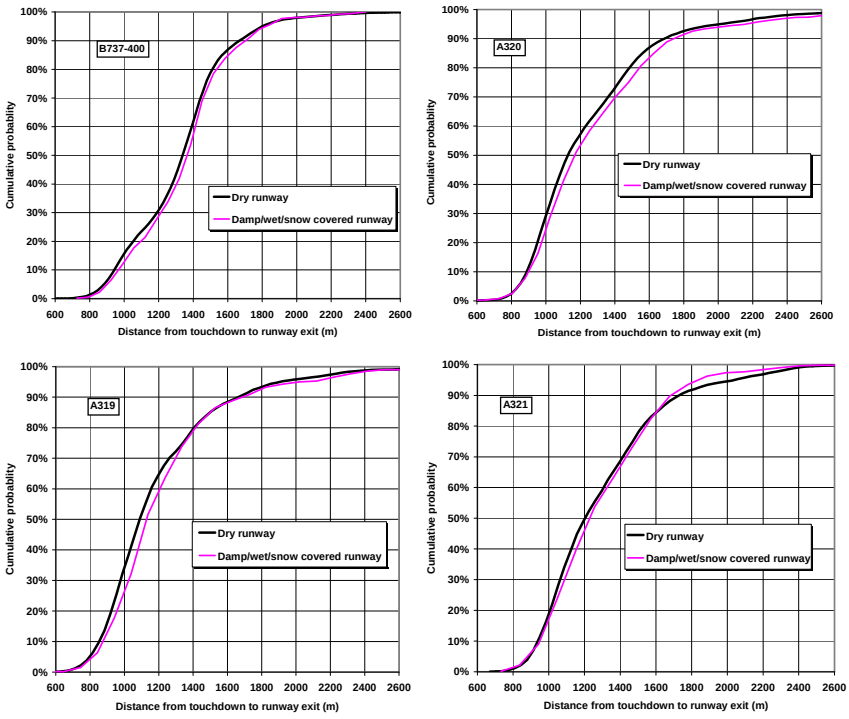

Figure 32. Influence of Runway Condition on Ground Roll Distance

All four aircraft models have thrust reversers installed. Thrust reversers are an effective means for stopping an aircraft on the ground. Thrust reverser efficiency is proportional to the square of the speed. It is therefore recommended to use reverse thrust at high speeds. This means that maximum reverse thrust should be selected immediately after touchdown. This also applies to the four aircraft models considered in this study. The standard operational procedure is to select reverse immediately after touchdown of the main gear. Figure 33 shows the distribution of the time from touchdown to thrust reverser engagement for the four aircraft. All four aircraft show similar pilot performance in selecting the thrust reversers. Figure 34 shows the frequency distribution of the thrust reverser use. The data show a large variation in the time that reverse thrust is used.

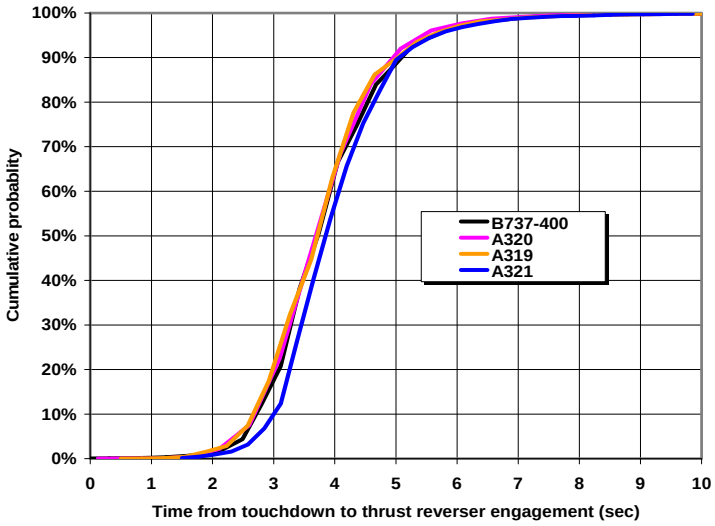

Figure 33. Time From Touchdown to Thrust Reverser Engagement

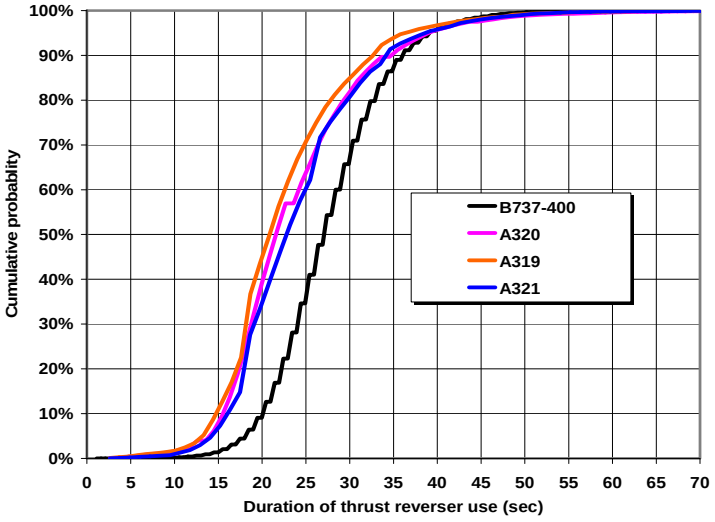

Figure 34. Duration of Thrust Reverser Use

For the A319, A320, and A321, it is recommended to use maximum reverse thrust down to an airspeed of 70 kt (36 m/s), whereas for the B-737-400, an airspeed of 60 kt (31 m/s) is recommended. Figure 35 shows the frequency distribution of the airspeed at which idle reverse is selected for the Airbus aircraft. In a large number of landings, the reverse thrust is used down nearly to the recommended speed.

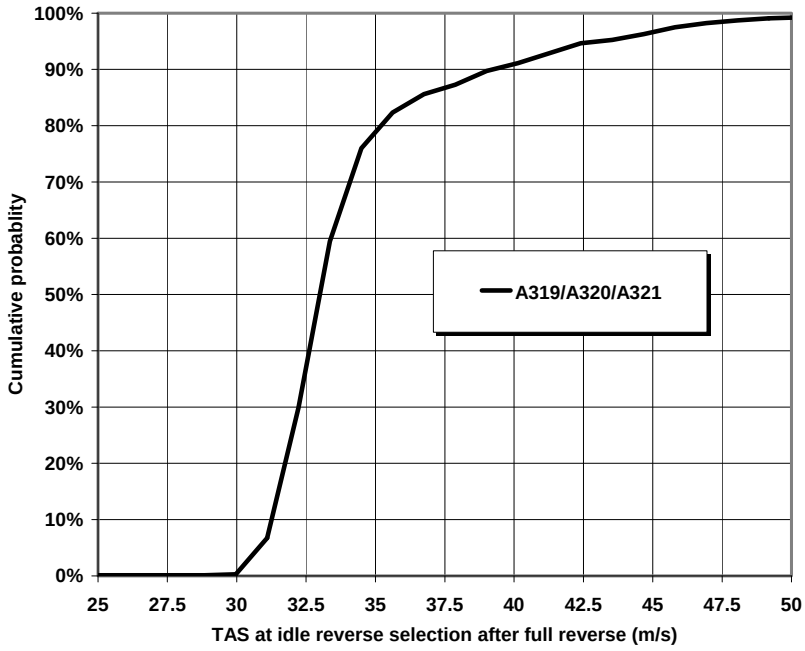

Figure 35. Airspeed at Idle Reverse Selection for the A319, A320, and A321 Aircraft

Although thrust reversers are an important means for stopping an aircraft, the ground roll data analyzed in this study did not show a clear correlation between thrust reverser use and ground roll distance, as shown in figure 36. Clearly, more variables are involved in stopping distance than thrust reverser use.

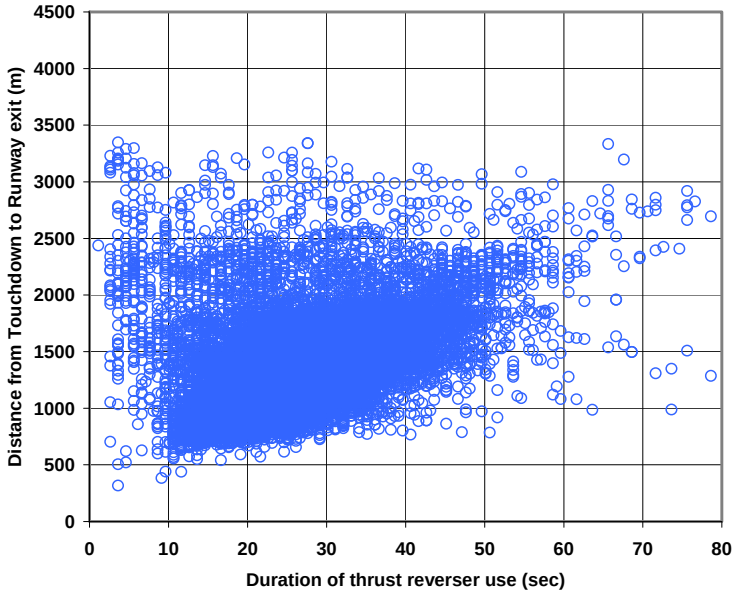

Figure 36. Influence of Thrust Reverser Use on Ground Roll Distance

5. BRIEF DISCUSSION OF THE RESULTS.

5.1 DATA PROCESSING.

The flight data used in the present project were obtained from quick access recordings. These data are retrieved regularly by the airlines for their flight data monitoring analysis. A disadvantage of these recordings is that some parameters are recorded at a low sampling rate. Time-critical recordings, such as touchdown point, can, therefore, not always be obtained directly from the raw data. As part of the present study, algorithms were developed (either based on existing material or newly developed) to overcome some problems of the low sampling rate. Also, data processing algorithms were developed for events during the landings for which no direct recorded parameters were available (e.g., the flare initiation point). The developed data processing algorithms were validated as much as possible. This showed that the algorithms gave credible results.

5.2 RESULTS.

The results presented in this report show that there a large number of variables that influence the overall landing field performance. The results also show that the variation of those variables can be large and that they can be related to each other. The results gave insight into the operational variation of a number of issues such as: autobrake selection, the use of thrust reverse, floating behavior. The following is a summary of the important findings.

- The airborne distance is strongly influenced by the threshold crossing height and the speed loss from flare initiation to touchdown.

- The airborne distance during autolands is, on average, shorter and shows a smaller variation than during manual landings.

- The flare initiation height is lower for the fly-by-wire aircraft than for the non-fly-by-wire aircraft examined.

- Lighting conditions do not affect the airborne distance.

- The ground roll distance is strongly affected by the available landing distance.

- Autobrake setting has a significant influence on the ground roll distance.

- Runway condition did not have a measurable influence on ground roll distance. In general, the reduced braking action on a slippery runway was counteracted by the use of higher autobrake settings. This explains why there appears to be no measurable affect.

Regarding LAHSO, it can be concluded that not all the data analyzed in this report are relevant. The available runway length has a strong influence on the overall behavior of the pilots during landing (e.g., figure 27). It seems, therefore, evident that for the relevance for LAHSO, only landings on the shorter runways should be considered for study. This requires further analysis of the data.

6. CONCLUSIONS.

The following conclusions were made based on the results of the present study.

- Data from quick-access recorders can be used to analyze aircraft performance. During this study, valuable insight and knowledge was gained on using quick access recorded data for aircraft landing field performance analysis.

- Aircraft landing field performance is influenced by many variables. Some variables were found to have a more dominating influence than others. Variables that were found to have a strong influence are height above the threshold, speed loss form flare initiation to touchdown, and the available runway length for landing. However, there is not one single factor that dominates the landing field performance.

- Not all the results presented in this study can be used for the analysis of Land and Hold Short Operations (LAHSO). It follows from the results that the ground roll performance is strongly influenced by the available runway length for landing. Therefore, for LAHSO study purposes, only landings on shorter runways should be considered.

7. RECOMMENDATIONS.

The following recommendations were made.

- It is recommended to collect and analyze flight data during the landing of other type of aircraft, such as small turboprops.

- It is recommended to further analyze the already collected flight data. In particular, operations on short runways should be addressed because they are relevant for use in a LAHSO study. Furthermore, the collected data should be used for other more detailed analyses on issues like the dynamics of the flare, use of manual brakes, etc.

8. REFERENCES.

1. Title 14 Code of Federal Regulations Part 25.125, "Requirements for Landing in Federal Aviation Regulations."

2. Advisory Circular 25-7A, "Flight Test Guide for Certification of Transport Category Airplane."

APPENDIX A—EXAMPLE TIME HISTORIES

Figures A-1 through A-8 show example time histories for normal operational flights.

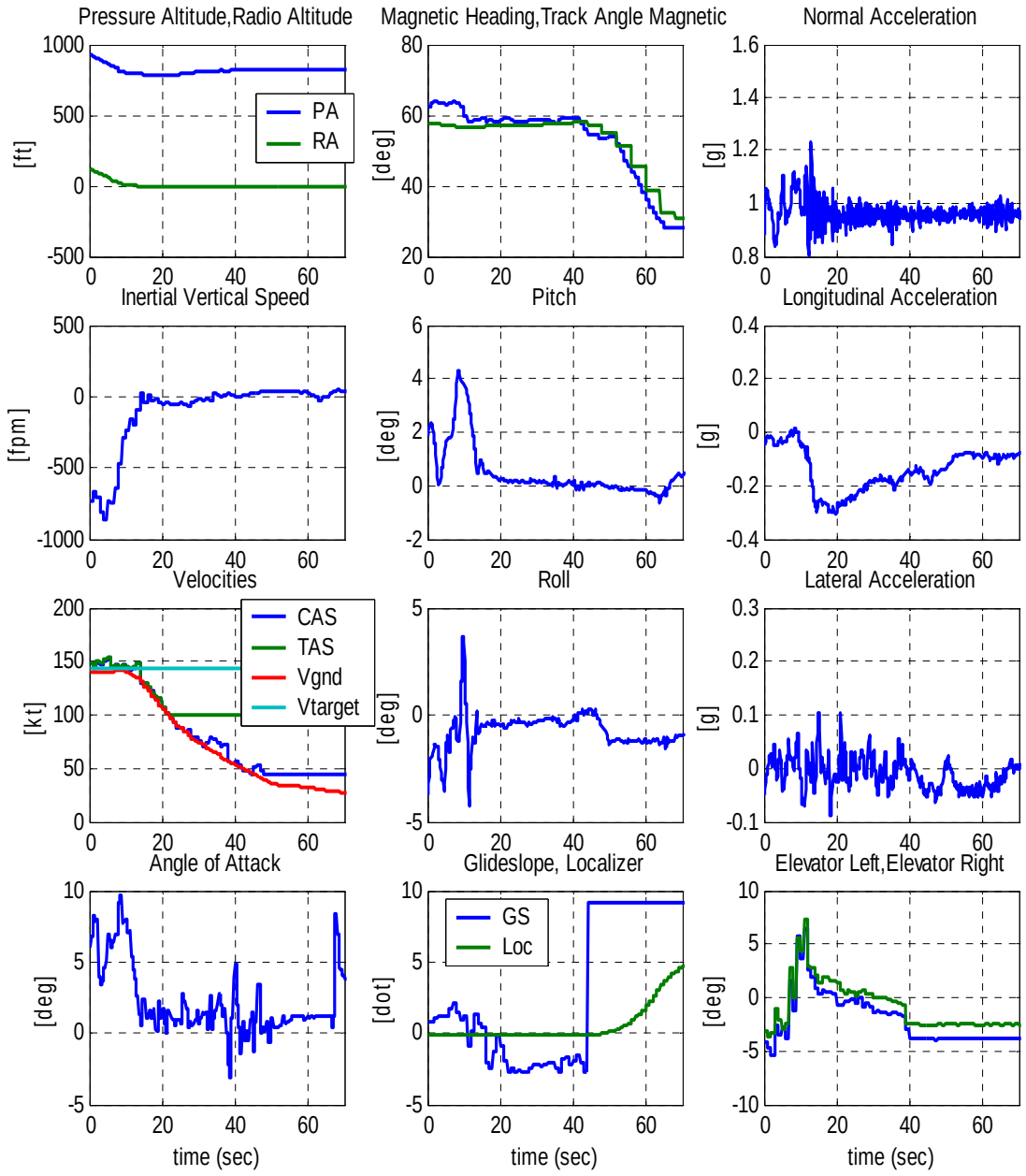

Figure A-1. Example Time Histories B-737-400, Parameter Series 1

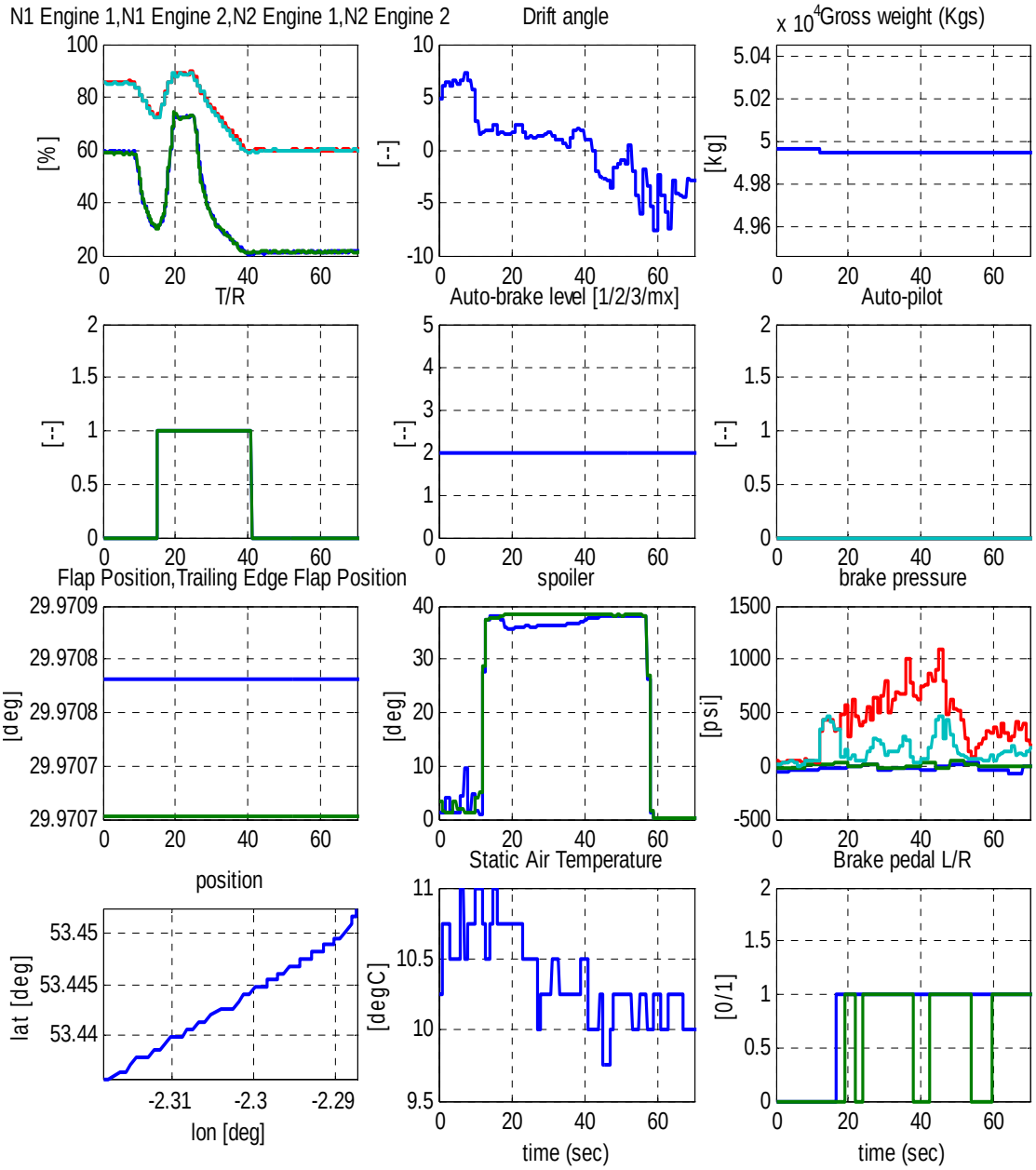

Figure A-2. Example Time Histories B-737-400, Parameter Series 2

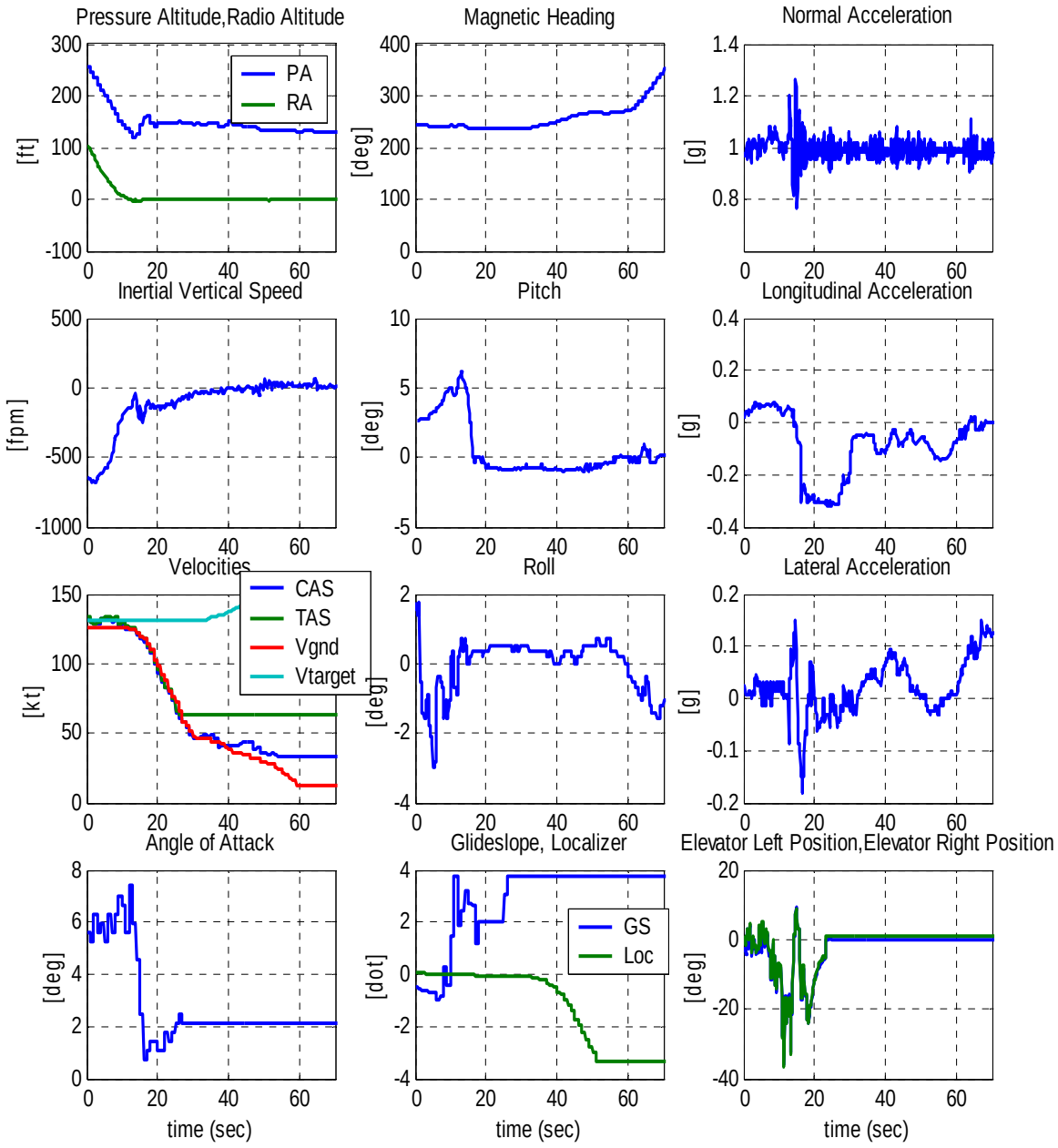

Figure A-3. Example Time Histories A320, Parameter Series 1

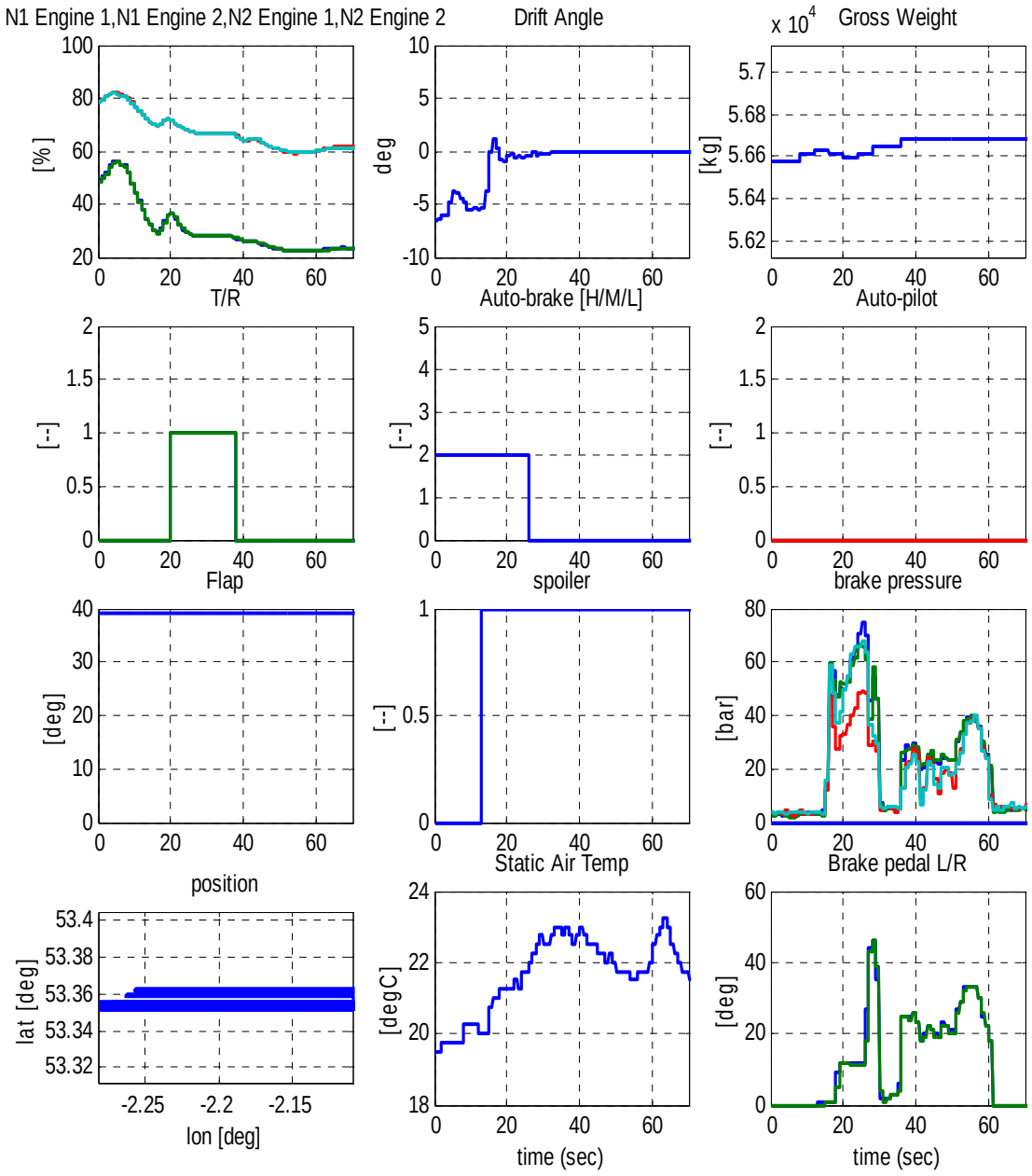

Figure A-4. Example Time Histories A320, Parameter Series 2

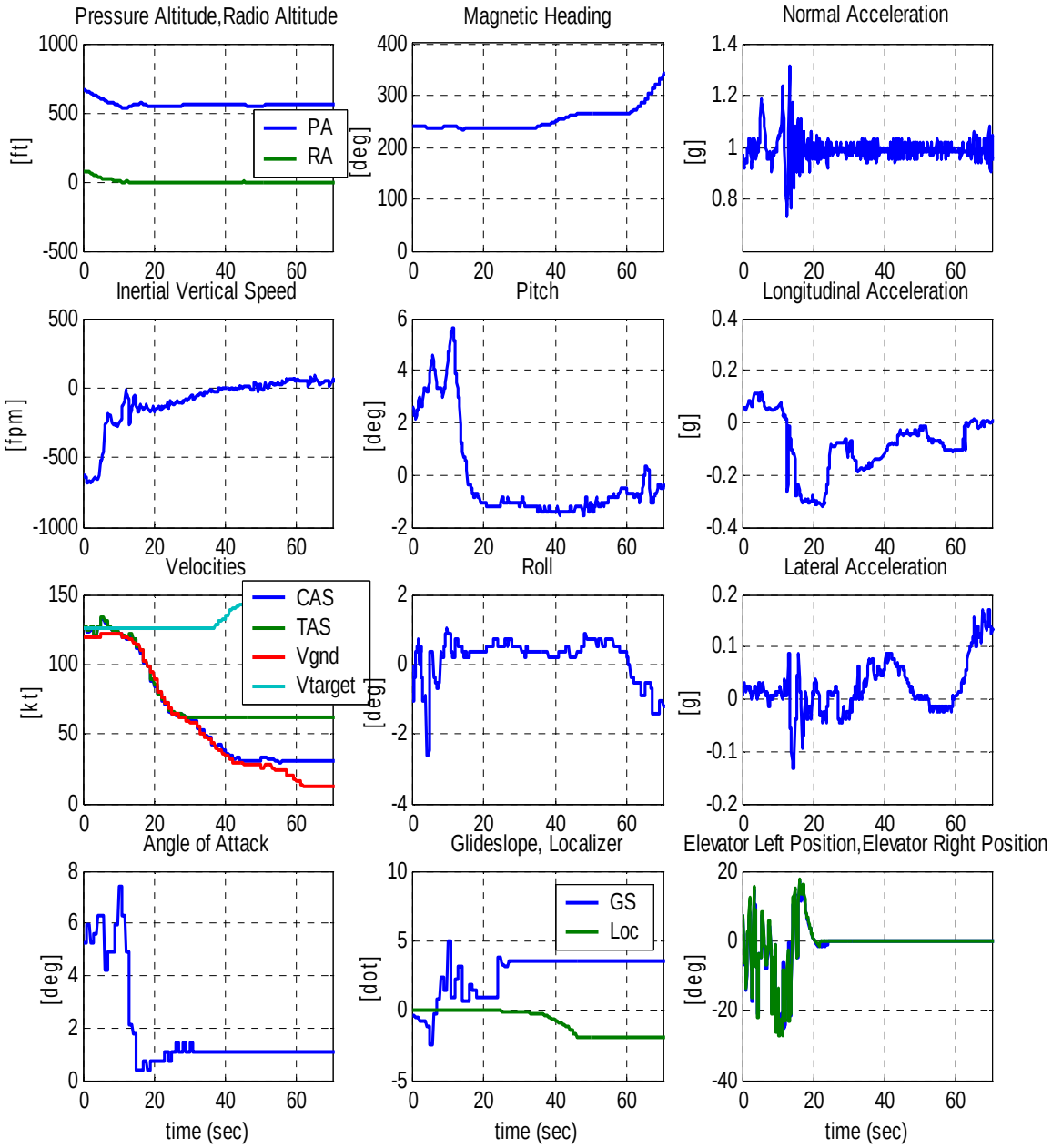

Figure A-5. Example Time Histories A319, Parameter Series 1

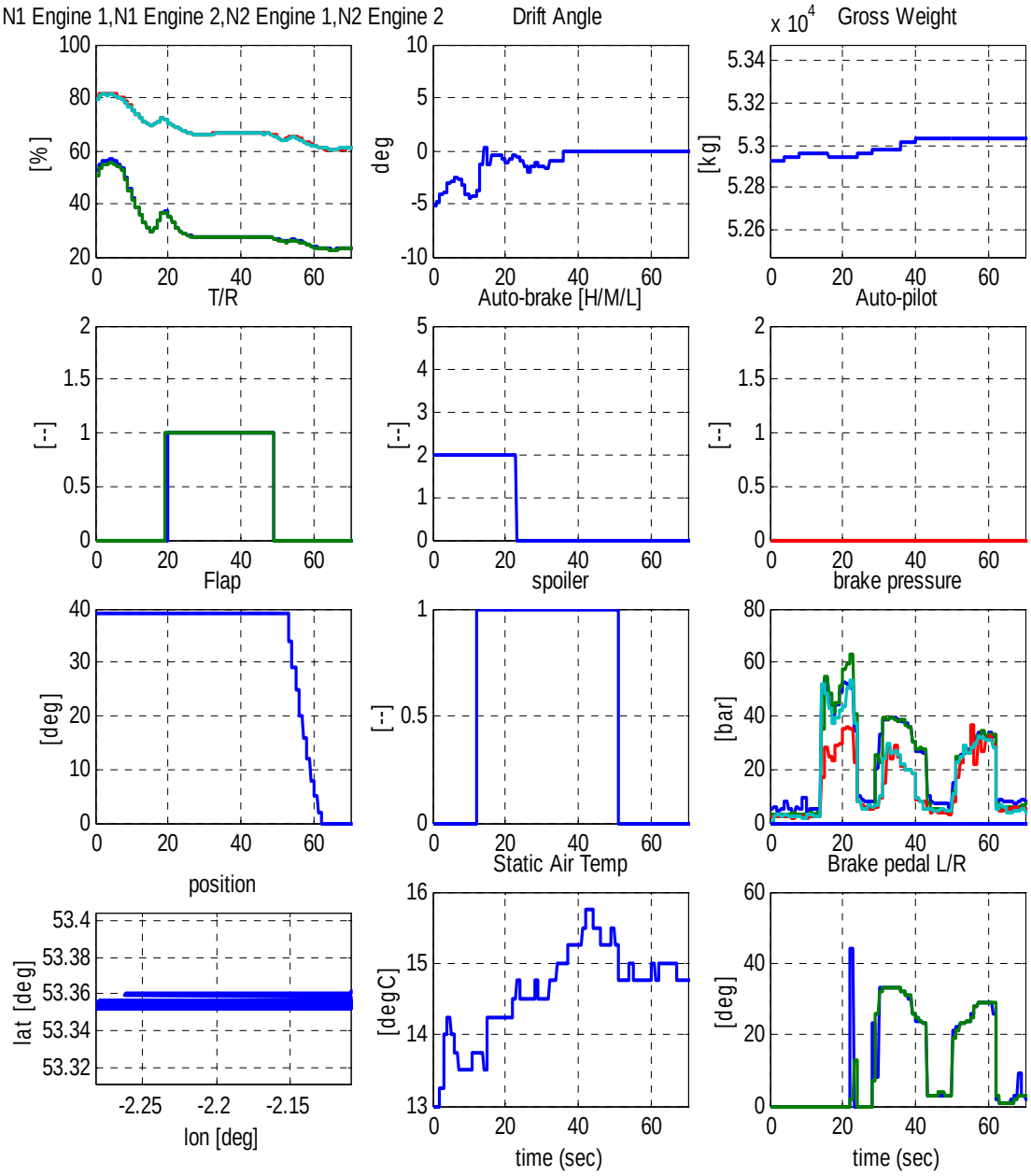

Figure A-6. Example Time Histories A319, Parameter Series 2

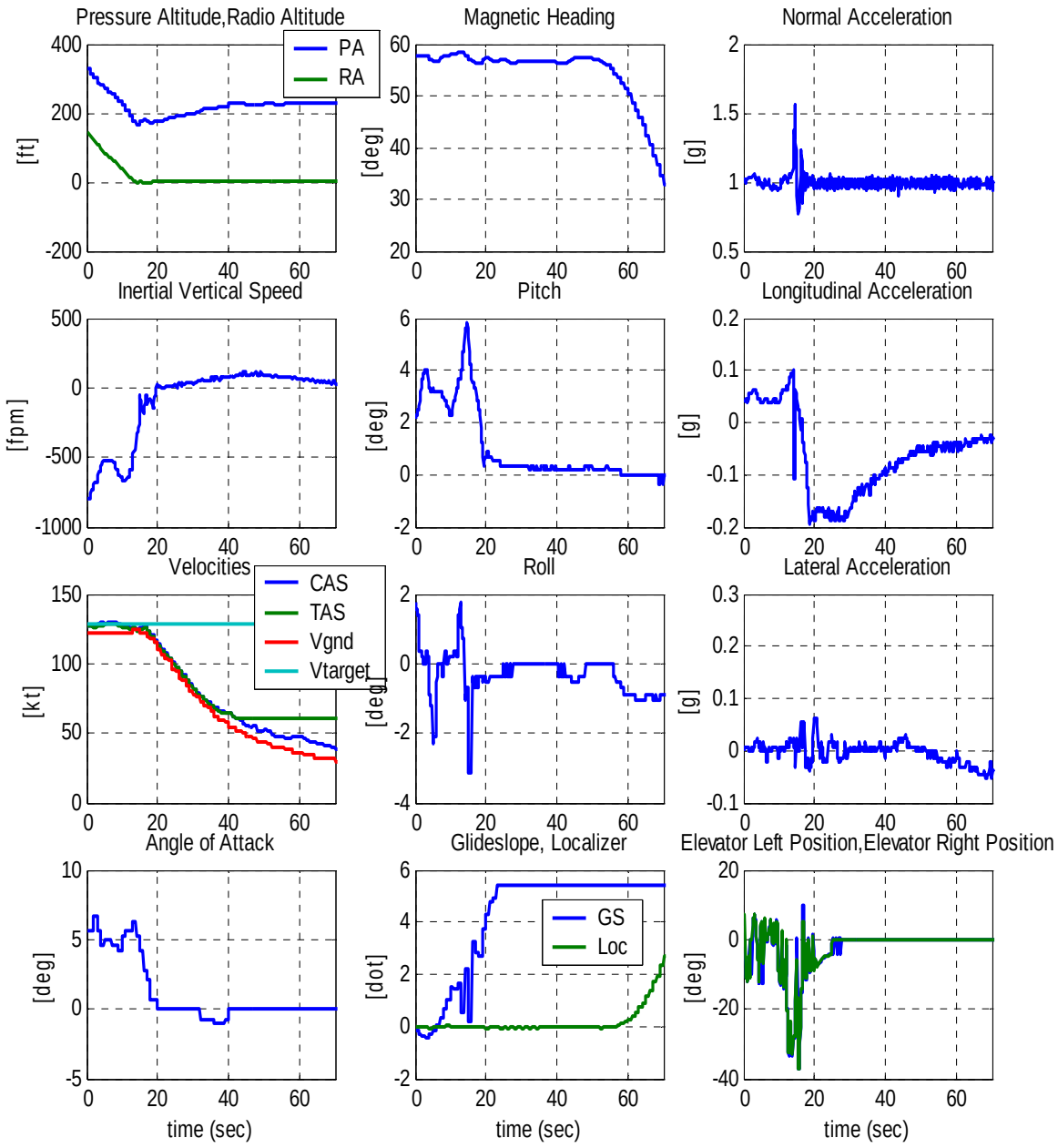

Figure A-7. Example Time Histories A321, Parameter Series 1

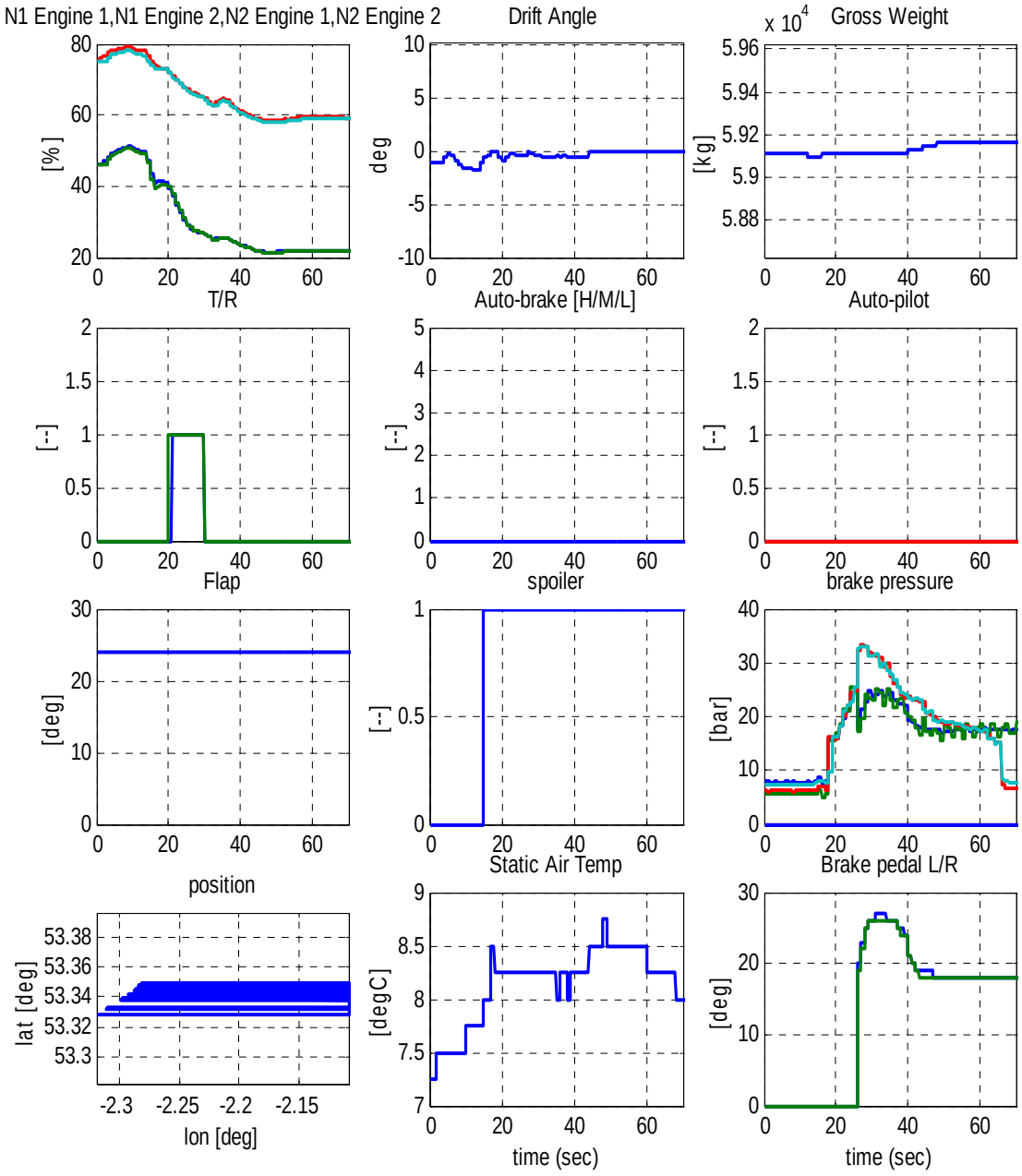

Figure A-8. Example Time Histories A321, Parameter Series 2

APPENDIX B—DEMONSTRATION OF DATA PROCESSING ALGORITHMS

B.1 EXAMPLE CASES WITH SMALL AND LARGE GLIDE SLOPE TRACKING ERROR.

Figures B-1 through B-30 are examples of the data that was collected during normal operational flights.

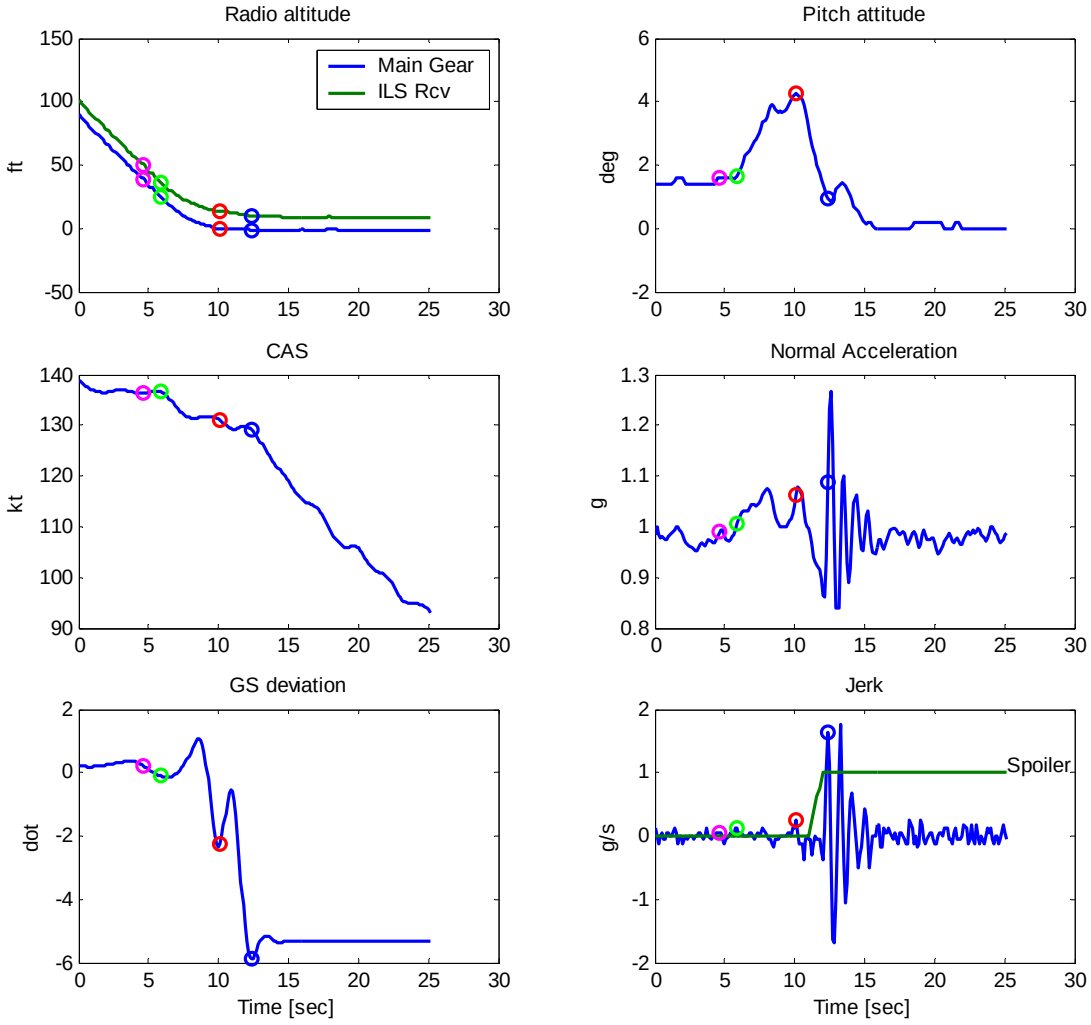

Legend:
O Threshold crossing
O Flare initiation
O Main gear touchdown
O Nosewheel touchdown

Figure B-1. A320 Nominal Conditions on Glide Slope

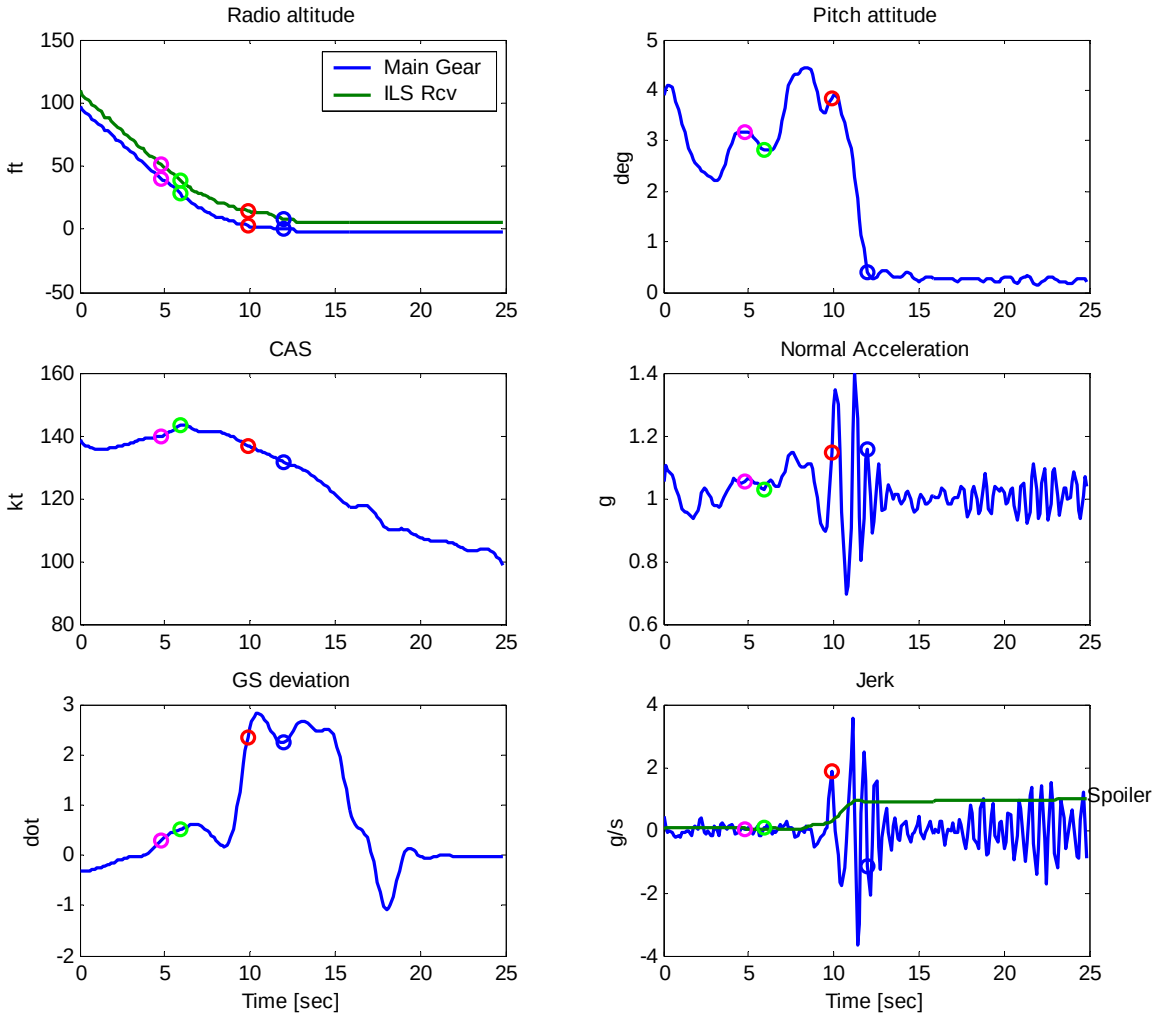

Legend:
O Threshold crossing
O Flare initiation
O Main gear touchdown
O Nosewheel touchdown

Figure B-2. B-737 Nominal Conditions on Glide Slope

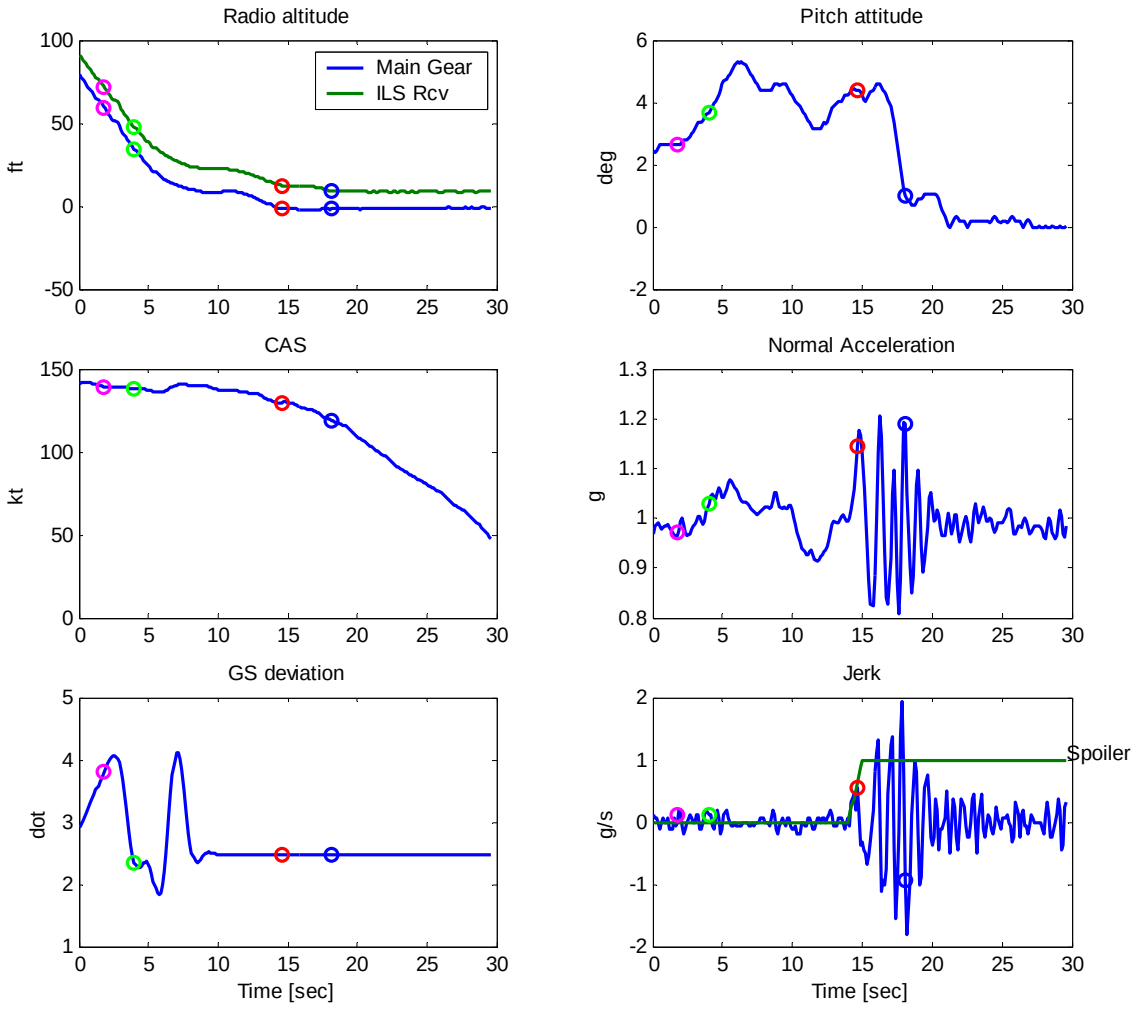

Legend:
O Threshold crossing
O Flare initiation
O Main gear touchdown
O Nosewheel touchdown

Figure B-3. A320 High THR Crossing

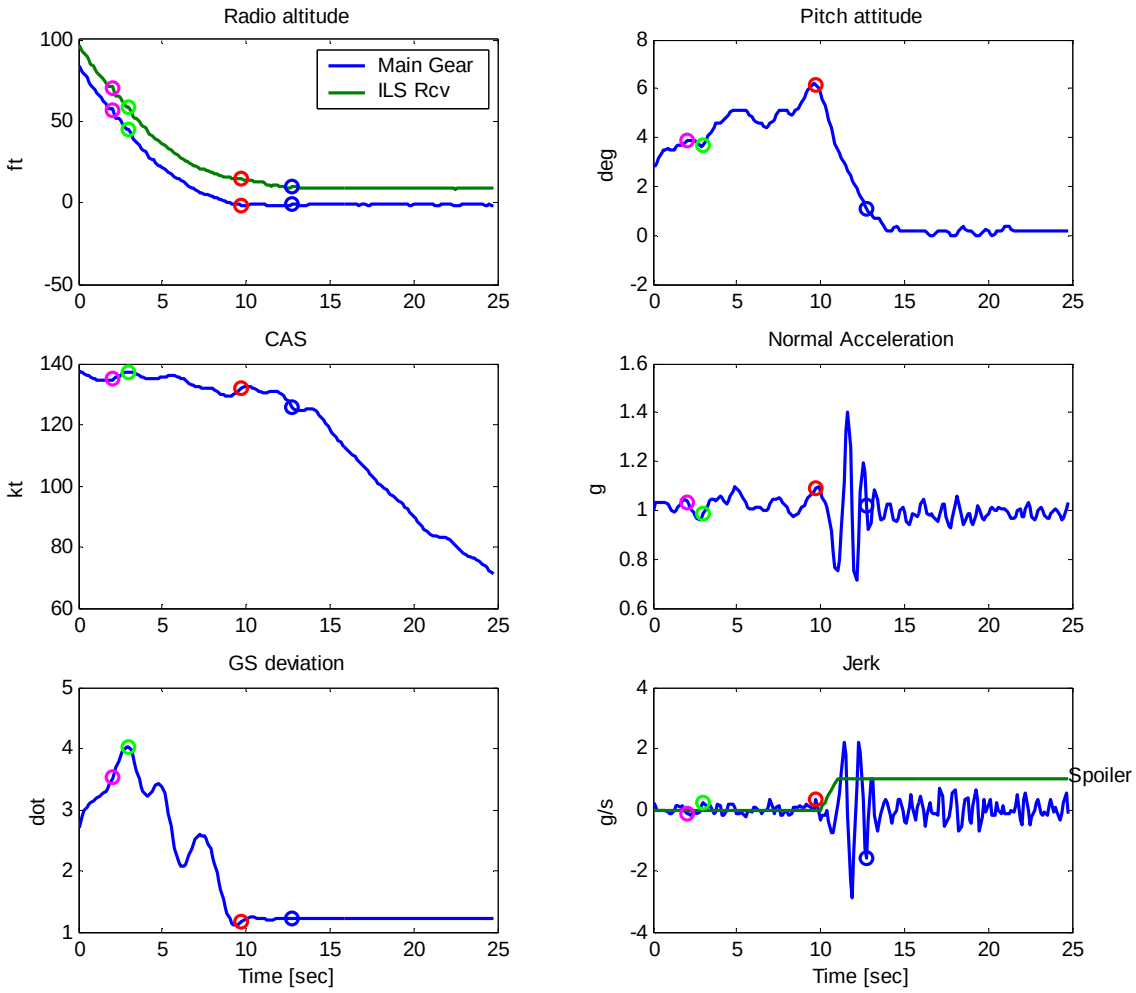

Legend:
O Threshold crossing
O Flare initiation
O Main gear touchdown
O Nosewheel touchdown

Figure B-4. A320 High THR Crossing 2

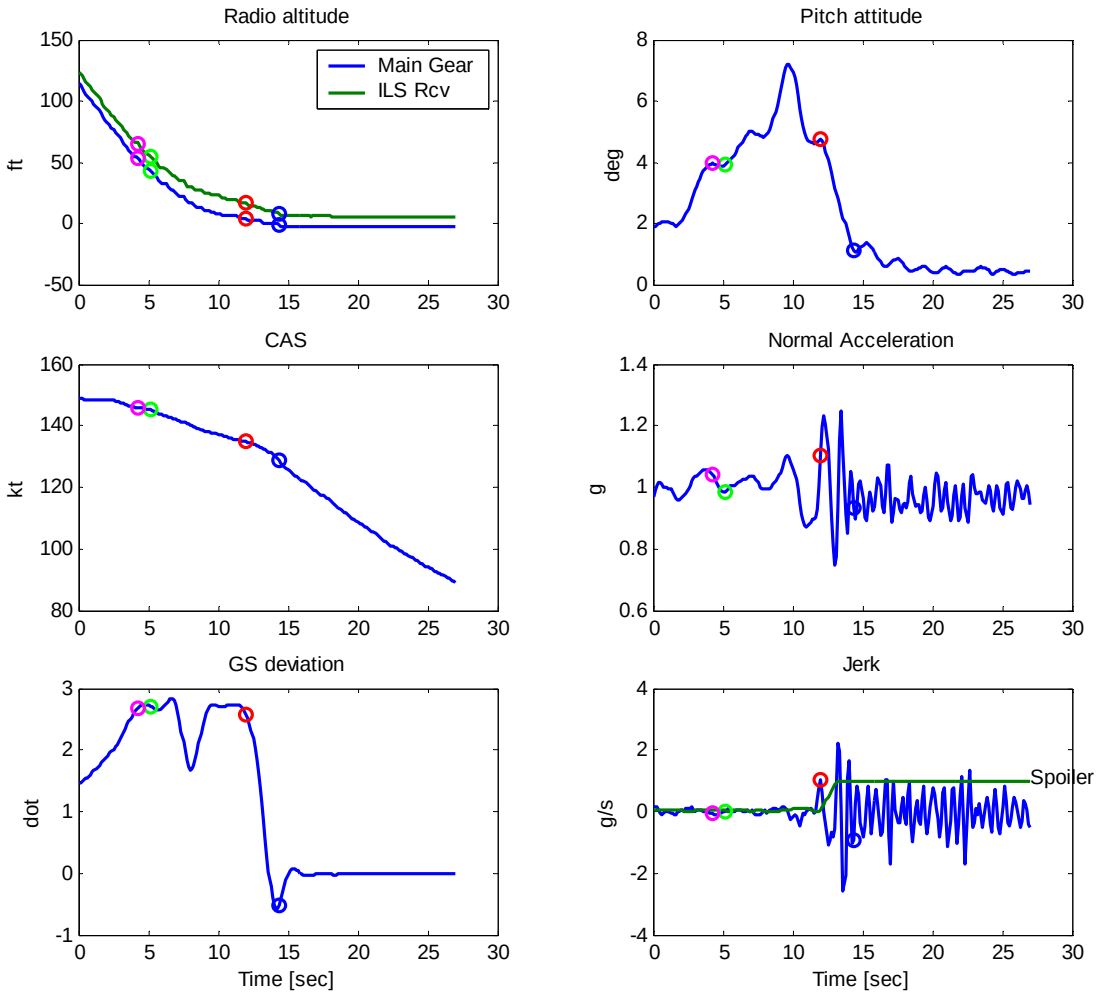

Legend:
O Threshold crossing
O Flare initiation
O Main gear touchdown
O Nosewheel touchdown

Figure B-5. B-737 High THR Crossing

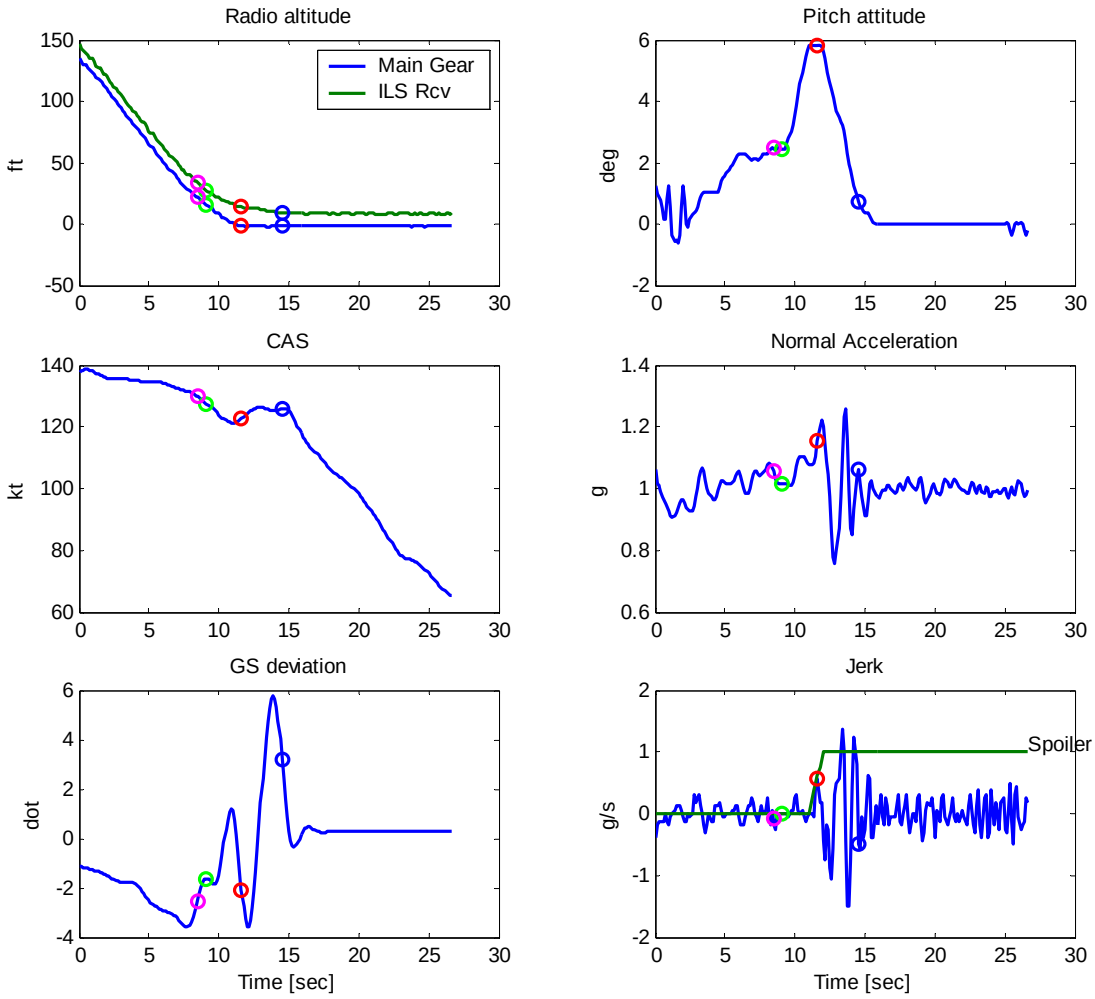

Legend:
O Threshold crossing
O Flare initiation
O Main gear touchdown
O Nosewheel touchdown

Figure B-6. A320 Low THR Crossing

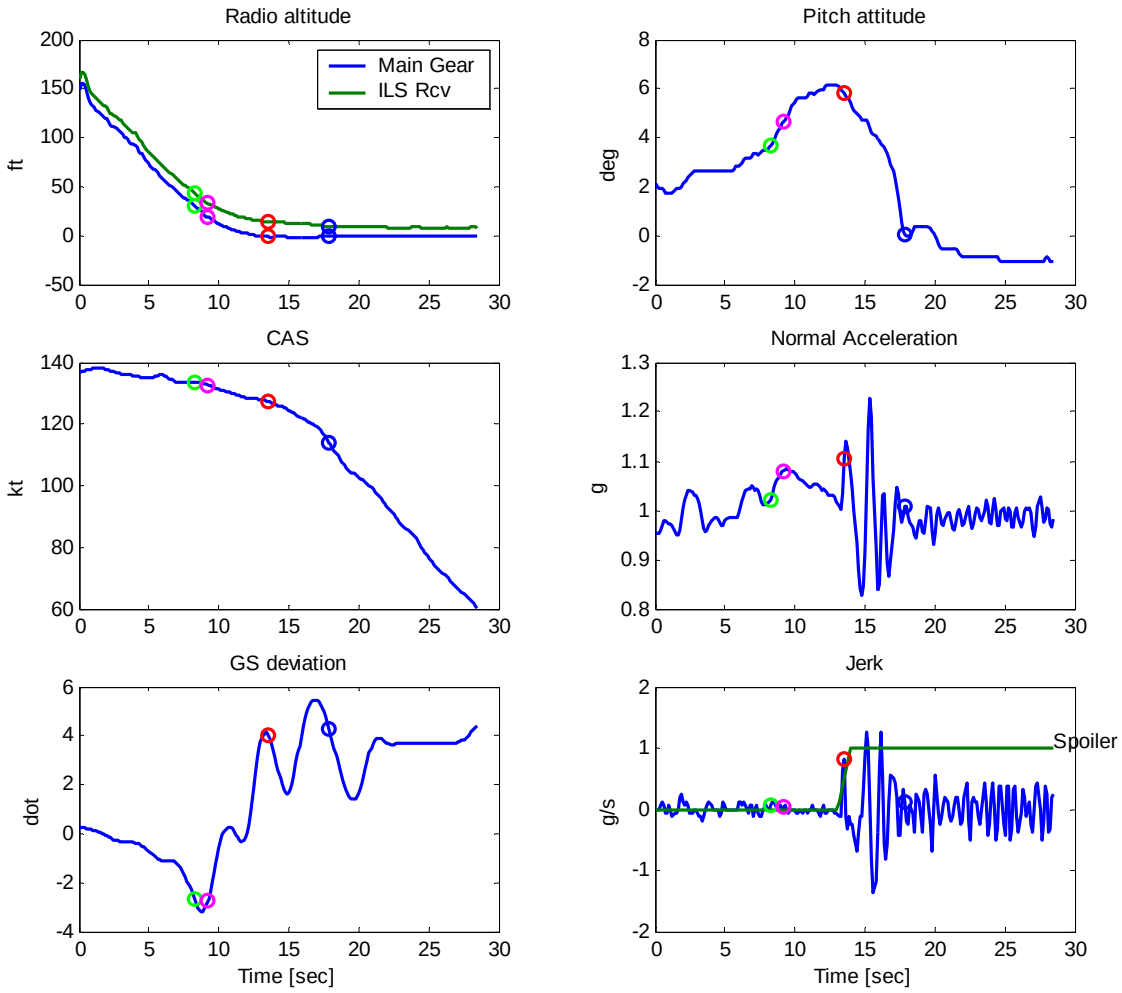

Legend:
O Threshold crossing
O Flare initiation
O Main gear touchdown
O Nosewheel touchdown

Figure B-7. A320 Low THR Crossing 2

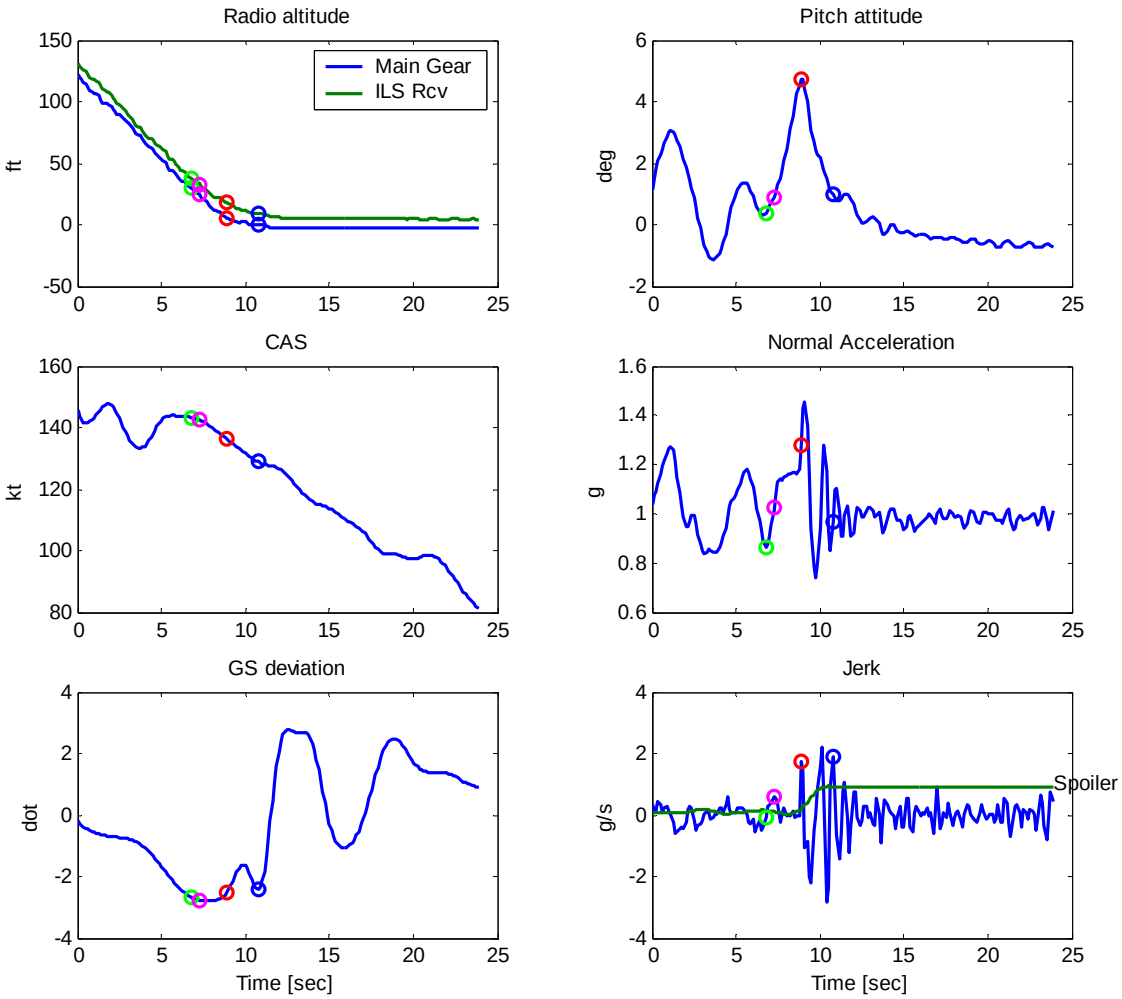

Legend:
O Threshold crossing
O Flare initiation
O Main gear touchdown
O Nosewheel touchdown

Figure B-8. B-737 Low THR Crossing

B.2 EXAMPLE CASES UNDER CALM WIND, HIGH WIND, AND SEVERE TURBULENCE.

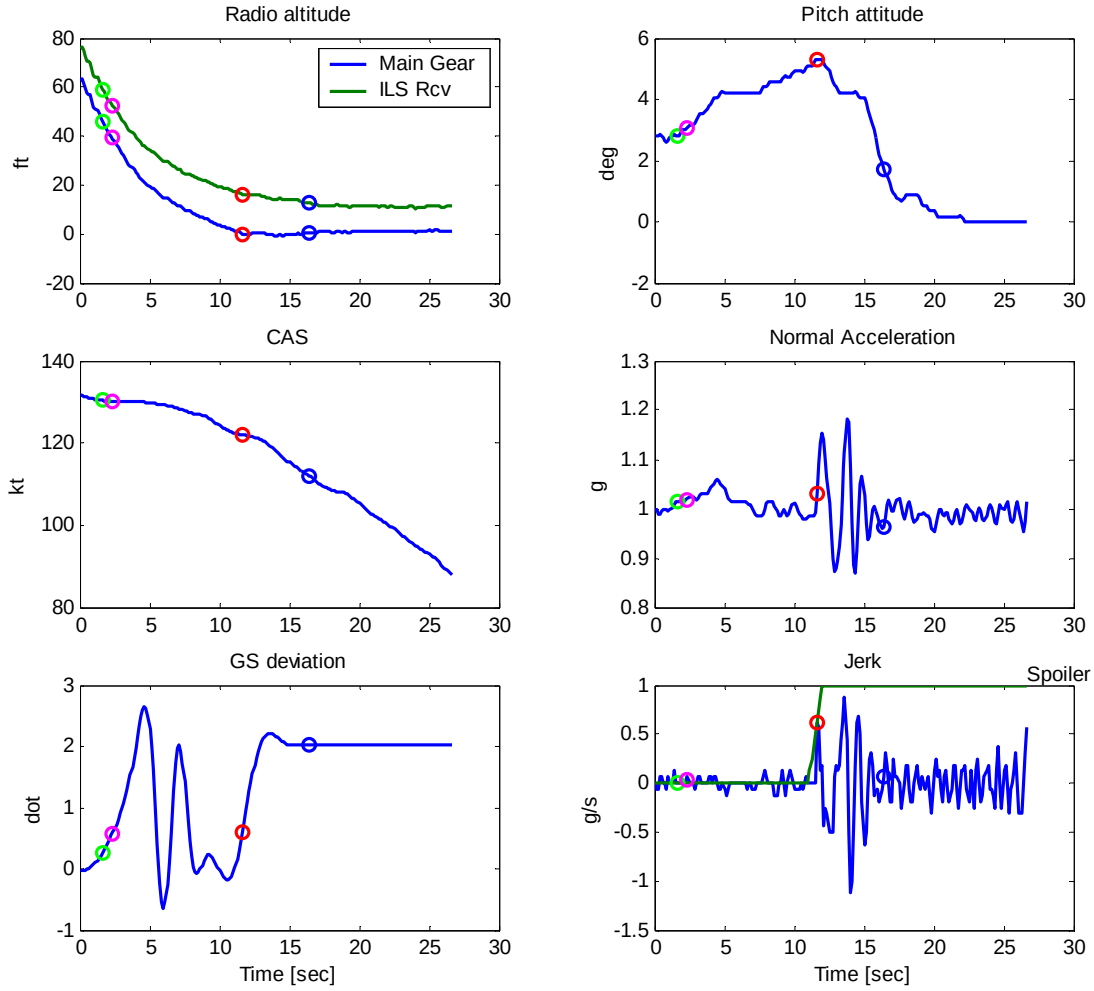

Legend:
O Threshold crossing
O Flare initiation
O Main gear touchdown
O Nosewheel touchdown

Figure B-9. A321 Calm Wind, no Turbulence

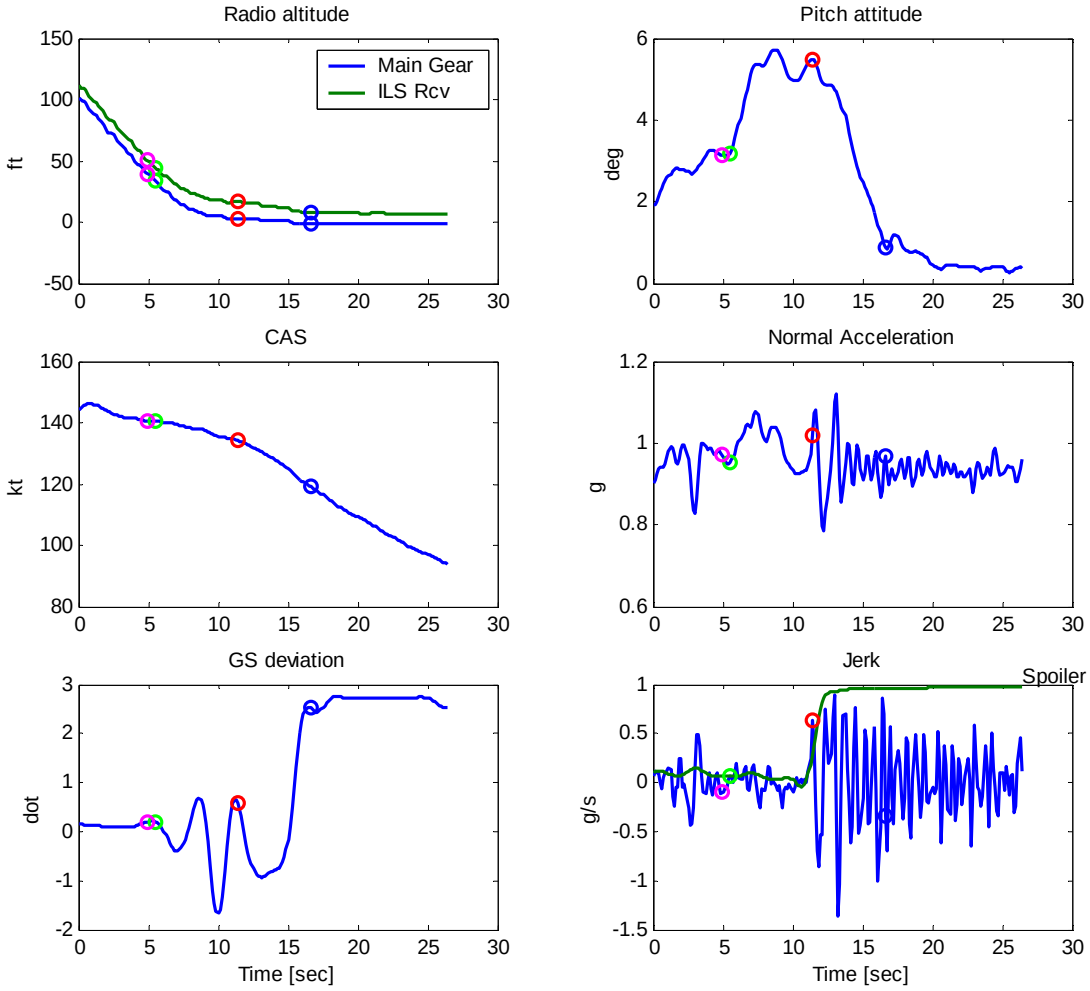

Legend:
O Threshold crossing
O Flare initiation
O Main gear touchdown
O Nosewheel touchdown

Figure B-10. B-737 Calm Wind, no Turbulence

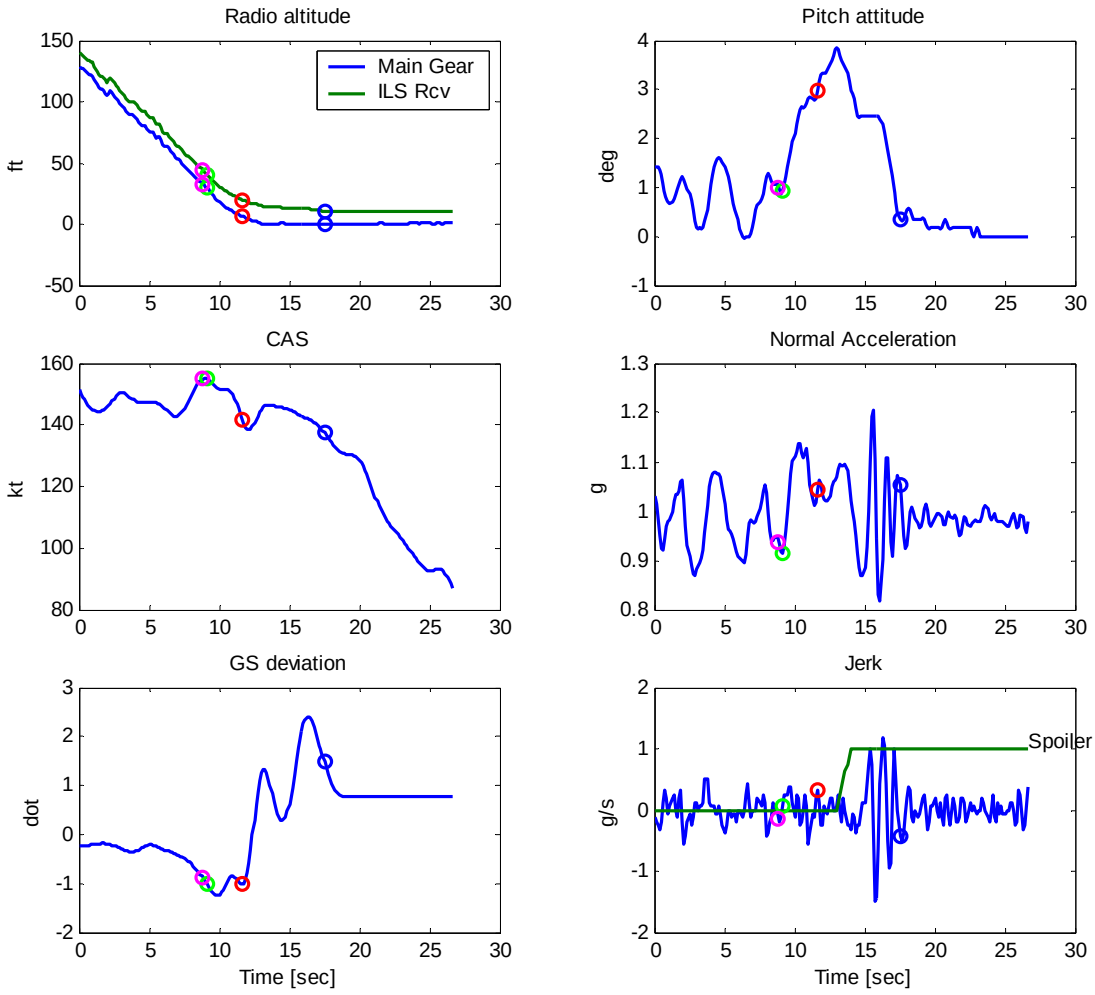

Legend:
O Threshold crossing
O Flare initiation
O Main gear touchdown
O Nosewheel touchdown

Figure B-11. B-737 Calm Wind, no Turbulence

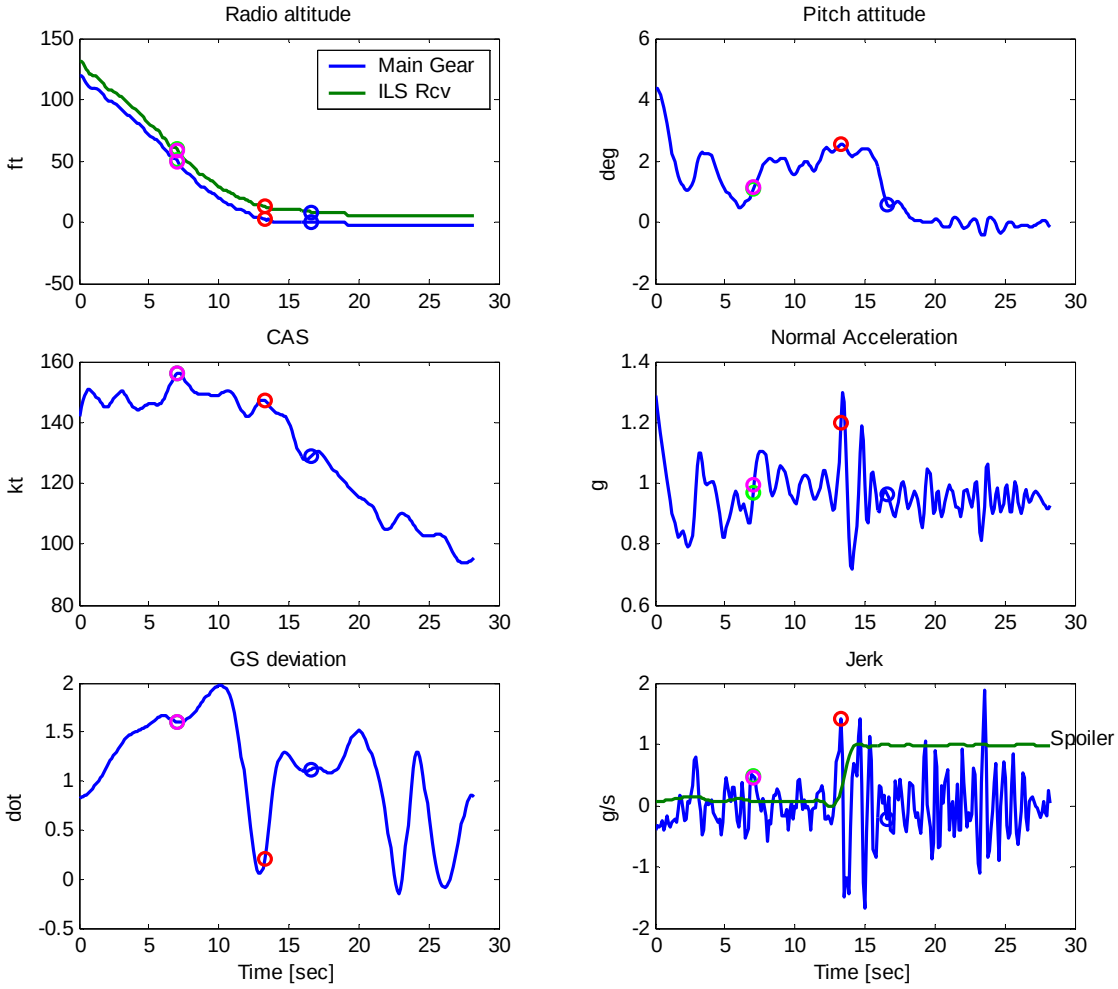

Legend:
O Threshold crossing
O Flare initiation
O Main gear touchdown
O Nosewheel touchdown

Figure B-12. B-737 Strong Wind (38 kt) and Severe Turbulence (gusting 52 kt)

B.3 EXAMPLE CASES WITH SHORT AND LONG AIR DISTANCE.

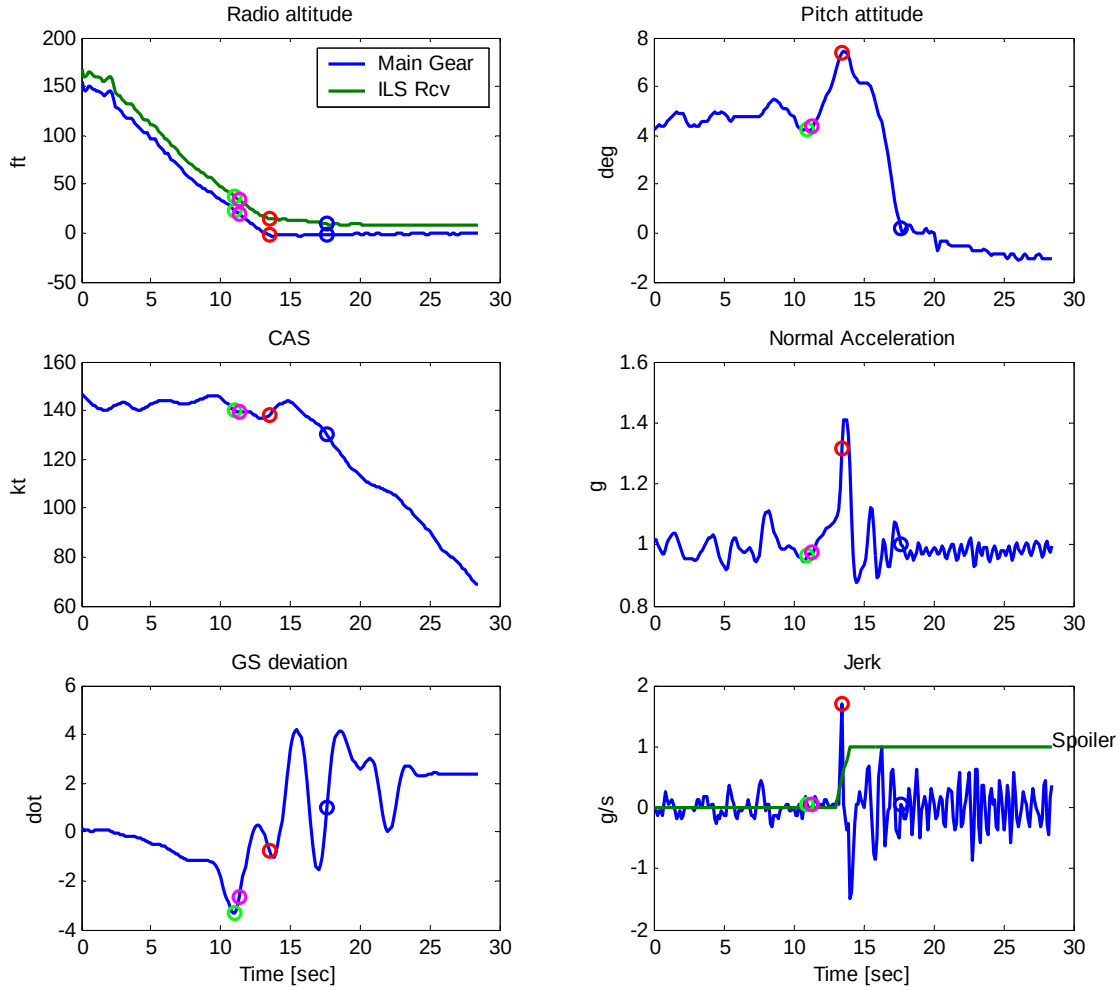

Legend:
O Threshold crossing
O Flare initiation
O Main gear touchdown
O Nosewheel touchdown

Figure B-13. A320 Short Landing (airborne distance = 463 ft)

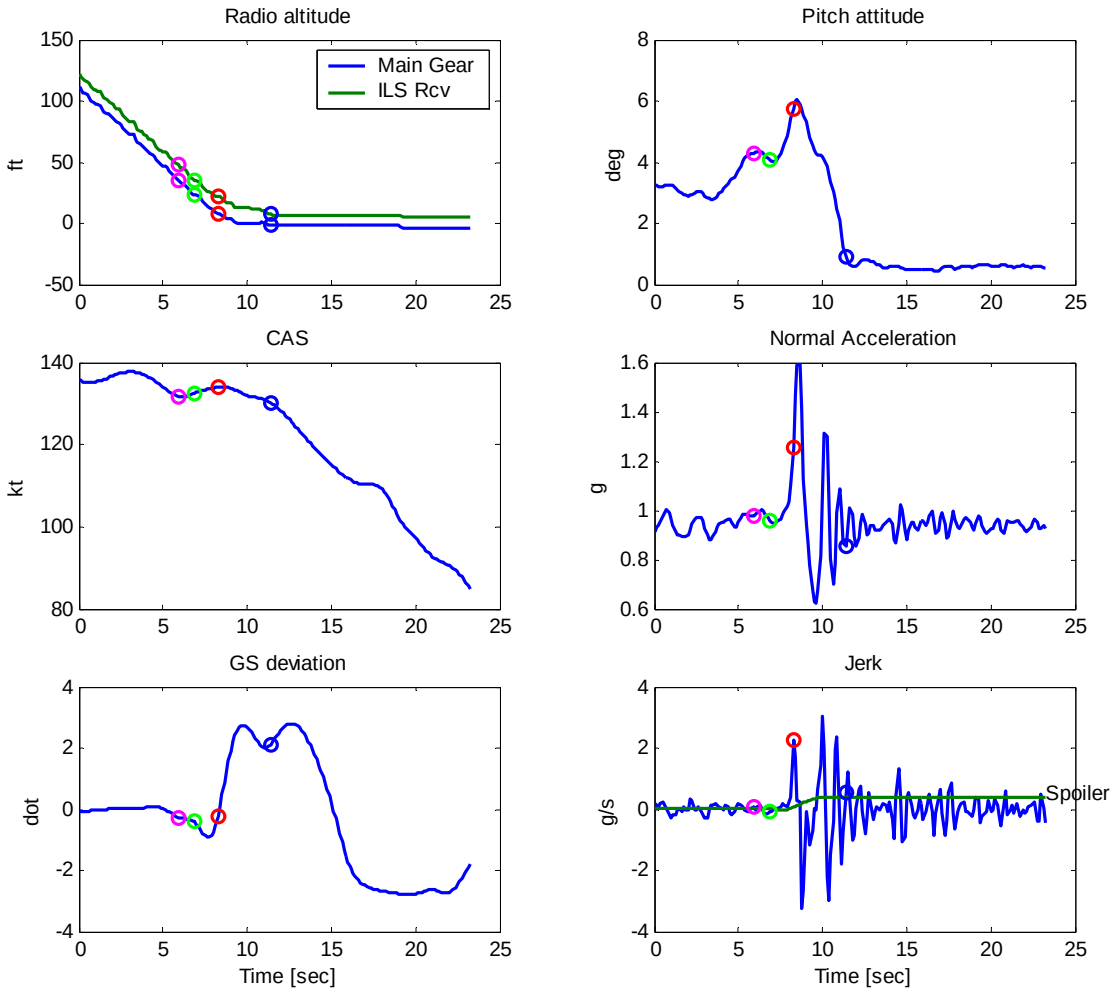

Legend:
O Threshold crossing
O Flare initiation
O Main gear touchdown
O Nosewheel touchdown

Figure B-14. B-737 Short Landing (air distance = 519 ft)

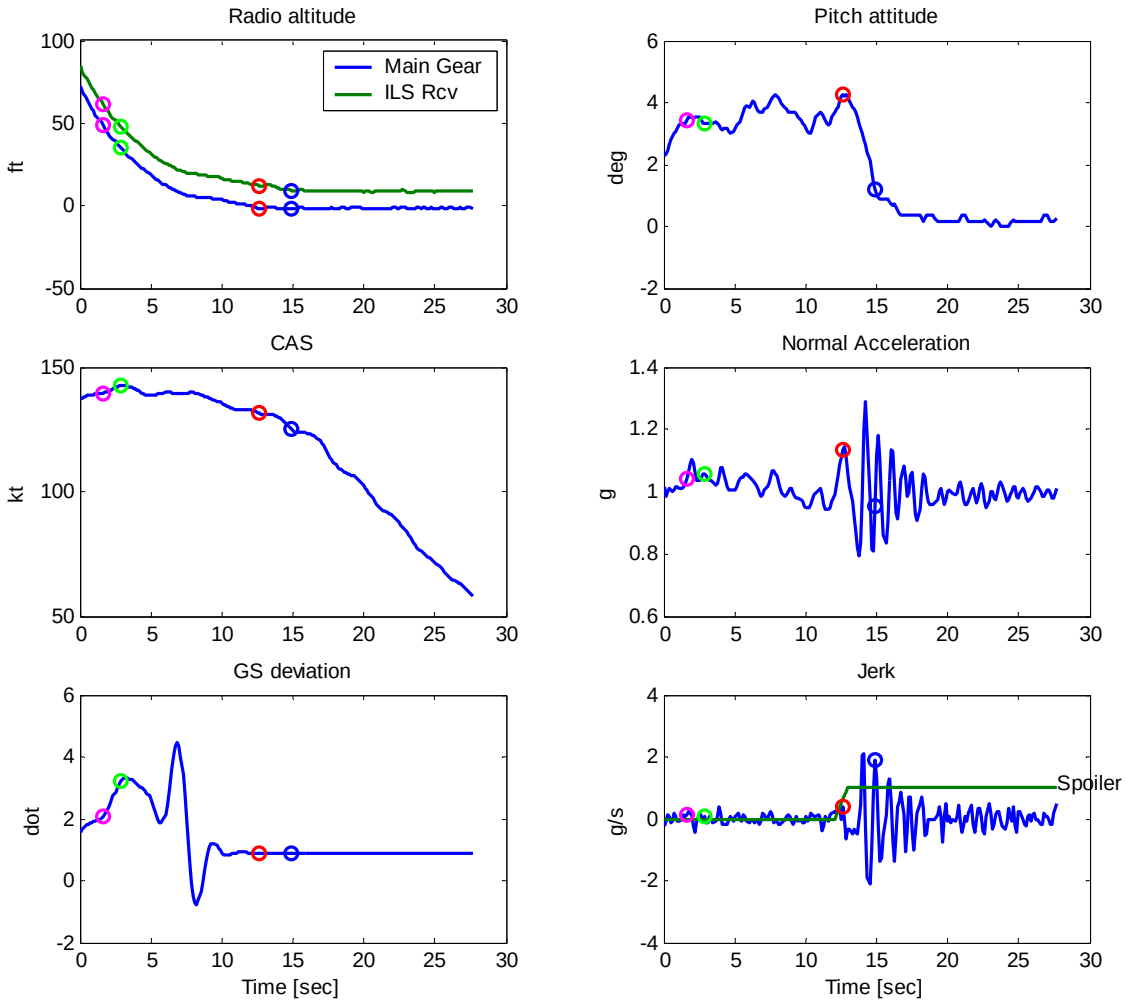

Legend:
O Threshold crossing
O Flare initiation
O Main gear touchdown
O Nosewheel touchdown

Figure B-15. A320 Long Landing (air distance = 2643 ft)

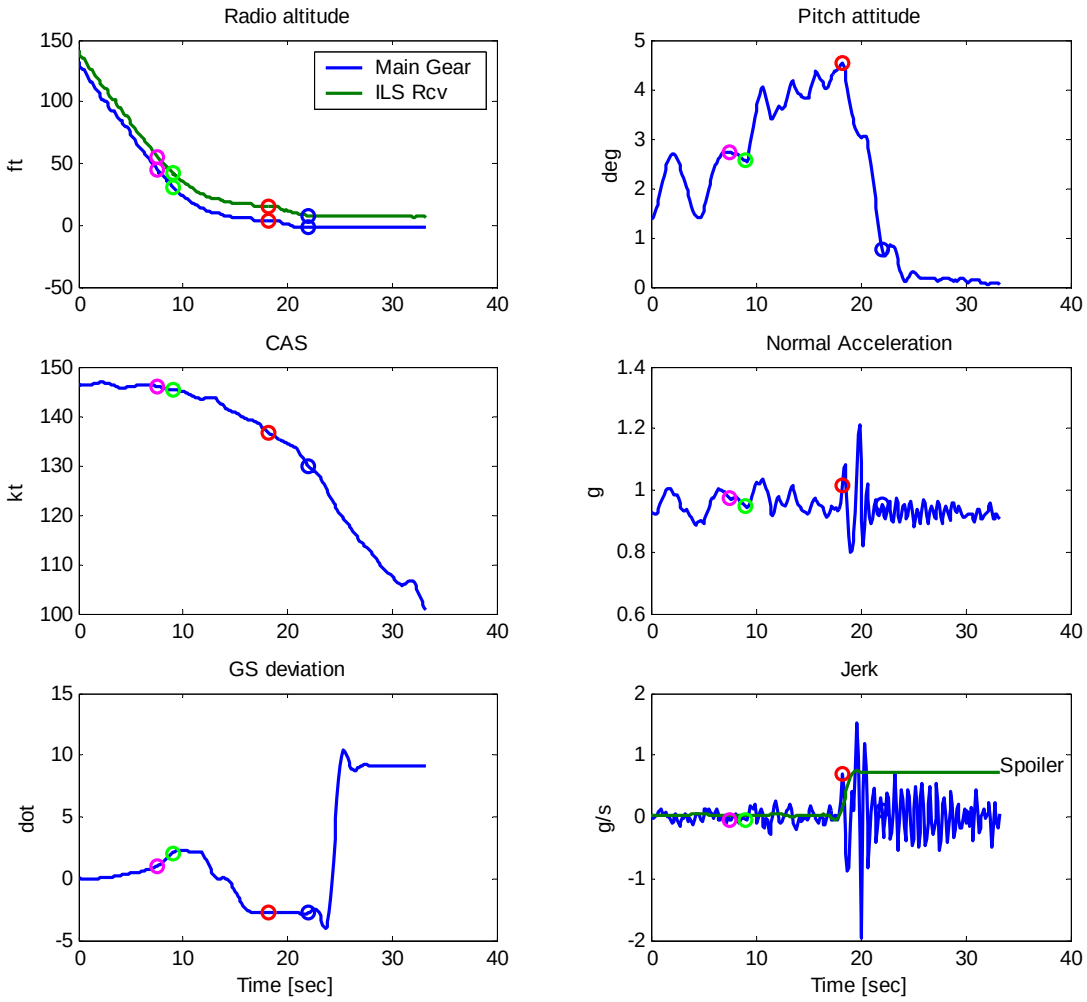

Legend:
O Threshold crossing
O Flare initiation
O Main gear touchdown
O Nosewheel touchdown

Figure B-16. B-737 Long Landing (air distance = 2642 ft)

B.4 EXAMPLE CASES WITH HARD AND SOFT LANDINGS.

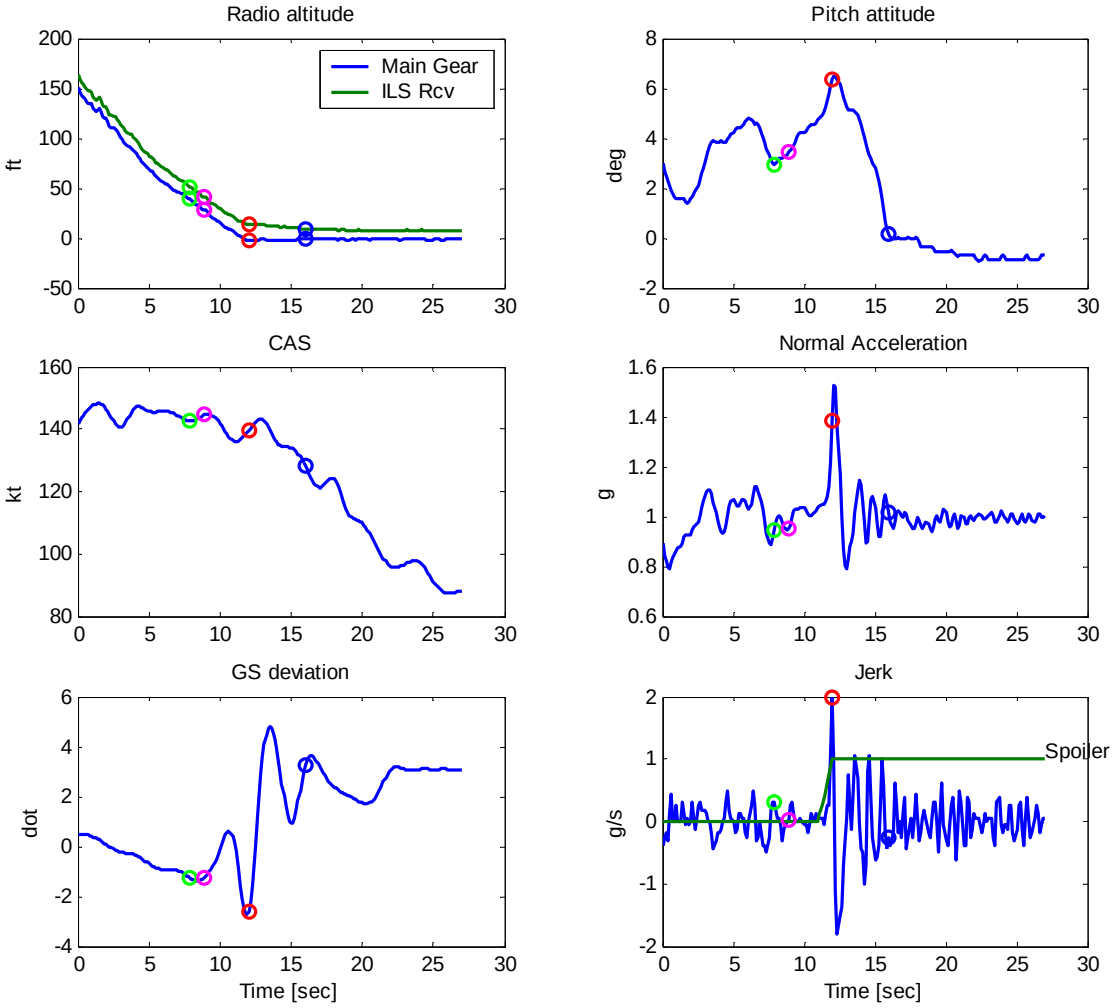

Legend:
O Threshold crossing
O Flare initiation
O Main gear touchdown
O Nosewheel touchdown

Figure B-17. A320 Hard Landing (air distance = 670 ft)

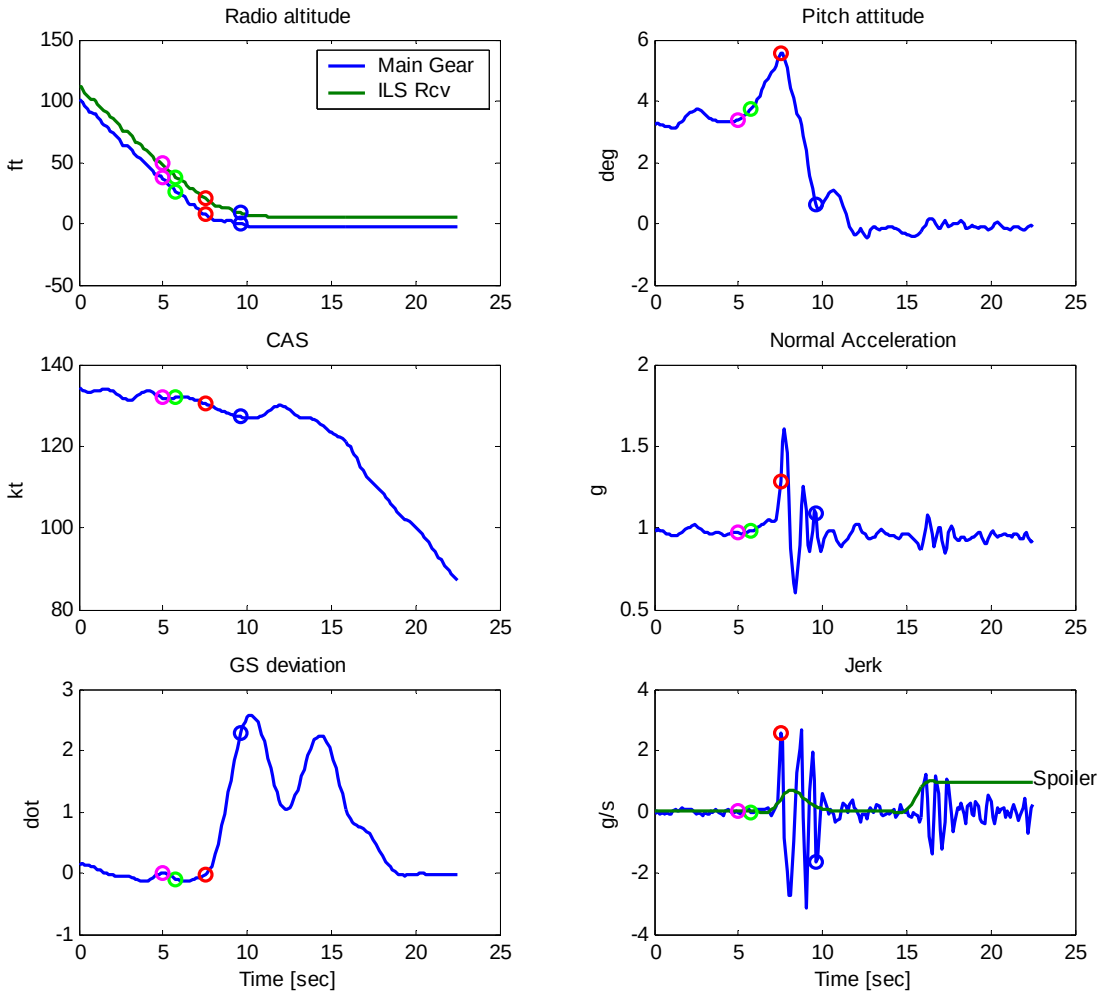

Legend:
O Threshold crossing
O Flare initiation
O Main gear touchdown
O Nosewheel touchdown

Figure B-18. B-737 Hard Landing (air distance = 552 ft)

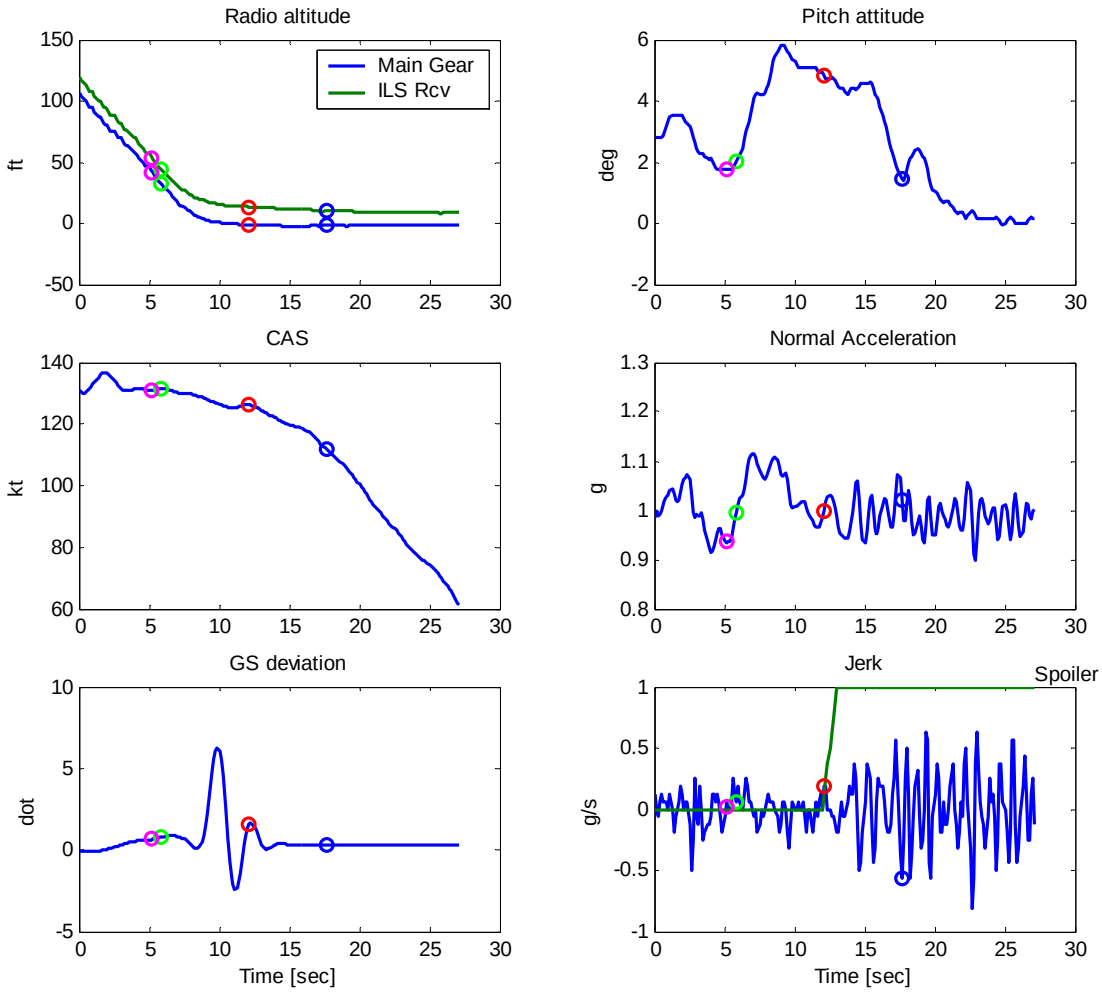

Legend:
O Threshold crossing
O Flare initiation
O Main gear touchdown
O Nosewheel touchdown

Figure B-19. A320 Soft Landing (air distance = 1607 ft)

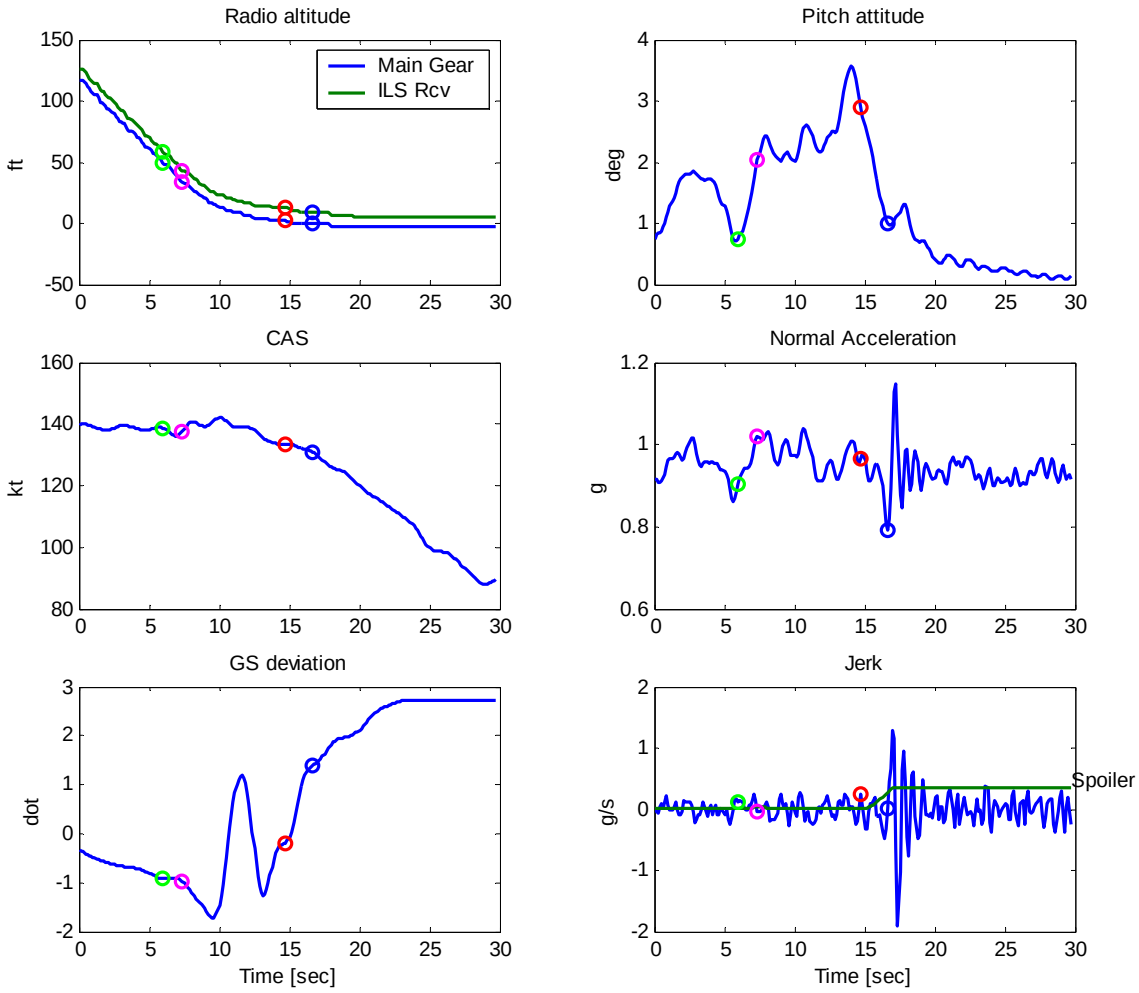

Legend:
O Threshold crossing
O Flare initiation
O Main gear touchdown
O Nosewheel touchdown

Figure B-20. B-737 Soft Landing (air distance = 1515 ft)

B.5 EXAMPLE CASES WITH HIGH AND LOW DESCENT RATE.

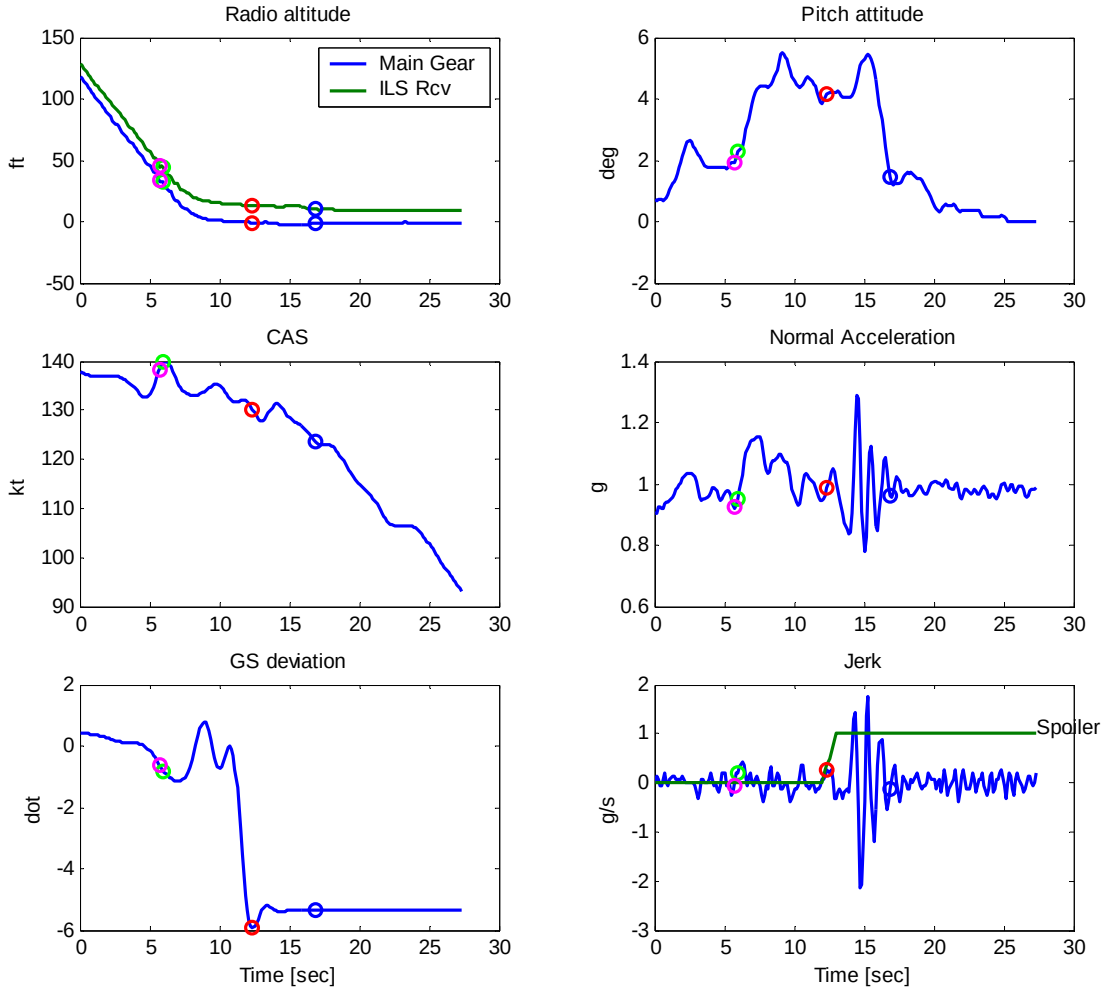

Legend:
O Threshold crossing
O Flare initiation
O Main gear touchdown
O Nosewheel touchdown

Figure B-21. A320 High Descent Rate at THR (V/S = 870 ft/min, air distance = 1720 ft)

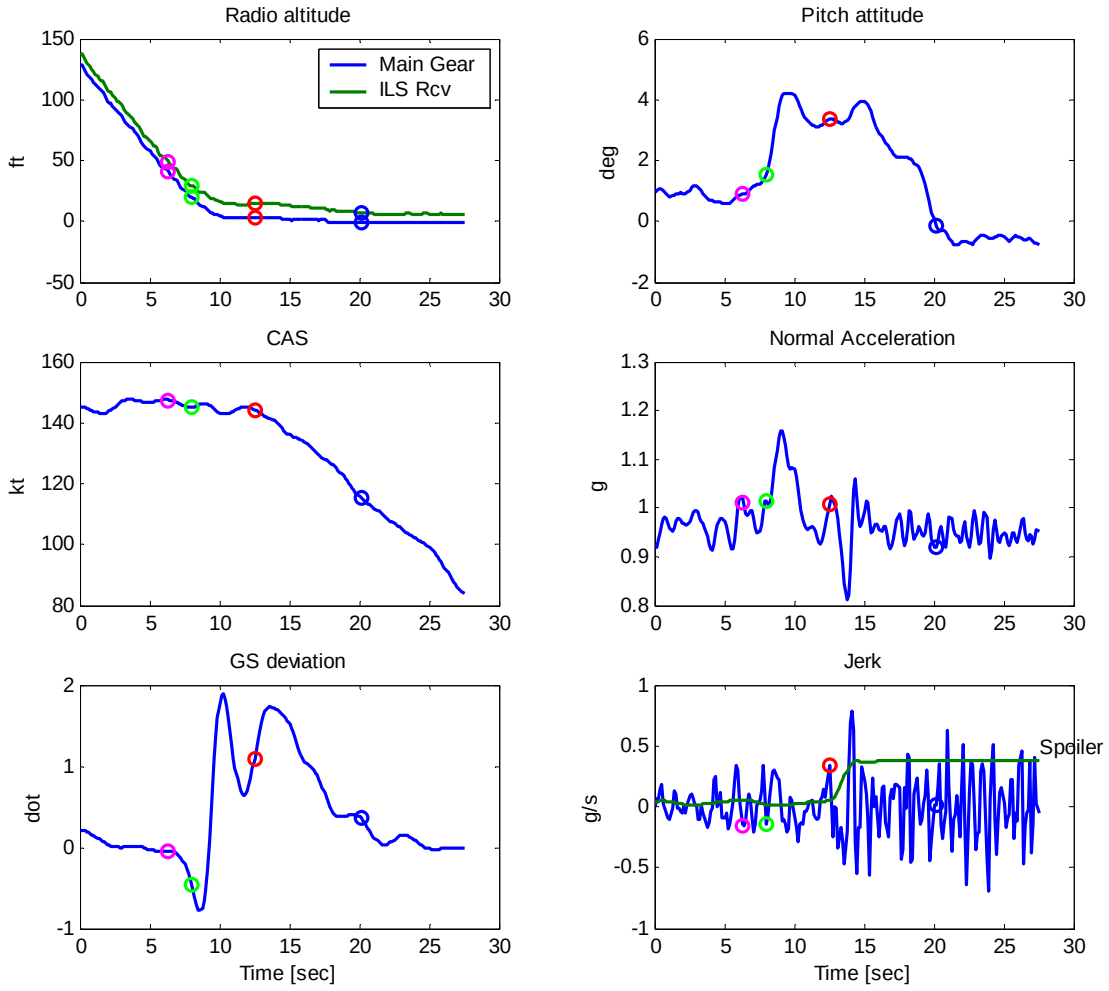

Legend:
O Threshold crossing
O Flare initiation
O Main gear touchdown
O Nosewheel touchdown

Figure B-22. B-737 High Descent Rate at THR (V/S=859 ft/min, air distance = 1330 ft)

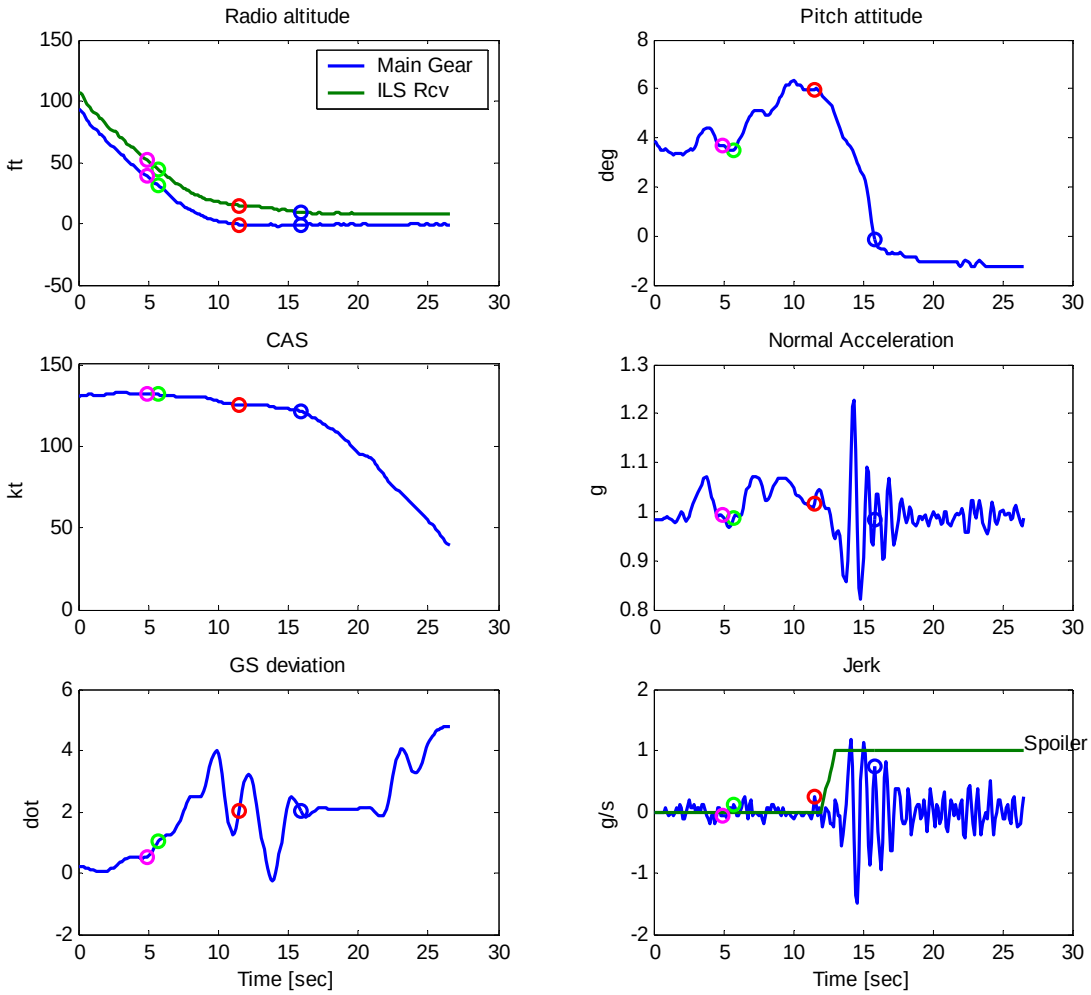

Legend:
O Threshold crossing
O Flare initiation
O Main gear touchdown
O Nosewheel touchdown

Figure B-23. A320 Low Descent Rate at THR (V/S=160 ft/min, air distance = 1398 ft)

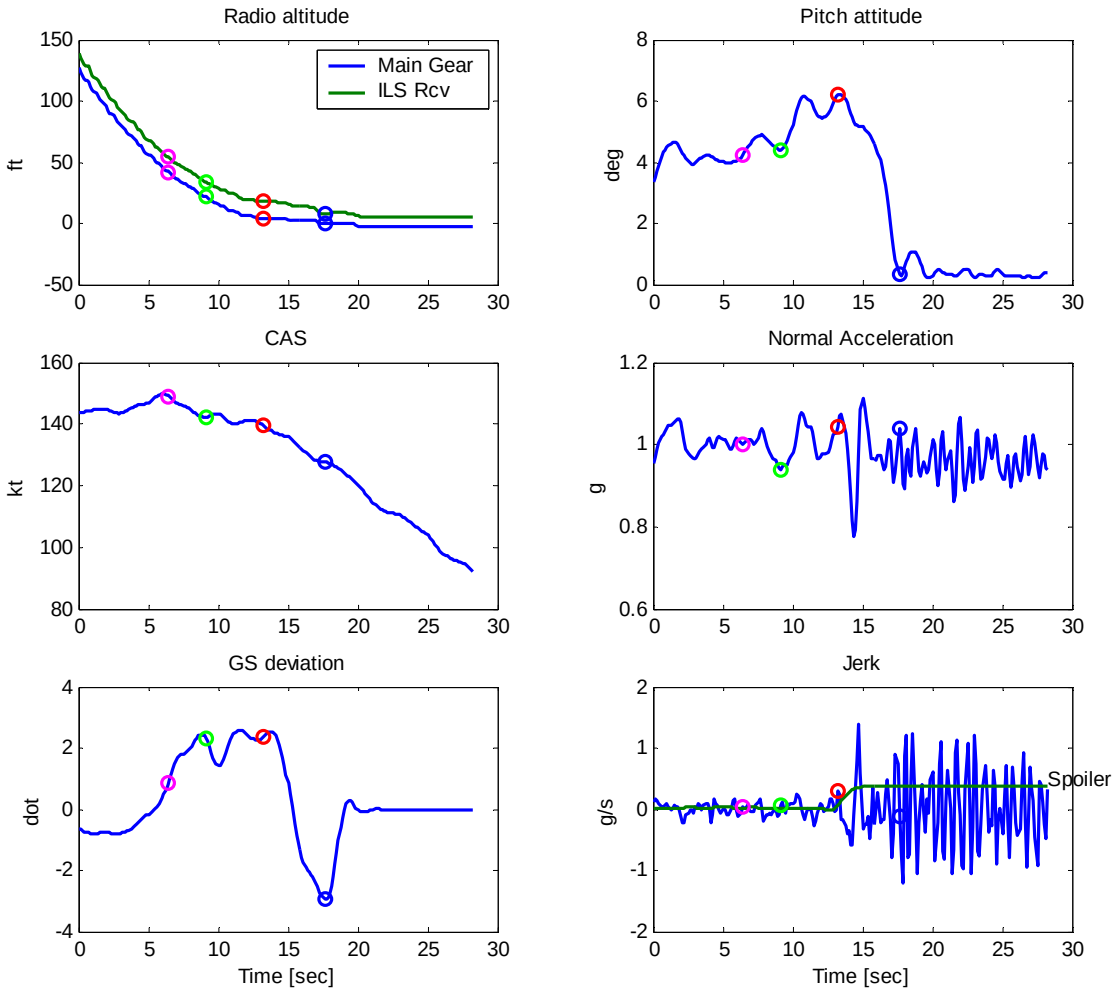

Legend:
O Threshold crossing
O Flare initiation
O Main gear touchdown
O Nosewheel touchdown

Figure B-24. B-737 Low Descent Rate at THR (V/S=314 ft/min, air distance = 1740 ft), Mean V/S~570 fpm

B.6 EXAMPLE FLARE CASES.

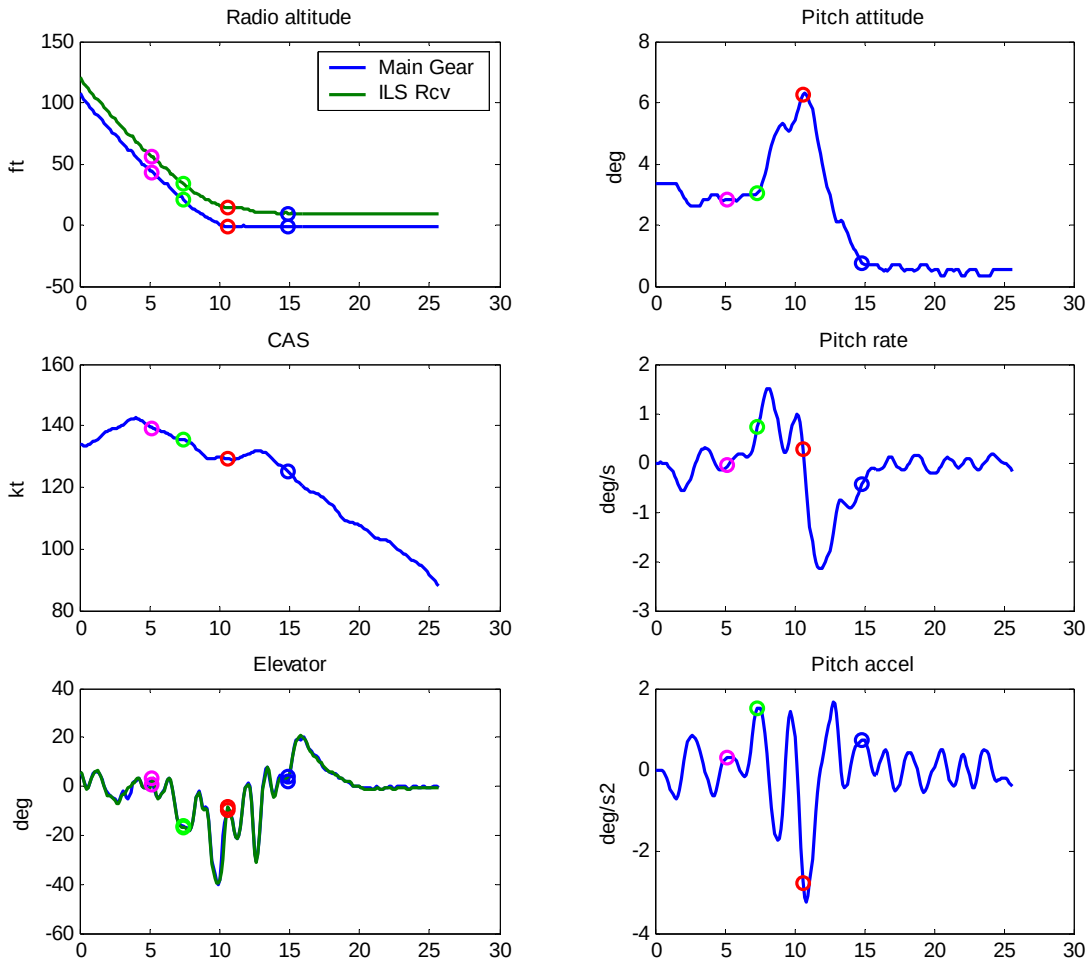

Legend:
O Threshold crossing
O Flare initiation
O Main gear touchdown
O Nosewheel touchdown

Figure B-25. A320 Normal Flare (NZ = 1.12 g)

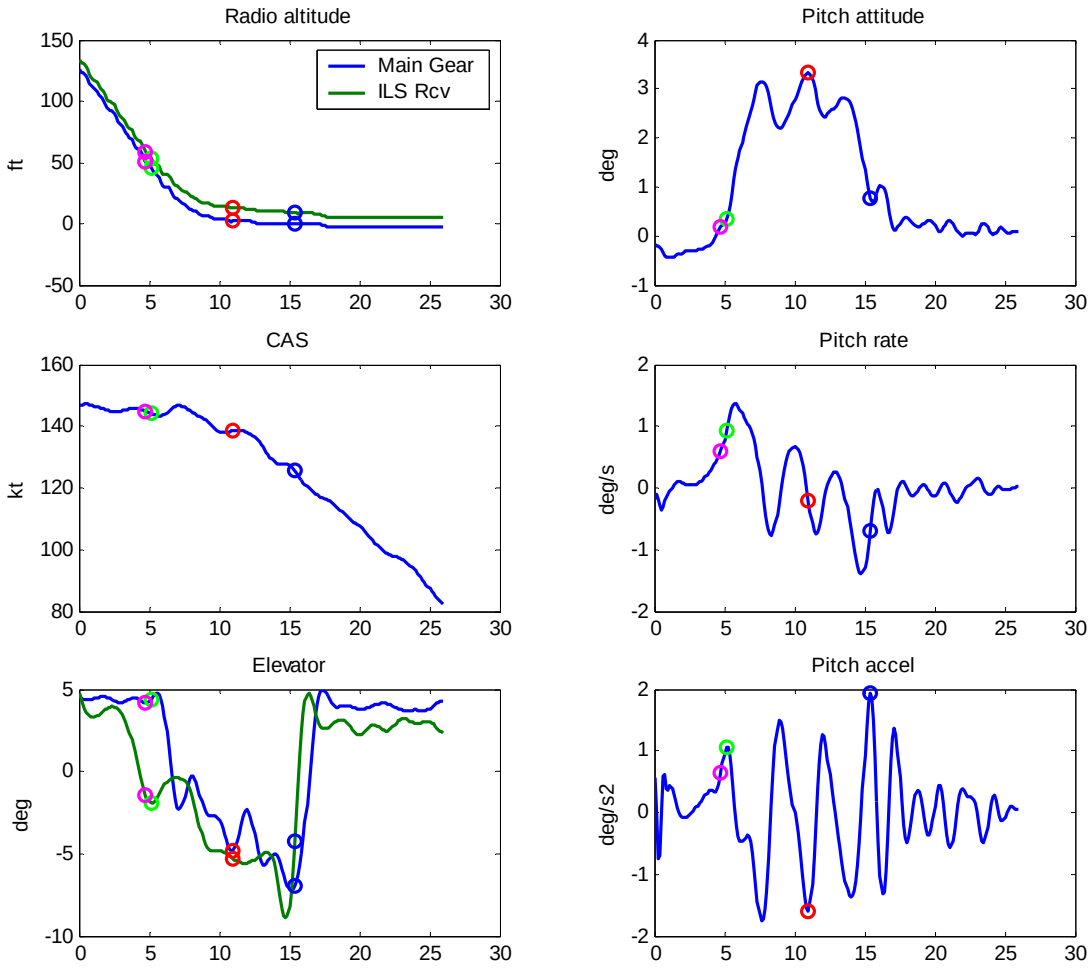

Legend:
O Threshold crossing
O Flare initiation
O Main gear touchdown
O Nosewheel touchdown

Figure B-26. B-737 Normal Flare (NZ = 1.12 g)

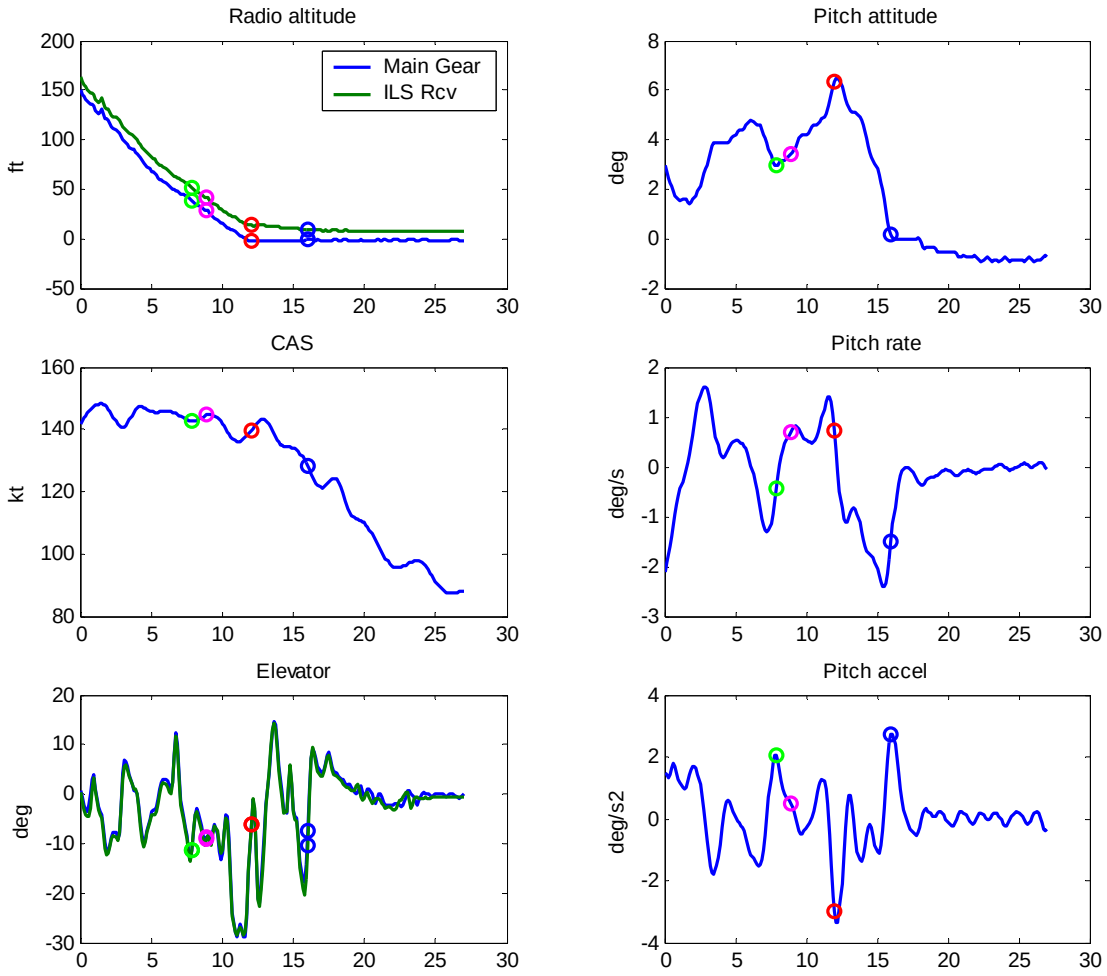

Legend:
O Threshold crossing
O Flare initiation
O Main gear touchdown
O Nosewheel touchdown

Figure B-27. A320 Aggressive Flare (NZ = 1.38 g)

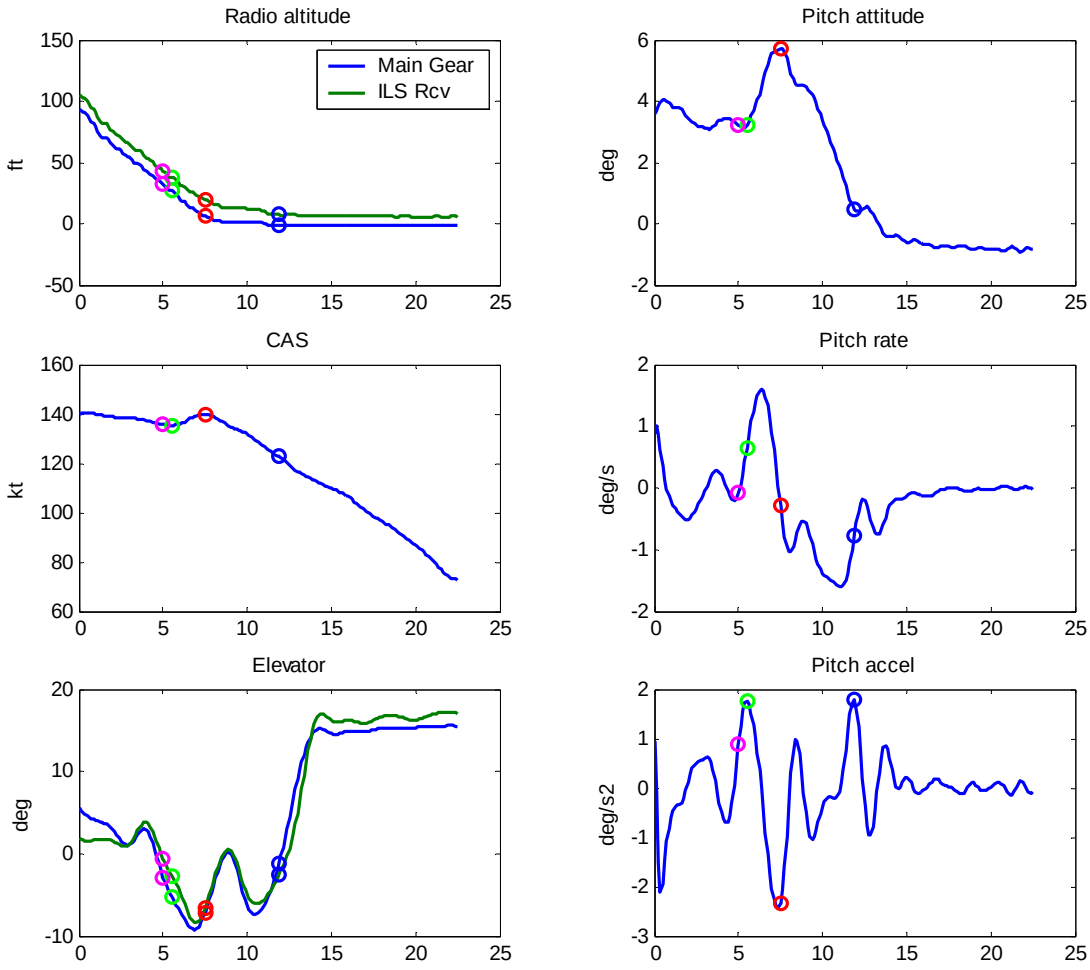

Legend:
O Threshold crossing
O Flare initiation
O Main gear touchdown
O Nosewheel touchdown

Figure B-28. B-737 Aggressive Flare (NZ = 1.4 g)

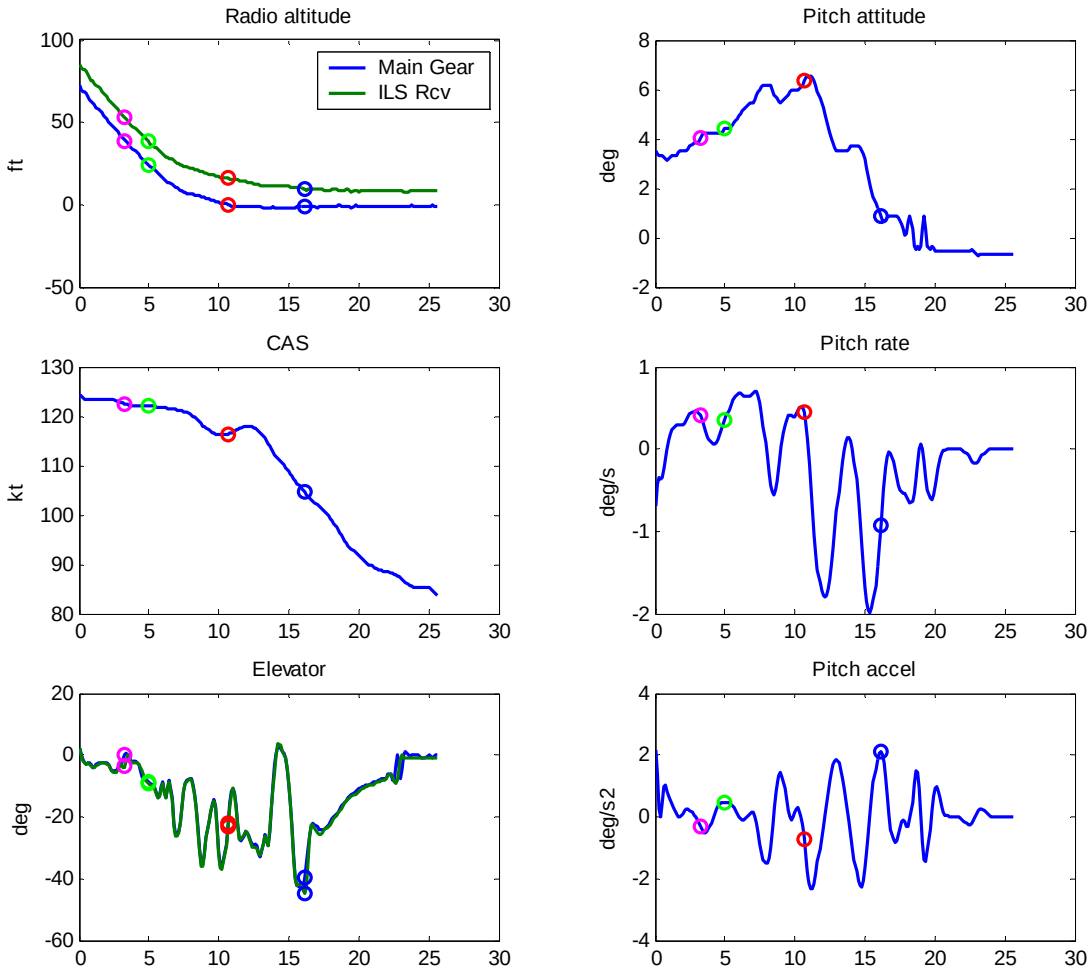

Legend:
O Threshold crossing
O Flare initiation
O Main gear touchdown
O Nosewheel touchdown

Figure B-29. A320 Slow Flare (NZ = 1.05 g)

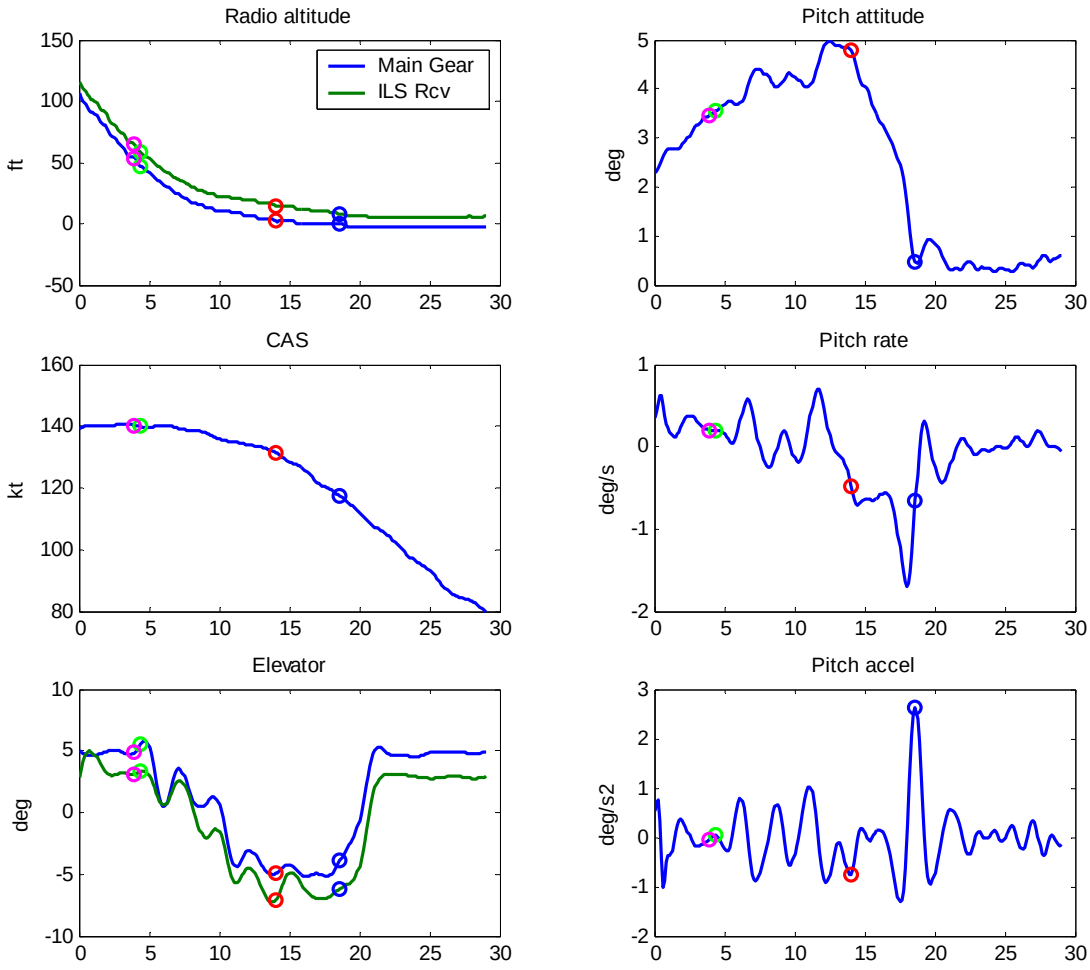

Legend:
O Threshold crossing
O Flare initiation
O Main gear touchdown
O Nosewheel touchdown

Figure B-30. B-737 Slow Flare (NZ = 1.02 g)